Politecnico di Milano

School of Industrial and Information Engineering

Department of Electronics, Information and Bioengineering

Master's Degree in Biomedical Engineering

Diffuse Reflectance Spectroscopy for Tissues Studies and Liver Vitality Check

Thesis Advisor:	Prof. Sergio Cerutti
Research Supervisor:	Vishnu Vardhan Pully

Candidate

Chiara Bignamini [766807]

Academic year 2012-2013

This Thesis was developed in collaboration with Philips Research, Minimally Invasive Healtcare Department, Eindhoven (NL)

and with the University Medical Center Groningen (UMCG), in Groningen, the Netherlands

Ai miei genitori.

Ringraziamenti

Acknowledgments

Al termine di questo lungo percorso, desidero fermarmi alcuni minuti per ringraziare chi ha fatto di questi cinque anni il periodo migliore della mia vita.
In the end of this long journey, I need to stop for a while to thank who contributed to the best period of my life.
Al final de este viaje, quiro pararme algunos minutos para agradecer toda la gente que ha sido responsable de los mejores años de mi vida.

Porgo un sincero ringraziamento al Professor Sergio Cerutti del Politecnico di Milano, che si è sempre dimostrato disponibile e comprensivo durante i nove mesi di stage che ho trascorso a Eindhoven, appoggiandomi con preziosi consigli e suggerimenti. Lo ringrazio particolarmente per la passione e l'entusiasmo che ha sempre dimostrato verso la Sua professione e che è in grado di trasmettere.

I wish to thank my supervisor in PHILIPS Research, Vishnu Vardhan Pully, who followed my project step by step, helping me with insightful discussions and precious tips.

I am deeply grateful to Renè Aarnink, who welcomed me in the Minimally Invasive Department of PHILIPS Research and gave me the possibility to live an amazing experience.
A special thank goes to Wilma, mum of all the students of the department and not only, who has always been available for any kind of help as well as for nice talks during morning coffees. I wish to show my gratitude towards the Photonic Group, which welcomed me during my nine months in PHILIPS Research and, in particular, I would like to thank Torre Bydlon, who kindly helped me with all the experiments and measurements.
Thanks also to Caren Kammen, from Life Science Facility at PHILIPS Research, who kept me updated about the availability of animal tissues for research purposes and helped me during the experiments, with the dissection of the animals.

Il GRAZIE più profondo va a coloro che hanno reso tutto questo possibile, sostenendomi sempre, nei momenti difficili e in quelli più facili, in quelli belli e in quelli meno piacevoli, insegnandomi con umiltà quegli inestimabili valori che oggi fanno di me la loro bambina cresciuta. Grazie a loro ho imparato ad affrontare con gioia ogni sfida, perchè è cadendo che ci si rialza, è sudando che si raggiungono le migliori soddisfazioni.
Questo ringraziamento va a mamma Angela e papà Antonio.

Un grazie speciale e sincero va a coloro che ci sono sempre state, che erano al mio fianco prima che l'università iniziasse e che tutt'ora lo sono. Grazie Vita, grazie Silva, grazie Laura, grazie Chiara, grazie Vanessa e grazie Alessia per le lunghe chiacchierate di venerdì sera, per gli sfoghi ed i pettegolezzi nonchè per avermi con-

tinuamente silenziosamente appoggiata.
Un enorme ringraziamento va poi a Veronica, che ci è sempre stata, per quanto vicine o lontane potessimo essere.

Se ricorderò per sempre questi cinque anni di università come i migliori che potessi mai aspettarmi, lo devo soprattutto a chi sapevo di trovare là, ogni giorno.
Ringrazio tutti i miei compagni di corso, con i quali ho condiviso gioie e dolori, esami e pranzi, fiorellini e numeri.
Grazie Gloria e grazie Anna perchè come eravamo brave noi tre a stare appollaiate al calorifero non lo era nessuno.
Grazie Lella, grazie Paolo, grazie Ste e grazie Fede, miei Amici per... la pelle!

Quiero agradecer también todos los Amigos que han compartido conmigo mis once meses en Zaragoza, siendo como hermanos y hermanas durante mi año de Erasmus. Gracias a Claudia, Emilio, Maria, Iñigo, Miguel, Javier, Juan, Alejandro y, otra vez, Lella.

Last but not least.. I really wish to thank all the Friends I met in Eindhoven during my internship at PHILIPS Research.
"Intern" is now a word full of meaning for me, because to be an intern probably means beeing a special person, or at least this is what this experience thought to me.
Thanks to Ale, who shared with me crazy moments of office night-life and not only, and thanks to Sasa for beeing the best housemates I could expect. Thanks to Rui, for beeing my best officemate ever and for supporting and understanding me in the

difficult part of my internship. Thanks to Giulia for being a friend, always bringing me love and verve, and thanks to Johan for introducing me to the amazing world of the iphone5. Thanks to Paki for his endless smile and to Yannick, for imitating my italian accent while ordering my ”grote bonen koffie”. Thanks to Cece, Deian, Bing, Toine, George, Tom, Emir, Pierre, Annika, Bente, Fleur, Libo and all other beautiful people I had the chance to meet.

Spero di aver lasciato qualcosa nel cuore di ognuno di voi.
I hope to have left something in each of your hearts.
Espero que haya dejado algo en el corazon de cadauno de vosotros.

Chiara

Summary

Diffuse Reflectance Spectroscopy (DRS) is an optical technique that enables tissue characterization by measuring the spectral response of the tissue-light interaction. Broadband light is emitted via an optical fiber and it is collected with another optical fiber after light absorption and scattering in the tissue. The collected light is acquired with a spectrometer that can resolve light in the visible and near infrared wavelength range below a micron.

The use of light is clinically appealing as it can detect physiological and biological changes whereas medical imaging only provides morphological information. The concentration of relevant chromophores in tissue can be extracted from its spectral response to light illumination.

This thesis project is mainly made by two different parts.

In the first period, the work has been focused on the use of DRS for the classification of different tissue types. The main goal behind it is to include DRS as a medical imaging tool for percutaneous guidance, to accurately guide interventional tools to the region of interest for an effective treatment. The aim is to provide a real time feedback on the tissue type touched by the sensor, such as on the physiological and biological changes in it.

Ex-vivo experiments on animal tissues have been performed, which resulted in high

sensitivity and specificity for the classification of fat, muscular and nerve tissues. Beside it, the effects of cold storage on tissues has been evaluated by remeasuring the tissue samples after freezing them at -8°C. A comparison between data from swine defrosted tissues and human cadavers tissues will be presented.

The goal of the second part of this thesis project is the evaluation of the potentials of Diffuse Reflectance Spectroscopy for monitoring liver vitality during preservation. Currently, pathology analysis are implemented for this purpose, but the results require too much time to be available compared to the maximum preservation time of a donor liver. Beside it, continuous monitoring is not possible.

DRS could have the potentials to be the real-time, mini-invasive and cheap substitute to pathology analysis.

This research has been developed in collaboration with the Groningen University Medical Center (UMCG), in Groningen (NL), where experiments on discarded human livers under normothermic perfusion are currently running. DRS measurements on one perfused and two not perfused livers have been acquired during a period of 6 hours and the output data have been analyzed.

The results of this study are promising, but new experiments on human discarded livers during perfusion are needed.

This thesis project has been performed at PHILIPS Research, Minimally Invasive Healthcare department, located at High Tech Campus - Eindhoven, The Netherlands.

Sommario

La Diffuse Reflectance Spectroscopy (DRS) è un tecnica mini-invasiva che sfrutta le caratteristiche ottiche dei tessuti biologici con scopi di diagnosi e/o di feedback durante procedure interventistiche percutanee.
La tecnica prevede l'utilizzo di un ago contenente due fibre ottiche, una delle quali funziona da sorgente di luce visibile e infrarossa, mentre l'altra riceve i raggi diffusi dal tessuto. Il segnale in uscita dal sistema dipende dalle caratteristiche ottiche del campione analizzato, ovvero dalla sua composizione. I principali componenti di un tessuto biologico che ne determinano le caratteristiche ottiche, assorbendo luce di differenti lunghezze d'onda, sono: sangue (principalmente emoglobina, ossigenata e non ossigenata), acqua, cellule lipidiche, fibre collagene e beta-carotene. La luce che non viene assorbita da tali componenti, detti cromofori, viene diffusa e rilevata dalla fibra ottica sensore. Dal segnale in uscita è possibile risalire alle concentrazioni dei diversi cromofori nel tessuto utilizzando un modello sviluppato da Farrell nel 1992[27].

Il progetto svolto si constituisce di due parti principali.

Per la prima parte del lavoro la DRS è stata utilizzata con lo scopo di valutarne le capacità di classificazione di diversi tessuti animali. L'idea dietro a questo studio prevede l'utilizzo futuro della DRS come tecnica di imaging che dia la possibilità

di avere un feedback in tempo reale durante procedure interventistiche percutanee. Diversi esperimenti ex-vivo sono stati effettuati con lo scopo di valutare le possibilità di questa tecnologia in tal senso. I tessuti analizzati sono stati ottenuti da due conigli, due topi e due suini, seguendo le relative normative etiche. I dati rilevati in tali esperimenti sono stati analizzati con buoni risultati in termini di sensitività e specificità nella classificazione di tessuto adiposo, muscolare e nervoso. I tessuti in questione sono stati in seguito congelati e nuove misure spettroscopiche sono state effettuate dopo lo scongelamento. Questo esperimento ha voluto valutare l'effetto della conservazione a freddo sui vari componenti biologici di ogni tessuto. I dati rilevati da tessuti di suino sono stati inoltre comparati con dati acquisiti durante esperimenti su cadaveri umani (anch'essi una volta scongelati) per la valutazione di eventuali differenze da specie a specie. I risultati ottenuti non hanno rilevato significative differenze.

La seconda parte del lavoro è volta all'utilizzo della DRS per il monitoraggio delle funzioni vitali del fegato durante il breve periodo compreso tra l'espianto e il trapianto. Attualmente, diverse malattie epatiche, come, per esempio, cirrosi o tumori, hanno elevato il numero di richieste di trapianto di fegato, allungando i tempi di attesa per i pazienti. Questo problema, aggiunto all'elevato costo di un trapianto di fegato, porta alla necessità di ottimizzazione delle procedure al fine di evitare rigetti o complicazioni post-operatorie. Ad oggi gli organi vengono analizzati prima del trapianto mediante studi patologici come, ad esempio, biopsie. I risultati, però, necessitano tempi di attesa troppi lunghi se confrontati con le 4-18 ore in cui un fegato può essere conservato. La DRS si collocherebbe come sostituto mini-invasivo, real-time ed economico alle analisi patologiche, preservando il tessuto e permettendone un monitoraggio continuo durante il periodo di conservazione.

Questa parte del lavoro è stata svolta in collaborazione con il Centro Medico Universitario della città di Groningen (UMCG), in Olanda, dove, ad oggi, si stanno svolgendo esperimenti per la valutazione di una nuova tecnica di perfusione per fegati destinati al trapianto, che si svolge a temperatura corporea. Attualmente gli organi vengono conservati a basse temperature, ma studi precedenti hanno dimostrato che la conservazione mediante perfusione a 37℃ porterebbe a migliori condizioni iniziali per il trapianto.

Misure spettroscopiche sono state rilevate su tre fegati durante 6 ore con e senza perfusione. I dati ricevuti dall'UMCG sono stati analizzati e hanno portato a promettenti risultati. Ulteriori esperimenti sono necassari per la validazione della tecnologia.

Questo progetto di tesi è stato sviluppato in PHILIPS Research, dipartimento di Minimal Invasive Healthcare, High Tech Campus - Eindhoven, Olanda.

Contents

List of Figures

Introduction

In current medical practice, there is a clear trend towards minimally invasive procedures in surgery and radiology. Medical imaging is very often used for diagnosis but also in percutaneous image guidance. One of the challenges that physicians still encounter is to accurately guide interventional tools such as needles to the region of interest for an effective treatment. Most percutaneous image-guided procedures such as tissue biopsy are performed under ultrasound, Computer Tomography, Magnetic Resonance or X-Rays. Using ultrasound is nowadays the best technique for tissue visualization in real-time, but it requires a lot of experience for proper and accurate needle guidance to the region of interest. X-Rays is another real-time imaging, which has the drawback of lacking soft tissue contrast information. CT and MR enables soft tissue visualization but they require to be combined with ultrasound or X-Ray for real-time guidance and visualization of the distal end of the tip of the interventional tools. Thus, there is a clear need to have sensing capabilities at the tip of the tools to confirm its position in the region of interest for an effective treatment. Several biomedical research groups investigated optical sensing at the tip of interventional probes to provide real-time feedback on the tissue type during a procedure and subsequenlty confirm the position of the tip in the region of interest. Diffuse Reflectance Spectroscopy (DRS) is an optical technique that enables tissue characterization by measuring the spectral response of the tissue-light interaction. Broadband light is emitted via an optical fiber and it is collected with another optical fiber after light absorption and scattering in the tissue. The collected light is acquired with a spectrometer that can resolve light in the visible and near infrared wavelength range below a micron.

The use of light is clinically appealing as it can detect physiological and biological changes whereas medical imaging only provides morphological information. The concentration of relevant chromophores in tissue can be extracted from its spectral response to light illumination. Different evaluation phantom based techniques have been used to validate a mathematical model that derives the physiological and biological tissue composition from the DRS signal. Multivariate data analysis methods and other statistical tools assessed the clinical performance of diffuse reflectance spectroscopy between 500 and 1800 nm for tissue diagnosis and confirmation of the location of the needle tip for tissue biopsy or treatment [8].

This thesis consists in a feasibility study to evaluate the potentials of DRS for tissue classification and tissue monitoring over time.

Chapter 1

Background

Diffuse Reflectance Spectroscopy (DRS) is an optical technique that enables tissue characterization by measuring the spectral response of tissue-light interaction.
Light in the infrared and visible range is emitted via an optical fiber and, after light absorption and scattering in the tissue, the return light is collected with another optical fiber.

Several biomedical research groups are currently studying this technology as a minimally invasive procedure for clinical diagnosis like, for example, for discrimination between healthy and tumor or dysplastic tissue. Another challenge that physicians are encountering is to include DRS as a medical image for percutaneous guidance, to accurately guide interventional tools to the region of interest for an effective treatment. The main aim is to provide a real time feedback on the type of tissue touched by the sensor, such as on the physiological and biological changes in it.

Optical parameters are obtained by converting measurements of observable quantities (ex.reflection) into parameters which characterize light propagation in tissue.

A number of methods have been proposed in order to measure the optical properties of tissues. These can be separated into two classes: direct and indirect. In direct techniques, optical properties are found using Beer's law, while in indirect techniques, a theoretical model of light scattering has to be built. Indirect techniques can be subdivided into iterative and non-iterative methods. A non-iterative method uses equations in which the optical properties are explicitly given in terms of the measured quantities while, in iterative methods these relations are implicit. In the second case the values for the optical properties are iterated until the calculated reflection and transmission match the measured values. These methods are the most cumbersome to use, but the optical model employed can be much more sophisticated than in the non-iterative methods [9].

In past years, investigators have reported values for the total attenuation coefficient , the effective attenuation coefficient, the effective penetration depth, the absorption and the scattering coefficient, and the scattering anisotropy factor for a variety of tissues at a variety of wavelengths. The majority of these results are based upon approximations to the radiative transport theory, like the diffusion theory [9], which enters in the category of the iterative indirect methods.

1.1 Light transport in biological tissues

In order to discuss the technique of DRS in more detail, it is important to understand how light propagates through biological tissues.

When incident light travels through biological tissues, photons can be absorbed or scattered.

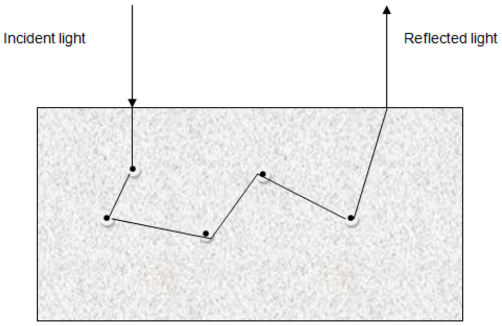

Figure 1.1: *Interaction between light and tissue*

A photon is absorbed if, after the interaction of one photon with the tissue, there is no re-emission of another photon, while scattering happens if another photon is emitted after the contact, in an elastic or inelastic way.

1.1.1 Light Absorption

The reflectance signal, in DRS measurements, gives information about the light absorption in the tissue. When light crosses a system of matter, the energy associated with the incident fields is most often dissipated as heat within the medium.

In 1729 Bouguer[10] firstly found a relationship between the thickness of the medium and the absorption of light and later, in 1760, Lambert[11] derived the mathematical expression for it, known as Lambert-Bouguer law

$$I = I_0 e^{-\mu_a l} \tag{1.1}$$

where I is the transmitted intensity through a distance l, I_0 is the incident intensity and μ_a is the absorption coefficient which can be interpreted as the probability that a photon will be absorbed by the medium per unit lenght.

In 1852 Beer determined that the absorption coefficient of a compound is linearly related to its concentration c diluted in a non-absorbing medium[12]

$$\mu_a = \alpha c \tag{1.2}$$

where α is the specific absorption coefficient. Substituting this value in equation (1.1) gives the relation know as Lambert-Beer law

$$I = I_0 e^{-\alpha c l} \tag{1.3}$$

which can be expressed like

$$I = I_0 10^{-\epsilon c l} \tag{1.4}$$

where ϵ is the molar absorptivity of a specific compound in solution, known also as specific extinction coefficient.

It is possible to define $A = \epsilon c l$ as the absorbance associated to one particular compound. In a solution containing n absorbing compounds, the total absorbance is the sum of the individual ones

$$A = A_1 + A_2 + \cdots + A_n = (\epsilon_1 c_1 + \epsilon_2 c_2 + \cdots + \epsilon_n c_n)l \tag{1.5}$$

. The Lambert-Beer law is valid only if the light which enters the medium is monochromatic and perfectly collimated, and if the medium itself is pure and uniformly absorbing. Those conditions will translate in errors during practical spectroscopic measurements.

The most important chromophores in biological tissues are water, lipids and hemoglobin, which are considered, for that reason, the most important parameters that response for absorption in spectroscopic measurements.
The most abundant chemical substance in the human body is water, which constitutes from 60 to 80% of total body mass[6], depending on tissue type, age and gender. As showed in Figure1.2 its absorption coefficient is not significant within the visible wavelength range, while it reaches maximum values in the infrared, around 970 nm, 1192 nm and 1453 nm . It has been demonstrated that changes in temperature cause shifts of the peaks[13].
As said, another important parameter that has to be taken in consideration while measuring biological tissues is the amount of lipids. Most of the lipid in the human body exists in form of triglycerides (neutral fat) and it is found in subcutaneous tissues and around the organs. Phospholipids, another group of lipids, are the main component of cell membranes and are thus found in every organ in the body.
Lipid concentration in the subdermis adipose tissue depends on age and gender, varying from 23 to 47% for infants and from 68 to 87% for adults[14] As shown in Figure1.3, the relevant absorption peaks are at 930 nm, 1040 nm, 1200 nm, 1392

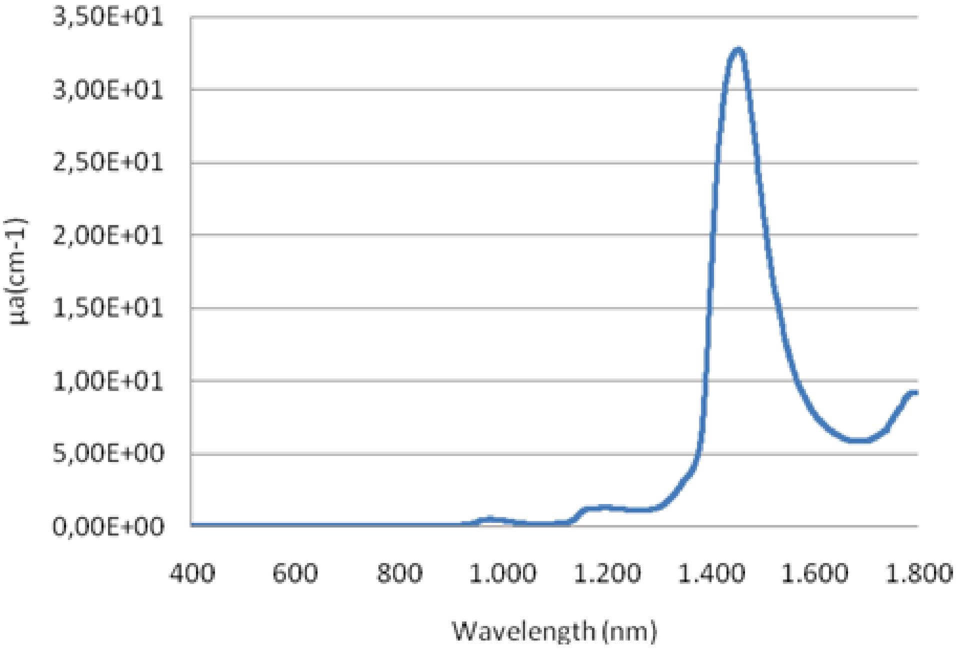

Figure 1.2: *Absorption coefficient of water at wavelength 400 to 1800 nm*[1]

nm, and 1413 nm.

The importance of lipid as an absorber in DRS depends upon the tissue in question. In some organs, like for example the liver, the amount of water is much greater than the fat and, for this reason, the ratio between fat and water plus fat (F/W+F) is considered to be much more useful to define the lipid content than the fat concentration itself. This will be one of the parameters extracted from the measurements (paragraph 1.2.2).

Besides water and fat, hemoglobin and its various derivates are the most dominant absorbers in the visible and near infrared wavelength range. Hemoglobin is carried in red blood cells, called erythrocytes, and constitutes approximately 40-45% of the whole blood. It is responsible for delivering oxygen from the lungs to the body cells and returning waste gases to the lungs to be eliminated. In the oxygenated

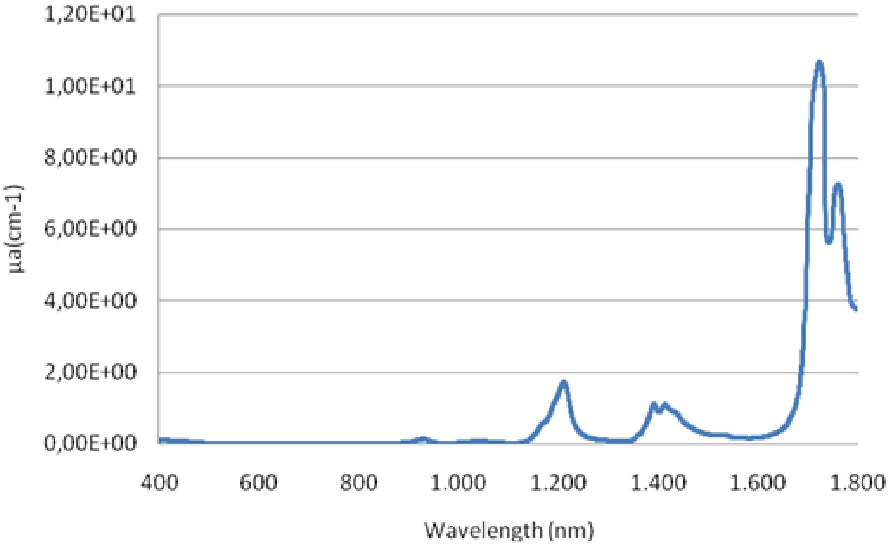

Figure 1.3: *Absorption coefficient of lipids at wavelength 400 to 1800 nm*[1]

state hemoglobin is known as oxyhaemoglobin (HbO_2), while in the de-oxygenated state it is known as deoxyhaemoglobin (Hb).

The third important derivate of hemoglobin is methemoglobin, in which part of the hemoglobin (less than 1%) is transformed. The absorption spectra of the three of them in visible and NIR wavelength range are shown in Figure1.4. Hemoglobin absorption coefficient reaches its maximum values at 445 nm and 560 nm, oxyhemoglobin ones at 415, 542, and 576 nm, while methemoglobin has characteristic peaks at 404, 508, and 635 nm.

In Figure1.5 the absorption spectra of important chromophores are shown. Among them it is also possible to visualize how the absorption coefficient of Bile and Beta-carotene vary for different wavelength. Recent studies proved that the fitting of tissue spectra can significantly improve by adding those two parameters[3]. As shown, bile has its main absorption peaks at 400 nm. Another peak is shown at 1450 nm but

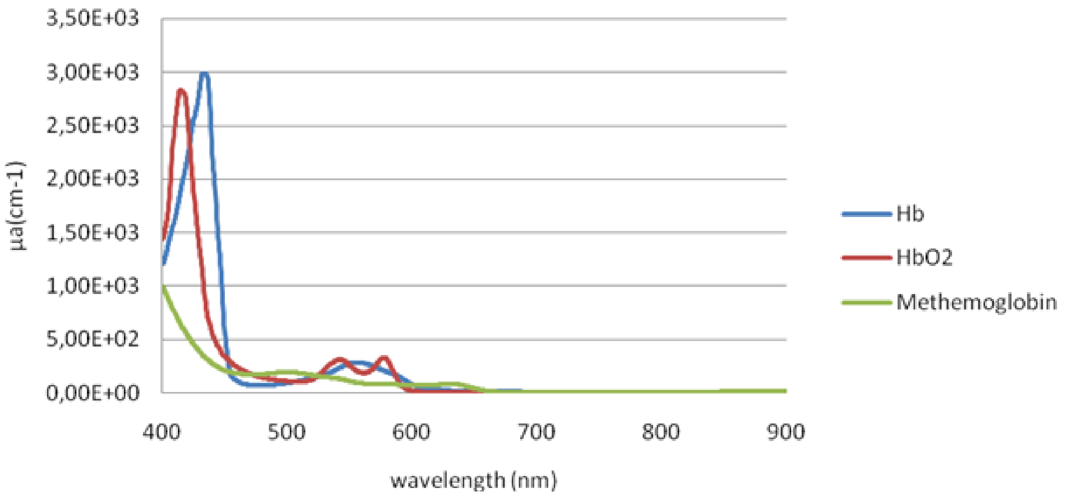

Figure 1.4: *Absorption coefficient of* HbO_2, HbO *and* $Methemoglobin$ *at wavelength 400 to 900 nm*[2]

it is mainly due to the presence of water[3]. Beta-carotene's main peak is displayed at 480 nm but it has been proved that it can vary depending on the substance in which the compound has been diluted[8].

Besides those, depending on the tissue in analysis, other relevant chromophores can be bilirubin[15], collagen[16] and melanin[17].

1.1.2 Light Scattering

Besides absorption, scattering is the other event that can occur to a photon which interacts with a particle. This happens when charged particles in a medium are set into oscillatory motion by the electric field of the incident wave and light is re-emitted (as opposed to absorbed) with a different direction of propagation in respect to the incident beam. It is possible to distinguish two different types of scattering: elastic, in which the energy of the incident particle is all conserved, and inelastic, in which some of that energy is lost or increased. Inelastic scattering

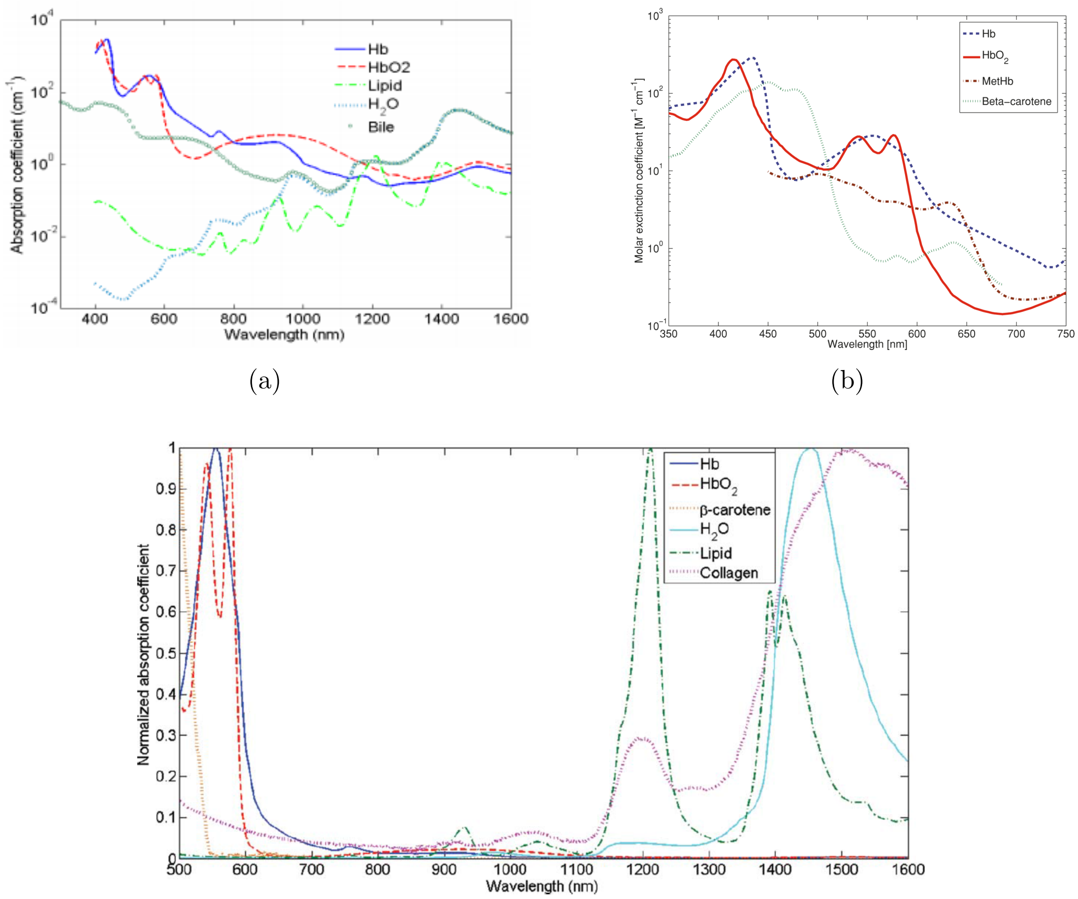

(a)

(b)

(c)

Figure 1.5: *[a]: Absorption coefficients of deoxygenated hemoglobin, oxygenated hemoglobin, lipid and water from 400 to 1600 nm. Absorption coefficient of bile from 300 to 1600 nm. The absorption coefficient axis is in a logarithmic scale[3].*
[b]: Absorption coefficients of deoxygenated hemoglobin, oxygenated hemoglobin and beta-carotene from 350 to 750 nm. Absorption coefficient of methemoglobin from 450 to 750 nm. The absorption coefficient is expressed per mole in a logarithmic scale[4].
[c]: Normalized Absorption coefficients of deoxygenated hemoglobin, oxygenated hemoglobin, beta-carotene, water, lipid and collagen from 500 to 1600 nm[5].

includes Brillouin, Raman and Compton effects, but in this section only elastic scattering will be discussed.

As a result of scattering, the velocity of light in matter is less than it is in vacuo.

In a medium in which the molecular separation is smaller than the wavelength of the incident light, atoms and molecules will scatter the primary radiation in all directions. The total scattered field in any direction is then a superposition of all the scattered wavelengths propagating in that direction. It interferes with the incident wave, modifying its phase and the velocity of the light through the medium[18].

The phase shift between the primary wave and the scattered one depends on the frequency of the incident light.

The refractive index of a substance (1.6) is a dimensionless number that describes how light, or any other radiation, propagates through that medium. It is defined as

$$n = \frac{c}{v} \tag{1.6}$$

in which c is the velocity of light in vacuo and v is the velocity of light in the studied medium.

It is possible to distinguish between two different types of elastic scattering, depending on the size and on the shape of the particles met by the incident wave: single and multiple scattering. Single scattering theory can be applied if the total scattered light is smaller then the incident wave. This happens if the particles concentration in the medium is low enough to have a sufficiently large separation between the particles[18]. If those particles have a small size compared to the wavelength of the incident light, Rayleigh scattering occurs (Rayleigh, 1871)[19], which means that the intensity distribution of the scattered light is on average angularly isotropic Figure1.6. Otherwise, if the scatterer size is of the same size order as the wavelength of the incident wave or larger, Mie scattering theory can be applied[20].

Mie theory[20] further describes both absorption and scattering by a spherical particle of arbitrary radius and refractive index. The analysis involves the formal solution of Maxwell's electromagnetic theory for homogeneous spheres using appropriate boundary conditions[18], which, in case of small particles, reduces to the solution for a Rayleigh scatterer.

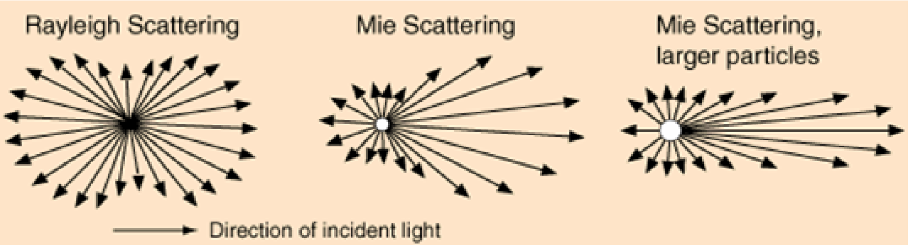

Figure 1.6: *Influence of particle size on scattering*

The exponential relationship expressed in equation (1.1), can be modified as

$$I = I_0 e^{-\mu_t l} \tag{1.7}$$

where μ_t is the total coefficient, given by

$$\mu_t = \mu_a + \mu_s \tag{1.8}$$

and μ_s is the scattering coefficient, which expresses the probability that a photon will be scattered per unit length. The reciprocal of the total scattering coefficient is known as free path.

Moreover, the new directions taken by photons after scattering do not occur with equal probability and this anisotropic behavior can be described by the differential scattering coefficient $d\mu_s(s, s')$, in which s and s' are respectively the directions of the incident and the scattered wave. The total scattering coefficient μ_s is calculated integrating it over all angles as follows:

$$\mu_s = \int_{4\Pi} d\mu_s(s, s')\, ds' \tag{1.9}$$

which depends on the angle between the incident and the scattered photons.

In many media μs is not independent of s, but they have orientation-dependent structures for which waves with particular directions are scattered with higher probability than others, so then the scattering coefficient will therefore depend on the incident direction. Normalizing the differential coefficient, the scattering phase function is obtained

$$p(s, s') = \frac{1}{\mu_s} d\mu_s(s, s') \tag{1.10}$$

such that $\int_{4\Pi} p(s, s')\, ds' = 1$.

Defining then θ as the angle between s and s', it is possible to introduce the anisotropy factor g as its mean cosine

$$g = \int_{4\Pi} p(\theta) cos(\theta)\, ds' \tag{1.11}$$

Combining the scattering coefficient and the anisotropy factor gives the transport scattering coefficient

$$\mu_s' = (1 - g)\mu_s \tag{1.12}$$

from which it is possible to modify the equation (1.1) as

$$\mu_t' = \mu_a + \mu_s' \tag{1.13}$$

and to define ${\mu'_t}^{-1}$ as the transport mean free path.

In reality, for the majority of the systems in nature, it is not possible to assume that particles are independent of one another and multiple scattering has to be taken in consideration.

Light Scattering in Biological Tissue

Biological tissues are mainly constituted by inhomogeneities which are responsible of mismatches in the relative refractive indexes, causing an increase of the overall light scattering.
Each microscopic object, in a cellular or sub-cellular level, will generate its own phase scattering function and contribute in defining the averaged scattering properties of the tissue.
Figure1.7 shows a 'generalized' cell[6], in which the main components are depicted. Cell sizes vary from the 4 μm of blood platelets till the meter that a nerve cell can reach, but they are all constituted by the same main elements: the cell membrane, the cytoplasm and the nucleus. The membrane surrounds the cell and it is made of a double layer of phospholipids which is approximately 8 nm thick, with numerous proteins embedded in it, while the cytoplasm constitutes the intracellular matrix and it is made by a water-based fluid, the cytosol, in which many organelles are suspended. Among those organelles, mitochondria are the ones responsible of giving energy supply to the cell. They are approximately 0.3-0.5 μm to 1-4 μm in size and they have an outer boundary similar to the cell membrane. The largest

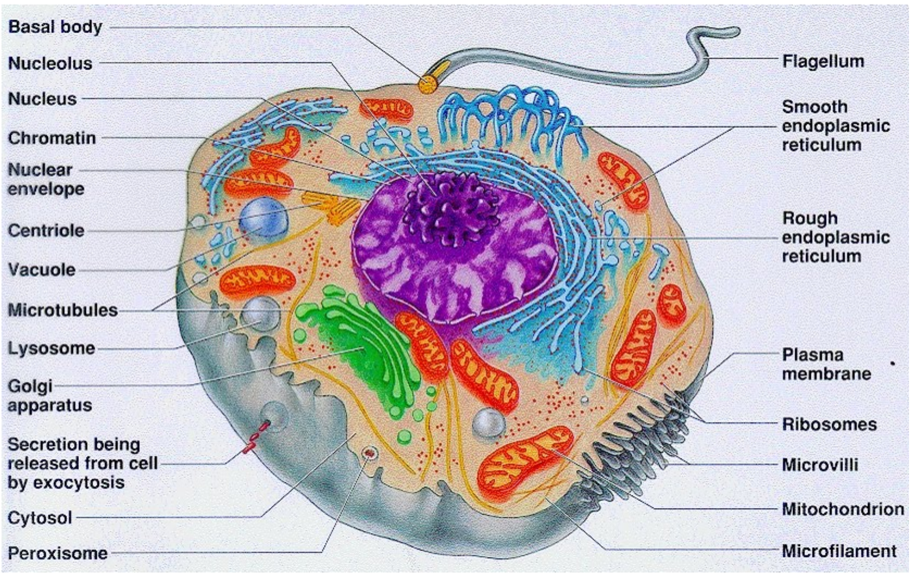

Figure 1.7: *Qualitative picture of a human cell*[6]

organelle in the cytoplasm is the nucleus, which is the control center of the cell. Its size varies with the cell type, with an average diameter in the order of 5 μ and, like the mitochondria, is surrounded by a phospholipid bilayered membrane[6]. Like shown in Figure1.8, while the cell membrane is responsible of Rayleigh scattering (its thickness is smaller than the near infrared wavelength), cytoplasm and nuclei cause Mie scattering.

The contribution of each type of particle to the mean scattering properties in tissue will depend on their individual properties and their relative concentrations, but, studying bulk tissue, what is important are the total effects of scattering and absorption. The typical mean refractive index for tissue is in the range 1.39-1.41, except of adipose tissue which is at 1.46[21]. Most tissue have a high g value, in the range 0.7-0.97[22], which means that the scatter is very forward-peaked.

It is important to take in account that computed values for the optical coefficients are inevitably prone to errors and that they may have been calculated under different

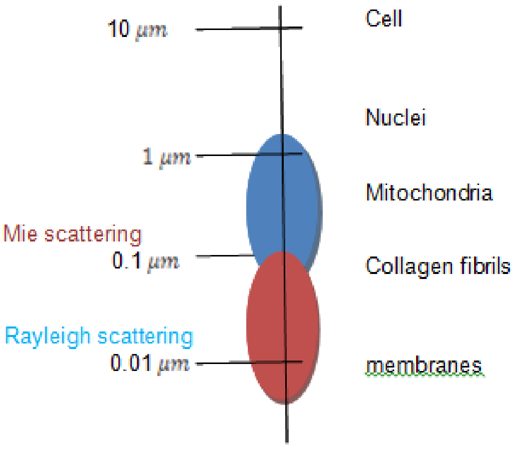

Figure 1.8: *Ultrastructure of tissue*

conditions like all (or any) of the following[9]:

- physiological conditions of the biological sample
    - hydration level;
    - homogeneity;
    - species variability;
    - frozen-unfrozen state;
    - in vivo - ex vivo;
    - fixed-unfixed;
    - surface smoothness of the sample slabs;
- irradiation geometry;
- boundary index matching-mismatching;
- orientation of detecting interstitial fibers with respect to the source fiber;
- numerical aperture of the sensing fibers;
- angular resolution of the photodetectors;
- separation of forward scattered light from unscattered light;
- theory used for the estimation of the parameters.

Beside those considerations, it is then relevant to take in account the intercellular order and the structures present other than cells, such as collagen fibers, which make multiple scattering of light becoming significant.

1.2 Diffuse Reflectance Spectroscopy (DRS)

Clinically relevant parameters can be obtained by modeling Diffuse Reflectance Spectroscopic measurements. Two important steps have to be done: (I) translate the spectral data into physical properties such as the absorption and reduced scattering coefficients for different wavelengths and (II) transform these optical properties into biological, biochemical and physiological parameters.

1.2.1 Models of Light Propagation in Biological Tissues

Analytical Models to translate DRS spectra into optical properties

To describe the light transport in a regime where multiple scattering is relevant it would be possible to use Maxwell's electromagnetic theory[23], but it has been noticed that the solution would be too complex and not compatible with practical applications like clinical use of DRS[24]. A more suitable description is given by the Radiative Transfer Equation (RTE), known also as Boltzmann transfer equation

$$\frac{1}{v}\frac{\delta}{\delta t}L(\vec{r},t,\hat{s})+\hat{s}\cdot\nabla L(\vec{r},t,\hat{s}) = -(\mu_a+\mu_s)L(\vec{r},t,\hat{s})+\mu_s\int_{4\Pi} L(\vec{r},t,\hat{s})p(\hat{s},\hat{s}')d\Omega' + S(\vec{r},t,\hat{s}) \tag{1.14}$$

in which the wavelike behavior of light is ignored and scattering and absorption of individual photons are considered. In this equation, $L(\vec{r},t,\hat{s})$ corresponds to the radiance, i.e. the energy at position $\vec{r}$, moving in direction $\hat{s}$ per unit of solid angle Ω, per unit of time t and per unit of normal area, v corresponds to the velocity of light in the medium, μ_a and μ_s to the absorption and scattering coefficients, p to the phase function and S is the radiation source term[25].

The RTE (1.14) can be reduced to a set of coupled differential equations thanks to the Diffusion Approximation, which is based on the following three assumptions:

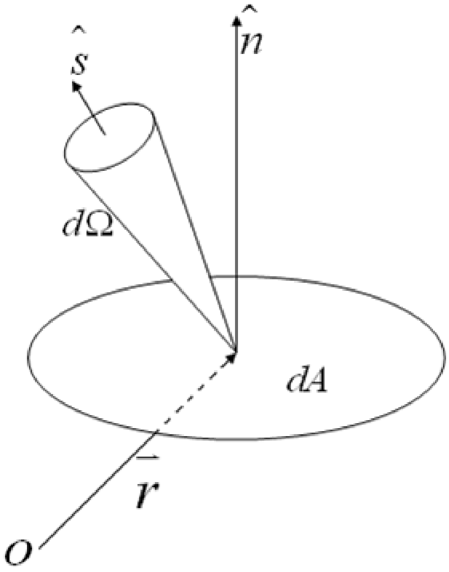

Figure 1.9: *Schematic of the energy flow through a differential area element dA at position $\vec{r}$ within a differential solid angle element $d\Omega$.*

- the highly forward scattering due to a medium with coefficient μ_s can be seen like an isotropic scattering with coefficient $\mu_s' = \mu_s(1-g)$;
- the tissue absorption is small compared to the reduced scattering while the inverse of the reduced scattering is larger then the source-detector distance;
- the source term in equation (1.14) is a distribution of single scattering sources along the axis normal to the boundary between the tissue and the source

surface[24].

With those approximations the RTE can be reduced to the Diffusion Equation given by *Patterson et al*[24]

$$\frac{1}{v}\frac{\delta\phi(\vec{r},t)}{\delta t} + \mu_a\phi(\vec{r},t) - D\nabla^2\phi(\vec{r},t) = S(\vec{r},t) \tag{1.15}$$

where ϕ is the photon density or fluence rate, related to the radiance as follows

$$\phi(\vec{r},t) = \int_{4\Pi} L(\vec{r},t,\hat{s})d\hat{s} \tag{1.16}$$

S is the isotropic source term and D is the Diffusion coefficient, given by

$$D = \frac{1}{3(\mu_a + (1-g)\mu_s)} \tag{1.17}$$

While going deep into the tissue, the fluence rate decreases[26], showing an exponential behaviour, which constant is known as the effective attenuation coefficient μ_{eff} calculated as follows

$$\mu_{eff} = \sqrt{3\mu_a(\mu_a + \mu_s')}. \tag{1.18}$$

according to the diffucion theory.

In an infinite turbin medium, the steady-state solution to the diffusion approximation for the fluence rate at a distance (ρ, z) from an isotropic point source at position $(0, z_0)$ is given by[27]

$$\phi(\rho, z_0) = \frac{1}{4\pi D}\frac{e^{-\mu_{eff}r_1}}{r_1} \tag{1.19}$$

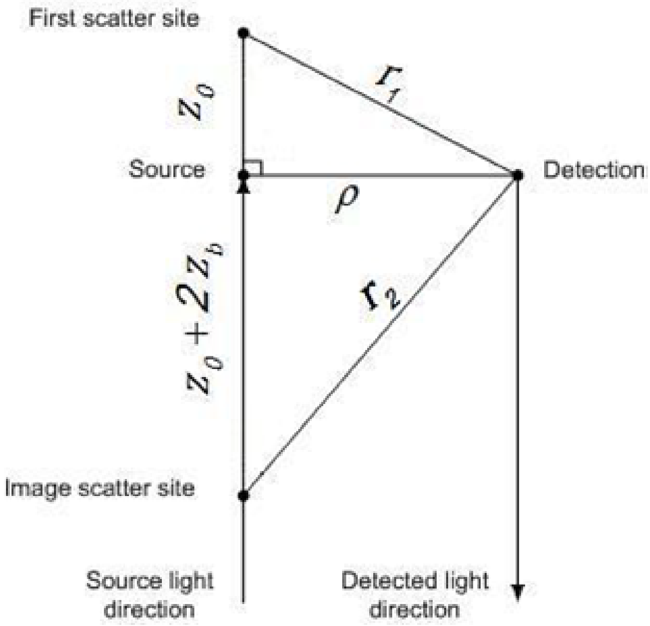

Figure 1.10: *Schematic representation of geometry and parameters. Source and detection fiber entrances are indicated with points. The light direction in the source and detector fiber is indicated with an arrow*

where r_1, the distance between the point source and the position (ρ, z) (see Figure1.10), is given by

$$r_1 = \sqrt{(z - z_0)^2 + \rho^2} \tag{1.20}$$

In a semi-infinite turbin medium, the boundary conditions at the surface of the medium become relevant. If there is no mismatch between the refractive indexes of the first and the second medium, there must be no photon current coming back into the scattering ones at the boundary. The expression for this is given by

$$\frac{\phi(\vec{r}, t)}{2D} = (\vec{\tau} \cdot \nabla\phi(\vec{r}, t)) \tag{1.21}$$

where $\vec{r}$ is a point on the interface and $\vec{\tau}$ is a unit normal vector into the tissue. This means that the fluence rate is equal to zero at a certain distance above the

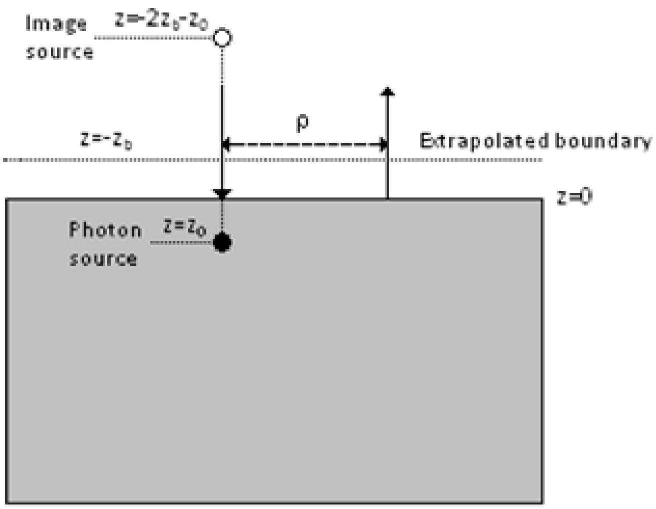

Figure 1.11: *Positions of photon source, extrapolated boundary and image source used in the model*

surface, known as "extrapolated boundary"[27], as shown in Figure1.11. If there is a mismatched refractive index at the media interface, then the position of the extrapolated boundary has to be adjusted. It has been shown[27] that this position is given by $z_b = 2AD$, where A is dependent on the indexes of the media and is equal to 1 if there is no mismatch.

The solution for a semi-infinite medium is given by

$$\phi(\rho, z_0) = \frac{1}{4\pi D}\left(\frac{e^{-\mu_{eff}r_1}}{r_1} - \frac{e^{-\mu_{eff}r_2}}{r_2}\right) \tag{1.22}$$

where r_1 was defined in equation (1.20) and r_2 is

$$r_2 = \sqrt{(z + z_0 + 2z_b)^2 + \rho^2} \tag{1.23}$$

which represents the distance between the image source and the collecting fiber.

The reflectance at the surface ($z = 0$) gives information about the fraction of light re-emitted from the medium at a distance ρ from the source and it is given as[28]

$$R(\rho, z_0) = -D\nabla\phi(\rho, z)|z = 0 \tag{1.24}$$

Combining equation (1.22) and (1.24) gives the law used to calculate the Diffuse Reflectance:

$$R(\rho, z_0) = \frac{1}{4\pi}\left[z_0\left(\mu_{eff} + \frac{1}{r_1}\right)\frac{e^{-\mu_{eff}r_1}}{r_1^2} + (z_0 + 2z_b)\left(\mu_{eff} + \frac{1}{r_2}\right)\frac{e^{-\mu_{eff}r_2}}{r_2^2}\right] \tag{1.25}$$

Analytical Models to translate optical properties into clinical parameters

The absorption coefficient can be seen as a linear combination of the absorption coefficients of all the single chromophores, which importance is proportional to their concentration in the tissue:

$$\mu_a(\lambda) = \sum_{i=1}^{N}[c_i] \cdot \mu_{a_i}(\lambda) \tag{1.26}$$

in which $[c_i]$ is the concentration of the i-th chromophore in the tissue out of the total amount N, and μ_{a_i} is its absorption coefficient. The absorption coefficients of each chromophore as a function of wavelength are known from literature (see paragraph 1.1.1) and they are used as a priori knowledge to estimate the concentrations $[c_i]$.

The reduced scattering can be expressed as a function of wavelength too[29]

$$\mu_s'(\lambda) = a_{Mie}\lambda^{-b} + a_{Rayleigh}\lambda^{-4} \tag{1.27}$$

where a_{Mie} and $a_{Rayleigh}$ respectively correspond to the Mie and Rayleigh reduced scattering amplitude and b is the reduced scattering slope and it is correlated with the average particle size. In particular it has been proved that it decreases with the average diameter of the particles[30].

Equation (1.27) can also be written as follows

$$\mu_s'(\lambda) = a\left(\rho_{MR}\left(\frac{\lambda}{\lambda_0}\right)^{-b} + (1-\rho_{MR})\left(\frac{\lambda}{\lambda_0}\right)^{-4}\right) \tag{1.28}$$

in which λ_0 is a normalization wavelength set to 800 nm and the parameter a corresponds to the reduced scattering amplitude at this specific wavelength. The reduced scattering corresponds to the sum of Mie and Rayleigh scattering and, therefore, ρ_{MR} is defined as the Mie-to-Rayleigh fraction of scattering[31].

The reduced scattering coefficient is assumed to be a power law function and, as said, the wavelength-dependency of the absorption coefficients is replaced by a priori knowledge of them. Those two considerations give the possibility to derive the chromophore concentrations and the reduced scattering amplitudes and slopes by simply combining (1.26) and (1.27). In this way, the fitting model locks onto the spectral features and shapes of the measured reflectance[8].

1.2.2 Empirical modifications on the models

Knowing the distance between the emitting and the collecting fibers and the chromophores of interest as input arguments, the measured spectra were fitted from 500 to 1600 nm with the model suggested by Farrell *et al*[27], which has been derived from the approximate diffusion theory using a Levenberg-Marquardt non-linear inversion algorithm in order to determine the absorption coefficient and the reduced scattering coefficient expressed in cm^{-1}[8]. The model was then validated using phantoms with known concentrations of different chromophores, including spectra calibration procedures. Investigators that were interested in determining blood volumes and levels of oxygenation in blood could not estimate them from known phantoms when the light was in a low wavelength range. At the beginning it was thought that one of the assumption for the approximate diffuse theory was not holding because of the high absorption of blood at short wavelengths[32]. However, in the mid-90s, some groups studied whether the cause was due to the inhomogeneous distribution of blood in tissues, which gives much higher chance to photons at wavelengths below 500 nm to be completely absorbed compared to photons at higher wavelength. Several groups investigated in order to find the best correction factors and nowadays the most used is the pigment packaging factor[33] given by

$$C(\lambda) = \frac{1 - e^{-2R\mu_a^{blood}(\lambda)}}{2R\mu_a^{blood}(\lambda)} \tag{1.29}$$

where R corresponds to the effective vessel radius and μ_a^{blood} represents the absorption coefficient of hemoglobin in blood, given by[31]

$$\mu_a^{blood}(\lambda) = (StO_2)\mu_a^{HbO_2}(\lambda) + (1 - StO_2)\mu_a^{Hb}(\lambda) \tag{1.30}$$

In this last equation $\mu_a^{HbO_2}(\lambda)$ and $\mu_a^{Hb}(\lambda)$ represent the basics extinction coefficient spectra of oxygenated and deoxygenated hemoglobin respectively, assuming blood content of 150 g/l (typical for humans). StO^2 is commonly known as the blood oxygen saturation and represents the oxygenated hemoglobin fraction in the total amount of hemoglobin $StO_2 = \frac{[HbO_2]}{[HbO_2]+[Hb]}$, where $[HbO_2]$ and $[Hb]$ correspond to the concentrations of oxygenated and deoxygenated hemoglobin respectively.

All these considerations lead to an empirical modification of the old equation for the total absorption coefficient (1.26), which is now calculated as follows

$$\mu_a(\lambda) = C(\lambda)\nu_{BL}\mu_a^{Blood}(\lambda) + \nu_{WL}\Bigg((1-\alpha_{WL})\mu_a^{Water}(\lambda) + \alpha_{WL}\mu_a^{Lipid}(\lambda)\Bigg) \tag{1.31}$$

where μ_a^{Water} and μ_a^{Lipid} are the absorption coefficients of water and lipids respectively (see paragraph 1.1.1, Figure1.2 and Figure1.3). In this last equation for μa some new coefficients are present, which multiply the absorption coefficient of the most important chromophores:

$$\nu_{BL} = [HbO_2] + [Hb], \tag{1.32}$$

$$\nu_{WL} = [H_2O] + [Lipid], \tag{1.33}$$

$$\alpha_{WL} = \frac{[Lipid]}{([Lipid] + [H_2O])} \tag{1.34}$$

in which $[H_2O]$ and $[Lipid]$ correspond to the concentrations of water and lipids (density of 0,86 mg/ml) respectively. Those coefficients represent the blood volume fraction (ν_{BL}), the total amount of water and lipids in the probe volume (ν_{WL}) and the lipid fraction within this volume (α_{WL}).

From the acquired spectra eight parameters are always derived: a, b, ρ_{MR}, R, ν_{BL}, StO_2, ν_{WL}, α_{WL}, three of them defining the reduced scattering coefficient and the other five the absorption coefficient, from which three are related to blood and two to water and lipid. Depending on the tissue studied, other parameters can be considered for the fitting by adding them in the model as follows[31]

$$\mu_a^{total}(\lambda) = \mu_a^{tissue}(\lambda) + \nu_{others}\mu_a^{others}(\lambda) \tag{1.35}$$

In this study collagen, beta-carotene, methemoglobin, bile, bilirubin and lycopene will be estimated.

Typically, in the 600-1300 nm range the optical coefficients for soft tissues (e.g. liver, brain, lung, skin) are μ_a equal 0.01-1 mm^{-1} and μ_s equal 10-100 mm^{-1}[26].

Chapter 2

Tissue Classification

2.1 Introduction

Understanding the propagation and the distribution of light in biological tissue is essential for effective and safe applications in medical diagnostics and therapeutics. As said in chapter 1, optical properties of body tissues depend on the concentration of the main chromophores in them. Knowing the compositions of body tissues and combining them with their spectroscopic measurements gives the capability to understand how those chromophores effectively affect the optical properties of a particular tissue. Nowadays, many research groups are trying to understand if it is possible to rely on this knowledge in order to associate each spectra to a particular tissue without knowing where exactly it was acquired. This actually could constitute the technological basis for many different medical applications, like, for instance, for remote optical feedback during tissue-specific laser surgeries or, in oncology, for discrimination between normal and tumor tissues during diagnosis or treatment (ablation) operations.

Laser surgery provides the advantages of high precision and sterility, combined with little trauma. However, those advantages are accompanied by a lack of haptic feedback during the tissue cutting. Laser ablation is a remote process in which the surgeon doesn't get precise real-time information about the exact depth of the laser beam penetration and the type of tissue ablated at the bottom of the cut end. Due to that, it comes with the inherent risk of an accidental destruction of critically important organs and tissues, such as blood vessel walls or nerves.

A technical feedback system may assist and control tissue-specific laser ablation if it is able to identify the type of biological tissue targeted to be either ablated or preserved during surgery. Such a feedback system is expected to work in a loop, warning about the results after nearly every laser pulse and operating a real-time control that stops the laser ablation when it reaches a different tissue layer or an anatomical structure that has to be preserved.

Diffuse Reflectance Spectroscopy provides a straight-forward and low resource-consuming approach to optical tissue differentiation that can be exploited remotely and that can be easily integrated into the hand piece of the laser scalpel[34]. This can be a real-time method because the integration time of the signal collection can be as short as a fraction of a microsecond.

Many studies in literature confirmed the possibility to use Diffuse reflectance spectroscopy for diagnostic purposes, to discriminate between normal/benign tissue and tumor/malignant or displatic ones. However, only a few confirmed the capability of DRS to be used for tissue-specifc laser surgery.

The main aim followed in this chapter is to understand if it is possible to use DRS to differentiate between regular types of tissue. Spectra from the most common types of tissue, like subcutaneous fat, muscle or nerve will be investigated.

2.2 Materials and methods

2.2.1 Measurement console

The spectra were collected from different samples with a setup which has been previously used for other studies[13, 31]. As shown in Figure2.1, it consists of a halogen broadband light source with an embedded shutter (Ocean Optics, HL-2000-HP), an optical probe with three fibers and two spectrometers that can resolve light from 400 to 1100 nm (silicon detector, Andor Technology, DU420A-BRDD) and 800 to 1700 nm (InGaAs detector, Andor Technology, DU492A-1.7), respectively. A filter that rejects light for wavelengths below 465 nm was mounted in front of the spectrometers to reject second order light at the detectors. The silicon detector is a matrix of 1024 by 255 pixels with pixel size of 26x26 micros whereas the INGaAs detector is a single array of 512 pixels with a pixel size of 500x50 micros. The spectral resolution for the silicon and InGaAs detectors are 4 and 10 nm, respectively.

Each measurement was simultaneously collected with both the silicon spectrometer

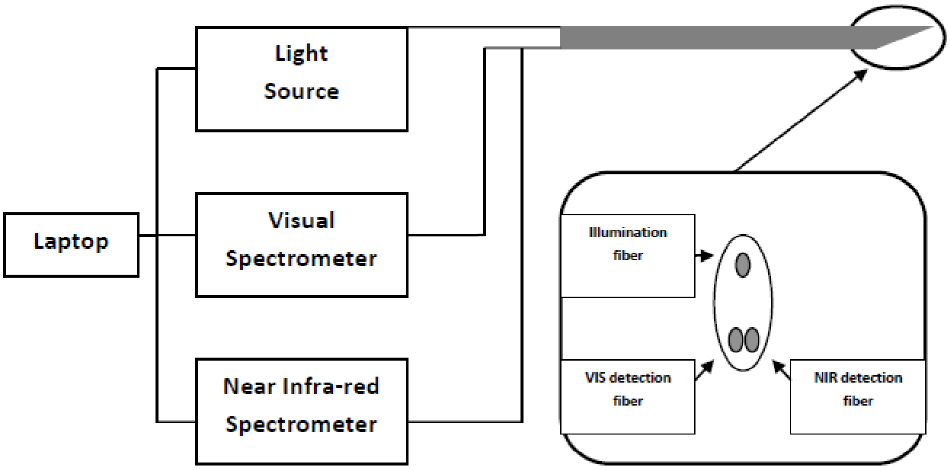

Figure 2.1: *Schematic overview of the diffuse reflectance spectroscopy system*

and the InGaAs one. The spectra are acquired in the visual range (400-1100 nm) and in the near-infrared range (800-1700 nm) and combined to a single spectrum. For all the acquisitions, the matching factor should ideally be equal to one but is on average 0.9±0.3. This is due to the fact that the light is collected via two fibers in an inhomogeneous medium and there might be a sampling error. To avoid this artifact, one single fiber was connected to a fiber splitter in order to collect the light from the same sampling volume. However, the use of a fiber splitter reduces the light transmission by more than 50% and thus longer integration times might be needed to achieve a good signal-to-noise ratio, making real-time feedback impossible[31].
For the spectral analysis the 400-1600 nm spectral range has been used, where the 400 to 1000 nm (VIS area) and 1000 to 1600 nm (NIR area) correspond to the data collected with the silicon and InGaAs detectors, respectively. All the spectra were acquired by placing the surface of the optical fibers at the distal end in contact with the tissue (by inserting the photonic needle in the tissue or placing it on its surface).
In Figure2.2, a picture of the photonic needle used during the experiments is shown.

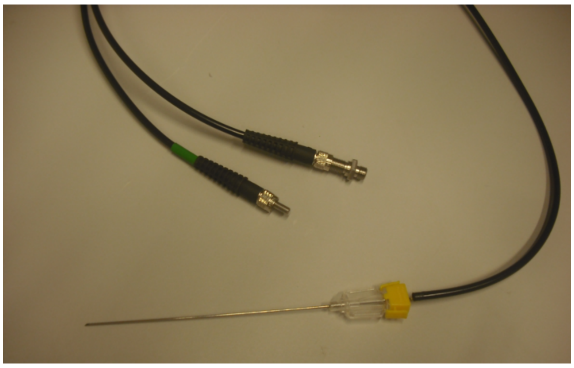

Figure 2.2: *Picture of the Photonic Needle*

The needle contains two fibers, one which will be connected to the light source (green connector in picture 2.2) and the other one (black connector in picture 2.2) which will go to the fiber splitter and, then, to the VIS and NIR detectors. The two fibers are separated, at the tip of the needle, by a distance of 0.87 mm, which implies that long distance (LD) DRS measurements will be performed. The thickness of the fiber is 200μm

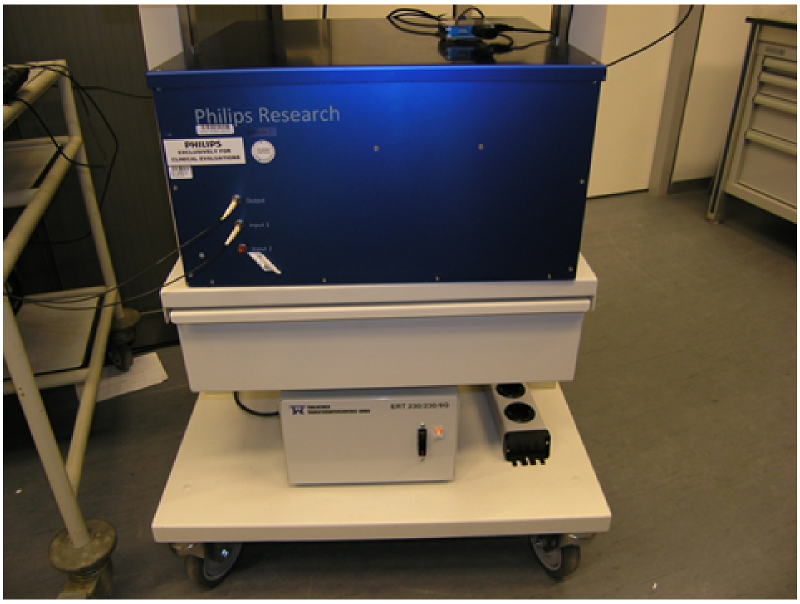

Figure 2.3: *Research Console for DRS measurements designed by Philips Research*

2.2.2 Calibration and Data pre-processing

The system was calibrated prior to each measurement on the tissue samples.

The calibration consists of several steps. First, the detectors is cooled down to -14°C. Once the temperature is stable, a wavelength calibration is performed to assign a wavelength value to each pixel of both detectors, fitting a second order polynomial to a set of atomic lines from Argon and Mercury light sources with peaks at known wavelengths.

The processed spectra $S(\lambda_i)$ are secondly calibrated by acquiring an intensity calibration spectra $C(\lambda_i)$. To do so, the reflectance signal of a white reflectance standard (spectralon LabSphere, WS-1-SL) is measured. A probe-holder is used to hold the probe tightly and keep the surface of the optical fiber at the distal end at a fix distance of 2-5 mm (see Figure2.4). The spectralon reflects the light uniformly over the probe surface generating the reflectance spectrum. This final signal corresponds to the system response and it is used to compensate for the spectral shape of the light emitted by the lamp, for the wavelength-dependent sensitivity of the detectors and for any wavelength-dependent sensitivity in the optics of the system[13]. Subsequently, a background measurement is carried out in order to minimize the impact of the ambient light, dark current and the electric offsets of the detectors.

As soon as the detector temperatures were stable, the calibration was performed before each set of measurements.

Once calibrated the system, each spectra was acquired averaging 15 DRS measurements each of them integrated in a time of 0.2 seconds for both the NIR and the VIS signals, to increase the signal-to-noise ratio. The spectrum of the tissue can be

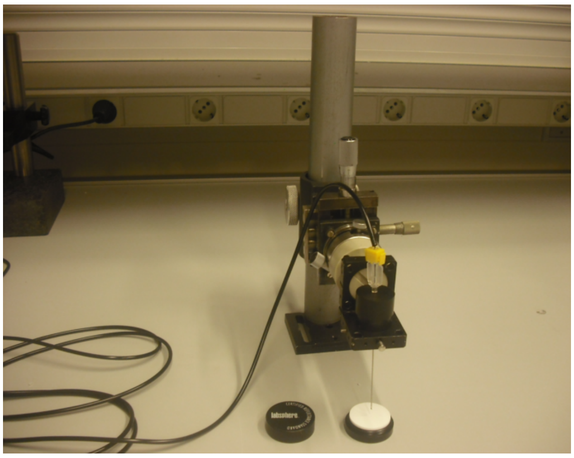

Figure 2.4: *Photonic Needle ready for the white reference calibration*

described as a function of wavelength with the following equation[13]:

$$C(\lambda_i) = \frac{T(\lambda_i) - T_{bg}(\lambda_i)}{C(\lambda_i) - C_{bg}(\lambda_i)} \tag{2.1}$$

where $S(\lambda_i)$, $T(\lambda_i)$, $C(\lambda_i)$ are the calibration spectrum, the effective measured tissue spectrum and the white reflectance standard measured spectrum, respectively, $T_{bg}(\lambda_i)$ corresponds to the background measurements acquired after each tissue spectra and $C_{bg}(\lambda_i)$ the one collected after each white reflectance standard spectrum.

2.2.3 Spectral measurements and Fit

Diffuse reflectance spectra were fitted over the wavelength range from 400 to 1600 nm. The parameters added in the model for the fitting of the results were collagen, beta-carotene and methemoglobin, together with the standard ones, described in paragraph 1.2.2. Figure2.5 shows an example of one spectra result. The blue signal represents the measured spectrum, while the red ones corresponds to the fitting result. Below the final result, the absorption coefficients of the single parameters are shown. Positive peaks in the single absorption coefficients correspond to the associated negative peak in the final spectrum. The main peaks are marked with arrows and the main parameters which influence the result are mentioned.

2.2.4 Statistical Analysis

The DRS-estimated quantification of each parameter in various tissue classes cannot in general be described by a parametric distribution such as a Gaussian distribution, so the measurement variables do not meet the normality assumption of an ANOVA. The statistical differences of each parameter in the defined tissue classes

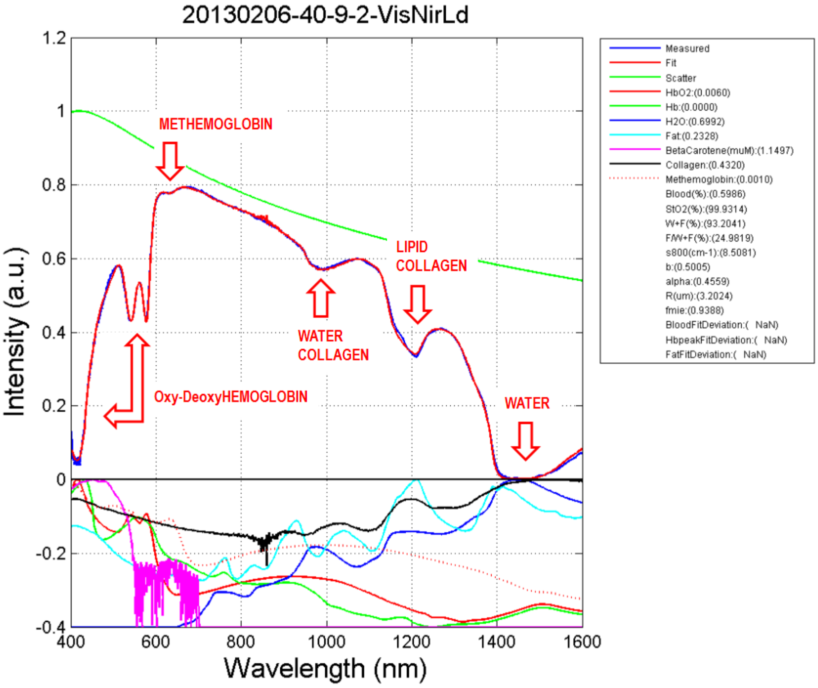

Figure 2.5: *Example of one fitted spectra*

were therefore determined using the non-parametric Kruskal-Wallis test[35], which does, however, assume that the observations in each group come from populations with the same shape of distribution. It is also used when the examined groups are of unequal size (different number of participants). Like the most non-parametric tests, it is performed on ranked data, so the measurement observations are converted to their ranks in the overall data set: the smallest value gets a rank of 1, the next smallest gets a rank of 2, and so on. Tied observations get average ranks; thus if there were four identical values occupying the fifth, sixth, seventh and eighth smallest places, all would get a rank of 6.5. The sum of the ranks is calculated for each group and then the test statistic, H, is calculated as follows:

$$H = (N-1)\frac{\sum_{i=1}^{g} n_i(\overline{r_i} - \overline{r})^2}{\sum_{i=1}^{g}\sum_{j=1}^{n_i}(r_{ij} - \overline{r})^2} \tag{2.2}$$

where

- n_i is the number of observations in group i
- r_{ij} is the rank (among all observations) of observation j from group i
- N is the total number of observations across all groups
- $\overline{r_i} = \frac{\sum_{j=1}^{n_i} r_{ij}}{n_i}$
- $\overline{r} = \frac{N+1}{2}$ is the average of all the r_{ij}.

H basically represents the variance of the ranks among groups, with an adjustment for the number of ties. The P value is the probability of getting a particular value of H by chance, if the null hypothesis is true.[35].

P-values smaller than 0.05 were considered statistically significant.

In the spectral data processing, different methods were used for the categorization of the tissues in different classes. A Classification And Regression Tree (CART) algorithm was used to automatically classify each collected tissue into one of the defined ones based on parameters derived from the measurements [5, 36]. With the CART algorithm, a decision tree is created based on the most significantly tissue chromophores and scattering parameters using a leave-one-out (LOO) cross validation scheme. The partition is developed by successive binary partitions based on the calculated thresholds on the different predictors in the decision tree. Each spectrum is separately classified and compared with the measurement knowledge in terms of sensitivity and specificity. Decision trees are very "natural" constructs, in particular when the explanatory variables are categorical. A variable is categorical if there are two or more categories and there is no intrinsic ordering to them. The main advantage of the CART method is that the results can be easily interpreted and correlated to clinical details, since the input parameters are the thresholds of the calculated values of the main tissue parameters. Moreover, this method is not sensitive to missing data [36].

Through CART methods results, sensitivity (Se) and specificity (Sp) will be given. They are calculated as

$$Se = \frac{TP}{TP + FN}, \tag{2.3}$$

$$Sp = \frac{TN}{TN + FP}. \tag{2.4}$$

in case two classes are involved. TP, FN, TN and FP correspond respectively to True Positive, False Negative, True Negative and False Positive values.

In case more than two classes are involved, sensitivity and specificity are calculated using formula (2.5) and (2.6), which elements are explained in Table2.1.

$$Se = \frac{TP}{TP + FN_1 + FN_2 + ... + FN_n}, \tag{2.5}$$

$$Sp = \frac{TN_{11} + TN_{22} + ... + TN_{nn}}{TN_{11} + TN_{22} + ... + TN_{nn} + FP_1 + FP_2 + ... + FP_n}. \tag{2.6}$$

$MeasuredTissue \mid DRS$	T	N_1	N_2	$\ldots$	N_n
T	TP	FN_1	FN_2	$FN_{\ldots}$	FN_n
N_1	FP_1	TN_{11}	TN_{12}	$TN_{1\ldots}$	FN_{1n}
N_2	FP_2	TN_{21}	TN_{22}	$TN_{2\ldots}$	TN_{2n}
$N_{\ldots}$	$FP_{\ldots}$	$TN_{\ldots1}$	$TN_{\ldots2}$	$TN_{\ldots}$	$TN_{\ldots n}$
N_n	FP_n	TN_{n1}	TN_{n2}	$TN_{n\ldots}$	TN_{nn}

Table 2.1: *Definition of True Positive, False Negative, True Negative and False Positive values in presence of more than two classes.*

2.2.5 Tissue Samples

The spectra were acquired ex vivo from three different animal species, in particular, from the upper part of the hind limb of two rabbits, one rat and two piglets. The rat and the rabbit tissues were collected from Life Science Facility at Philips Research, while swine's samples were provided by HemoLab, a company owned by the TU/e Holding BV, which is dedicated to research and development (R&D) services in the field of biomedical technology, in particular cardiovascular engineering.

All the samples were excised and measured within 12 hours after sacrificing the animal under standard procedures. There was no local or systemic illness of the animals to cause any pathological tissue alterations prior to sample extraction.

Five different tissue types were measured, in particular muscle, subcutaneous fat, sciatic nerve, cartilage and ligament. Cartilage and ligament samples were extracted only from one rabbit and one piglet respectively. An expert in animal anatomy from Life Science Facility helped recognizing the different tissue types during the dissection of the different limbs.

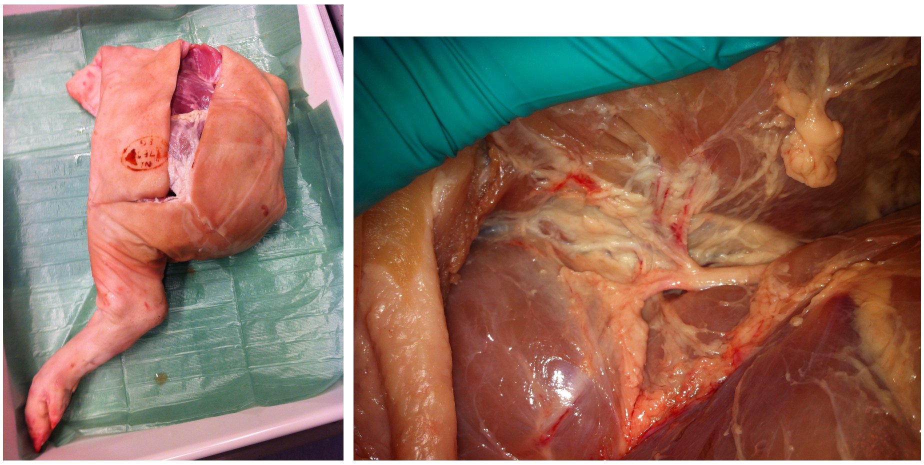

Figure 2.6: *Example of a measured swine hind limb with a particular of the measured sciatic nerve*

2.2.6 Spectra Acquisition

The first experiments were implemented on two rabbit limbs, from which 25 spectra per four locations in each tissue type were collected. The same day rat tissues were investigated, following the same protocol used for the rabbit ones, but it was not possible to take spectra from cartilage because of the small dimensions of the sample. Besides those, samples from muscle, subcutaneous fat and sciatic nerve from two swine hind limbs were measured, collecting 10 spectra from different locations per each tissue type. From one of the two samples it was also possible to acquire spectra from different locations on a ligament.

2.3 Results

2.3.1 Spectral Measurements and Fitting Results

In this section the measurements results and the corresponding fitting for the various tissues will be discussed. Only one spectra for each tissue type will be presented. In appendix A, more examples are shown

Muscle Tissue

Figure2.3.1 shows one result given by a measurement collected from rabbit muscle tissue.

Three main peaks are visible. As seen in paragraph 1.1.1, all of these peaks can be related to important chromophores, according to literature.

The first peak, between 400 and 600 nm, is due to the relevant presence of blood in muscles. In particular, the shape of the peak between 400 and 500 nm is related to the presence of oxyhemoglobin and deoxyhemoglobin, while mathemoglobin absorbs at higher wavelengths, around 630 nm. As all the experiments were conducted ex vivo, it is possible that hemoglobin already converted in methemoglobin[2]. Collagen is another important chromophore in muscle tissues and its presence is shown in the result displayed. Its typical absorption peaks are visible at around 1000 nm and between 1100 and 1300 nm. As said, all cells are surrounded by a membrane made of lipids, which have their main absorption peak at 1210 nm. Even if they are not main components of muscle tissue, lipids influence the shape of the peak between 1100 and 1300 nm. The presence of water is evident from the main visible peak in the infrared region, between 1300 and 1500 nm 1.1.1.

The fits of the measured spectra are in general good.

Subcutaneous Fat Tissues

In Figure2.8 an example of one spectra collected from swine subcutaneous fat is presented.

Lipids are the main components of fat tissue and, as concluded in previous studies,

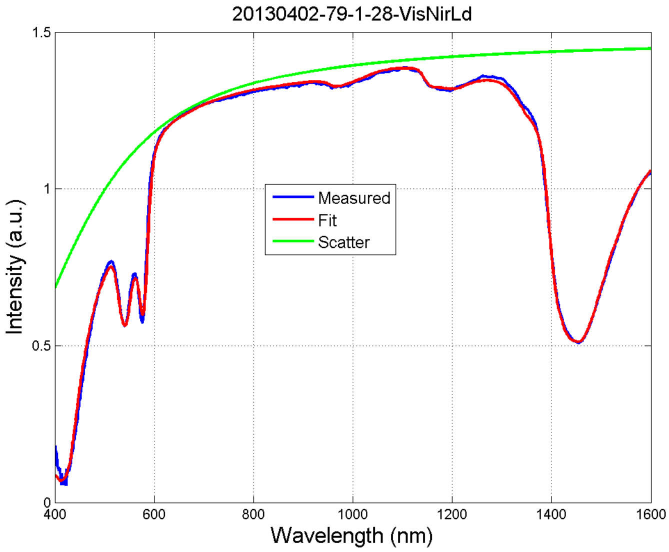

Figure 2.7: *Examples of spectra collected from muscle tissues in rabbit*

they are responsible for the absorption peak at 1210 nm[13]. In the shown result, the lipids main peak is visible and it is clear how their concentration is more preponderant with respect to the muscle samples which spectra is shown in Figure2.3.1. This peak is the typical feature which characterizes fat tissue spectra and enables their classification. In Figure2.8 is shown that subcutaneous fat spectra are influenced by blood, water and collagen in their absorption wavelegth ranges, which have been mentioned previously (see 1.1.1).

As noticed for muscle results, the fits of the measured spectra are in general good.

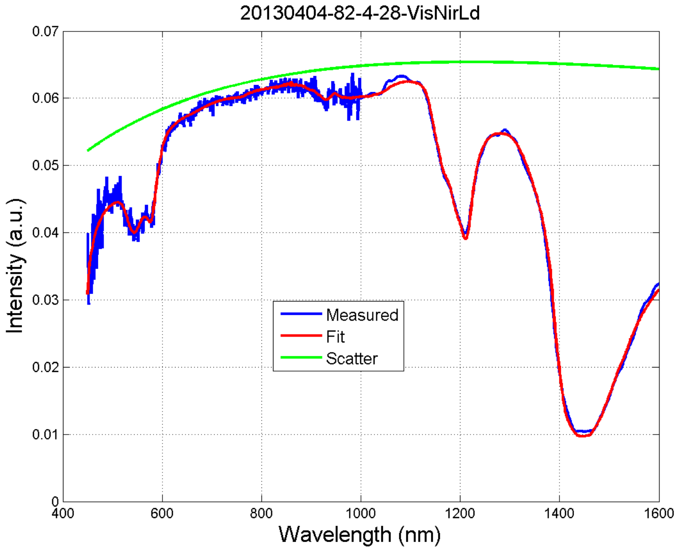

Figure 2.8: *Example of spectra collected from subcutaneous fat tissues in swine*

Nerve Tissue

In Figure2.9 a spectra from swine nerve tissues is shown.

Like in the previous results presented (Figure2.3.12.8), the influence of water is evident from the main visible peak in the infrared region, between 1300 and 1500 nm and the peak at 600 nm, which is supposedly due to the presence of methemoglobin, is still present. Similarly to the results showed for muscle spectra, the oxy-deoxyhemoglobin peak is present in the wavelength range between 400 and 600 nm. Blood supply is in fact crucial in nerves more than in fatty tissue, which consists of more capacious energy storage cells with a relatively low metabolic rate[34]. The peak at around 1210 nm, related to the presence of lipid, is less preponderant with respect to the fat tissue analyzed previously, but it is sharper than the one in the muscle spectra. This is in agreement with the anatomy of nerves, from which it is known that they are surrounded by a myelin sheath that contains 75% of lipids [34].

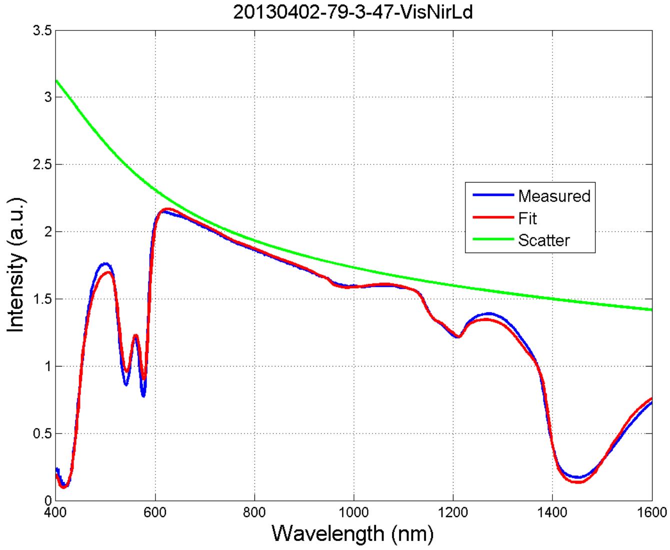

Figure 2.9: *Examples of spectra collected from nerve tissues in animals (a, b, c, d and e)*

As seen for muscle tissue (Figure2.3.1), the presence of collagen causes the small peak at 1000 nm and influences the shape of the lipid peak, between 1100 and 1300 nm.

Besides those, another particular feature noticed in nerve spectra is the sharp shape of the slop between 600 and 800 nm, which appears more leaning for nerve spectra than for muscle or fat ones.

The measured spectra show fitting results which are in general good (see appendix A).

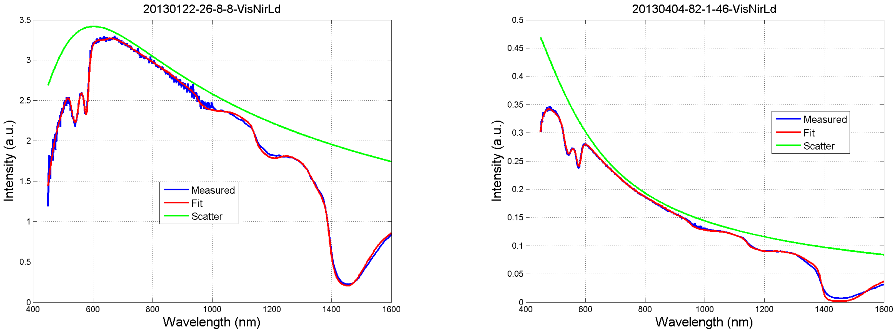

(a) Spectra from Rabbit Cartilage (b) Spectra from Piglet Ligament

Figure 2.10: *Examples of spectra collected from cartilage and ligament tissues in animals (a and b)*

Cartilage and Ligament Tissues

In Figure2.10 results if measurements on rabbit cartilage and swine ligament are shown.

As seen in the previous results, water and lipids peaks are visible. Beside those, hemoglobin and methemoglobin influence the shape of the spectra.

Both lipid and hemoglobin contents are not as important as seen for fat and muscle tissue respectively, but their contribution is still visible from the shape of the spectra.

The influence of collagen is visible at 1000 nm and, as explained in paragraph 1.1.1, it may contribute to the peak between 1100 and 1300 nm, even if the lipid's component is preponderant.

As in the results previously showed, also for ligament and cartilage spectra the fits of the results are in general good.

2.3.2 Collective Analysis

Diffuse reflectance spectral data were analyzed by fitting procedures which were further quantified with mean and standard deviations values for each tissue parameter. The results were shown using boxplots, which are useful to easily compare the amounts of the different parameters in two or more different types of tissues.

Due to the higher amount of data acquired from different animals, fat, muscle and nerve tissues will be evaluated in this analysis.

Figure2.11 shows the results of this comparisons for the main chromophores, which were considered statistically significant to differentiate different tissue types.

From these boxplots it is possible to observe that fat tissues can be well discriminated on the basis of the fat ration, which is defined as $\frac{fat}{(water+fat)}\%$, as said in paragraph 1.1.1. Muscle tissues have in most cases a higher level of total hemoglobin with respect of other tissues, while lipid cells are general the one with the less quantity of their slow metabolism and this is also shown from the results. Besides, the level of collagen is shown to be higher in muscles than in nerves, while it is almost absent in subcutaneous fat tissues, which is in agreement with histology. Another statistically significant parameter is the scattering coefficient value at 800 nm, which is higher for subcutaneous fat than for muscles and nerves.

In conclusion, the main parameters chosen for fitting DRS spectra show a clear distinction between the different types of tissue considered.

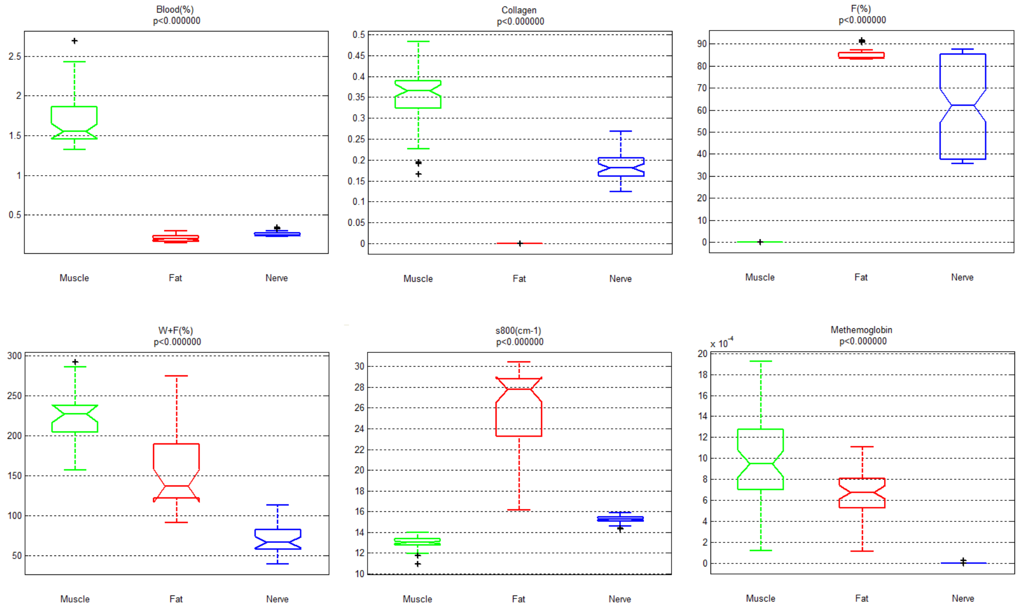

Figure 2.11: *BoxPlots of the relevant parameters values in different tissue types*

2.3.3 Tissue classification analysis

As explained in paragraph 2.2.4, a Classification And Regression Tree (CART) algorithm was used to automatically classify each collected tissue into one of the defined tissue types based on the parameters derived from the measurements[36]. With CART algorithm, the decision tree shown in Figure2.12 is created based on the six most significantly different tissue cromophores and scattering parameters, which are blood percentage, amount of collagen, fat percentage, water plus fat percentage and scattering coefficient value at 800 nm. Leave-One-Out cross validation scheme was used[36].

Table2.2 displays the classification accuracy of the decision tree in Figure2.12 for all optical DRS measurements considered in the study when compared with the experimental knowledge. As shown, a total of 375 spectra out of 402 for fat, 430 out

$MeasuredTissue/DRS$	F	M	N
$F(402)$	375	0	27
$M(508)$	0	430	78
$N(820)$	181	4	635

Table 2.2: *Confusion Matrix associated to the classification*

of 508 for muscle and 635 out of 842 for nerve were correctly classified, which gives the following sensitivity and specificity values:

$Se_{fat} = 93\%$, $Sp_{fat} = 85\%$,

$Se_{muscle} = 85\%$, $Sp_{muscle} = 99\%$,

$Se_{nerve} = 77\%$, $Sp_{nerve} = 88\%$.

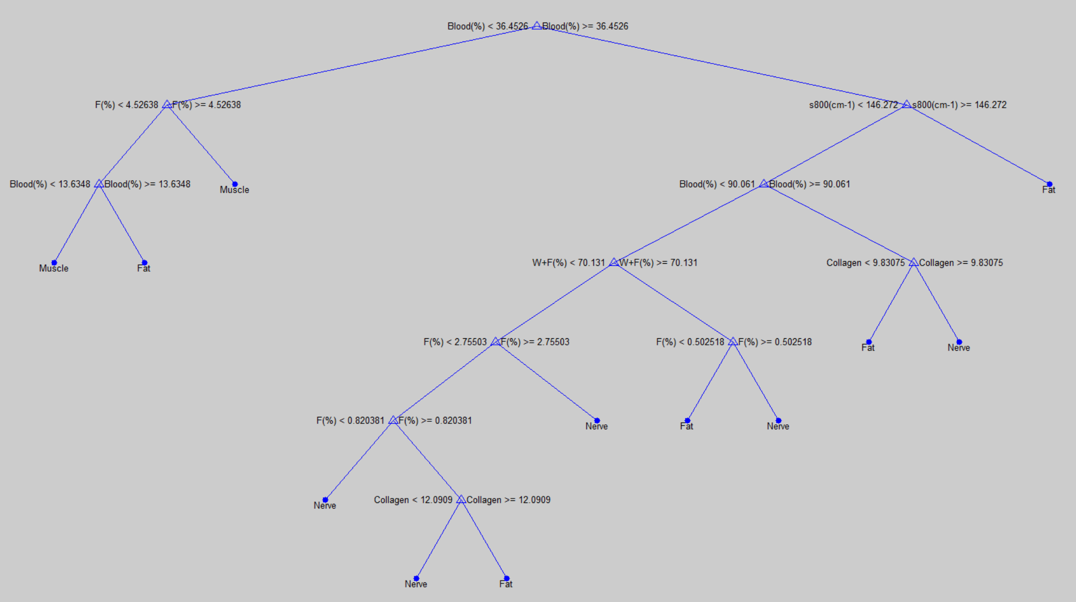

Figure 2.12: *Decision tree for the LOO method for muscle, fat and nerve tissues*

2.3.4 Per Animal Analysis

The same parameters used for the CART analysis were used to evaluate the classification results per each animal experiment. The evaluation was implemented comparing two tissues each time and calculating the percentage of successful classifications in each session of measurements. Figure2.13 shows the average values of the percentages per each comparison between tissue types. As shown, the more successful and repeatable results were obtained comparing fat and muscle tissues, considering the fat percentage as parameter for the classification. Comparing these two tissues, also the total hemoglobin amount (blood(%)) and the water plus fat percentage resulted to be good classifiers. Fat percentage resulted to be the best classifier comparing fat and nerve tissues, followed by the water fraction, the scattering coefficient value at 800 nm and collagen content. Those parameters are also responsible for Muscle/Nerve classification.

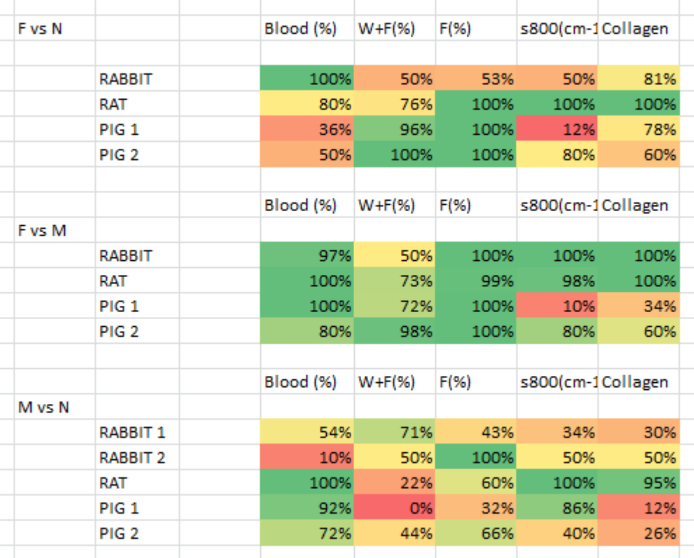

F vs N			Blood (%)	W+F(%)	F(%)	s800(cm-1	Collagen
	RABBIT		100%	50%	53%	50%	81%
	RAT		80%	76%	100%	100%	100%
	PIG 1		36%	96%	100%	12%	78%
	PIG 2		50%	100%	100%	80%	60%
			Blood (%)	W+F(%)	F(%)	s800(cm-1	Collagen
F vs M							
	RABBIT		97%	50%	100%	100%	100%
	RAT		100%	73%	99%	98%	100%
	PIG 1		100%	72%	100%	10%	34%
	PIG 2		80%	98%	100%	80%	60%
			Blood (%)	W+F(%)	F(%)	s800(cm-1	Collagen
M vs N							
	RABBIT 1		54%	71%	43%	34%	30%
	RABBIT 2		10%	50%	100%	50%	50%
	RAT		100%	22%	60%	100%	95%
	PIG 1		92%	0%	32%	86%	12%
	PIG 2		72%	44%	66%	40%	26%

Figure 2.13: *Per animal classification*

2.4 Conclusions

In this section, the feasibility of tissue types classification with diffuse reflectance spectroscopy has been investigated.

From this study DRS resulted to be a good technique for classification of fat, muscle and nerve tissue. The spectra acquired showed characteristics which are known from literature to be associated to particular chromophores in each tissue type. It was possible to visibly recognize spectra from muscle, fat and nerve tissue from the relevant peaks shown. After a statistical analysis based on CART algorithm, sensitivity values between 77% and 93% and sensibility value between 85% and 99% have been calculated. The parameters which resulted to be the most important for classification are the fat percentage, the total blood content and the water fraction, followed by the scattering coefficient at 800 nm and the collagen content.

Chapter 3

Parameters Variability

In this chapter variations of the parameters used for the fitting of the resulted spectra will be discussed. In particular, changes in the main parameters with time and temperature will be evaluated.

Beside it, eventual interspecies differences will be discussed, comparing results that were collected from different animals under the same conditions. Data from human cadavers will also be compared to assess if there are some important changes in the main chromophores concentrations which could eventually influence the possibility of using DRS for clinical applications.

3.1 Parameters Variability after cold storage

In this section changes in the main chromophores and scattering properties in tissues after cold storage will be discussed. Samples were frozen, defrosted and remeasured as soon as possible, when they reached again the room temperature. The results were compared with the ones collected from fresh tissue samples.

3.1.1 Tissue Samples

One of the two piglet hind limbs and one of the two rabbit thighs were involved in this study.

For the rabbit study, contacts with the Science Facility of Philips were taken and, as soon as one rabbit was ready to be euthanized for other purposes, the set up was shifted in one of the laboratories of the facility. The animal was euthanized, a small cut was performed on the skin of the thigh and DRS measurements were taken from the muscle and the sciatic nerve within one hour after death. Afterwards, the involved part was extracted from the animal and shifted to the Photonic Tool Lab, where previous DRS measurements were conducted, and remeasured around 5 hours after euthanasia.

The pig fresh samples were measured within 12 hours after death.

As soon as the measurements of the fresh tissues were over, both samples from rabbit and pig were put in a freezer at -8°C and left over night. The day after they were taken out of the freezer and put in a 4°C fridge till they were completely defrosted. The swine limb took three days to be completely unfrozen, while for the rabbit thigh the defrosting procedure was faster and it took only one night (12 hours). After that the tissues were left outside the fridge, in the laboratory, to be measured at room temperature afterward. The pig leg was measured after one night, while the rabbit thigh was ready after five hours.

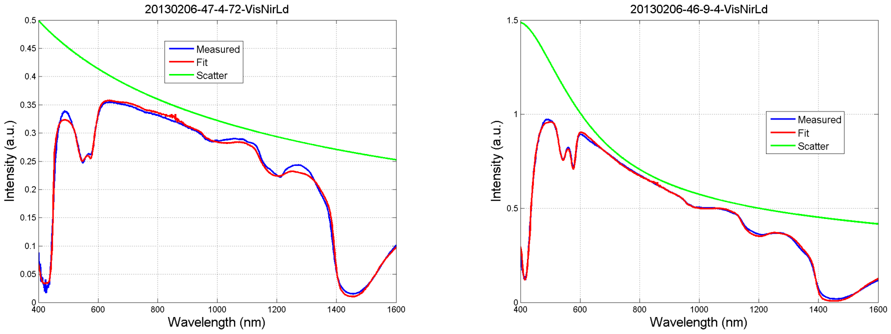

(a) Muscle

(b) Nerve

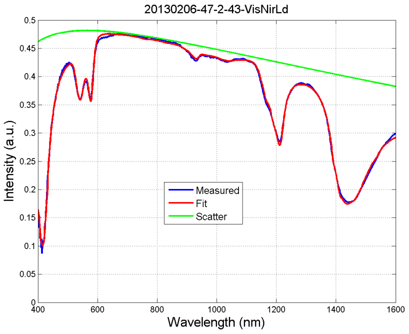

(c) Subcutaneous Fat

Figure 3.1: *Examples of spectra collected from defrosted Muscle (a), Nerve (b) and Fat (c) tissues*

3.1.2 Spectral Measurements and Fitting Results

Figure3.1 shows examples for the spectra collected from the different defrosted tissue, one from muscle tissue, one for nerve and a third one for subcutaneous fat. In all of them, the typical peaks and shapes explained in chapter2 are present. In particular, the water peak between 1300 and 1600 nm, the collagen peak at 1000 nm, the blood influence between 400 and 600 nm and the fat/collagen ones at around 1200 nm are visibly recognizable.

The fitting of the measured spectra resulted to be good inserting all the same parameters used in previous analysis (see paragraph 2.2.2).

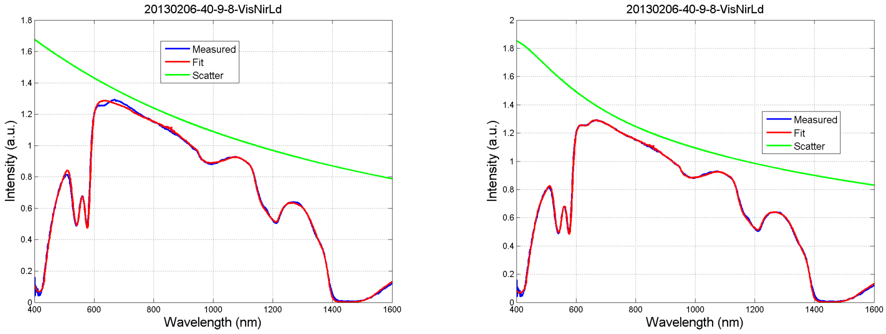

(a) fitting without methemoglobin (b) fitting with methemoglobin

Figure 3.2: *Example of fit results without (a) and with (b) methemoglobin as input parameter of the model*

As said, during tissue preservation, part of the oxy-hemoglobin is expected to transfer to methemoglobin[37]. Figure3.2 shows the spectra from 400 to 1600 nm measured from defrosted muscle tissue of the pig, fitted without and with methemoglobin as a parameter in the model. In the first one (Figure3.2(b)) there is a clear residual between the measurement and the fit curve observed at around 630 nm, where one of the absorption peaks of methemoglobin is. The result improves by including methemoglobin in the model (Figure3.2(a)).

3.1.3 Comparison between fresh and defrosted tissue

As done in previously, box plots were used to evaluate the behavior of the main chromophores and scattering elements used for fitting the collected spectra. The aim of the study was to investigate the eventual presence of particular changes among fresh and defrosted tissue. Different types of tissue were studied separately, in order to preserve the known trends for all the parameters considered.

In Figure3.3, the results from the comparison between measurements taken from fresh subcutaneous fat and defrosted one are displayed. As said, fat measurements

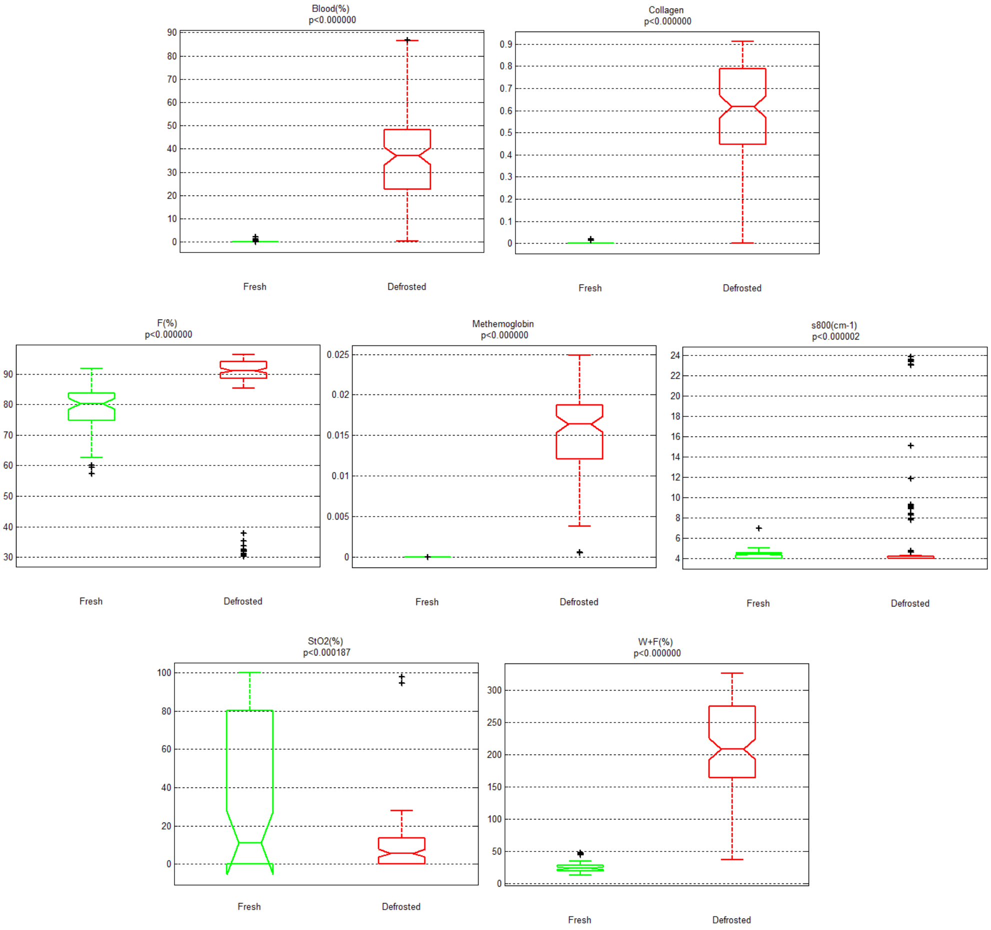

Figure 3.3: *Time-Temperature variability of chromophores concentrations in Pig Fat tissue*

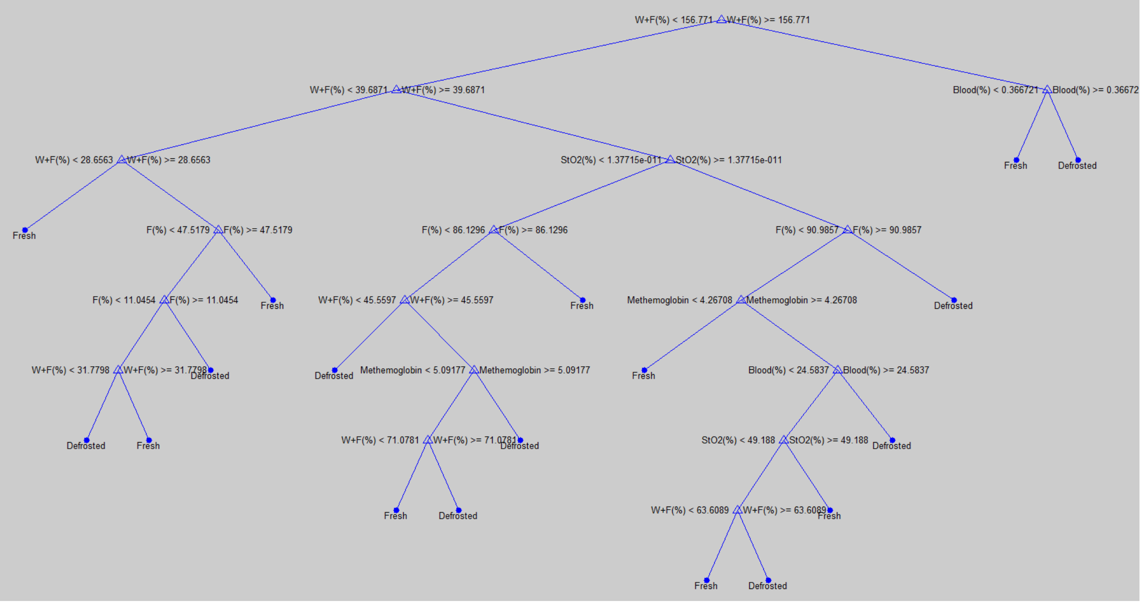

Figure 3.4: *Decision tree for fresh/defrosted tissue classification*

were performed only during the pig experiment. As shown, results for defrosted tissue are higher for blood content (%), fat (%), water plus fat (%), collagen and methemoglobin if compared with the ones for fresh samples. Dead tissues which are stored in cold temperatures have a slow metabolism, which implies a less oxygen request from cells and accordingly, less blood consumption[37]. Besides, time causes fibrosis of tissue, which is responsible for the presence of higher concentrations of collagen. Furthermore, as discussed previously, it is known from literature than the older the dead tissue, the higher the level of methemoglobin[37].

The results of the comparison for muscle and nerve tissues, for both pig and rabbit experiments are presented in appendix B. For both tissue types, the same trends noticed for fat tissue can be observed and the same considerations can be made. Results show that blood content (%), water plus fat (%), collagen and methemoglobin increase after cold storage.

$MeasuredTissue/DRS$	F	D
$F(710)$	689	30
$D(410)$	43	367

Table 3.1: *Confusion Matrix associated to the classification*

As done in paragraph 2.3.3, a Classification And Regression Tree (CART) algorithm was used to automatically classify each collected spectra as one from a fresh or defrosted tissue[36]. With CART algorithm, the decision tree shown in Figure3.4 is created based on the five most significantly different tissue cromophores and scattering parameters, which are blood percentage, fat percentage, water fraction, oxygen saturation percentage and methemoglobin. Leave-One-Out cross validation scheme was used[36].

Table3.1 displays the classification accuracy of the decision tree in Figure3.4 for all optical DRS measurements considered in the study when compared with the experimental knowledge. As shown, a total of 689 spectra out of 710 for fresh tissue and 410 out of 367 for defrosted tissue were correctly classified, which gives the following sensitivity and specificity values:

$Se_{fresh} = 96\%$, $Sp_{fresh} = 90\%$,

$Se_{defrosted} = 90\%$, $Sp_{defrosted} = 96\%$.

3.2 Interspecies differences

In Chapter2, samples from different animals have been analyzed. However, there could be some interspecies differences of the optical tissue properties which may significantly influence the final spectra.

In this section, differences in the chromophore's concentrations in each tissue type for each different animal will be investigated and compared. Data collected from two human cadavers will be added to this comparison.

3.2.1 Data Collection

For this studies, the same data used in the previous analysis were used (see paragraph 3.1.1). In particular, data acquired from defrosted tissues were considered. The only types of tissue that were collected from all the different species were subcutaneous fat, muscle and nerve, which were involved in this study. Data from ligament and cartilage were considered not enough and excluded.
Data from human cadavers were also available for this study. These data were previously acquired for other purposes following the standard ethically correct procedures. The human cadaver tissues were measured at room temperature when defrosted.

3.2.2 Collective analysis

As done in Chapter2, boxplots were used to evaluate the behavior of the main chromophores and scattering elements used for fitting the spectra in three different animals and in human cadavers. The aim of the study was to investigate the eventual presence of particular changes among the species. Similarly to what was done in paragraph3.1.3, different types of tissue were studied separately, in order to preserve the known trends for all the parameters considered.

In Figure3.5, the results of this comparison for subcutaneous fat tissue are displayed. These show higher values of blood content (%), water plus fat (%) and methemoglobin for humans than for animals. It has to be considered that the hu-

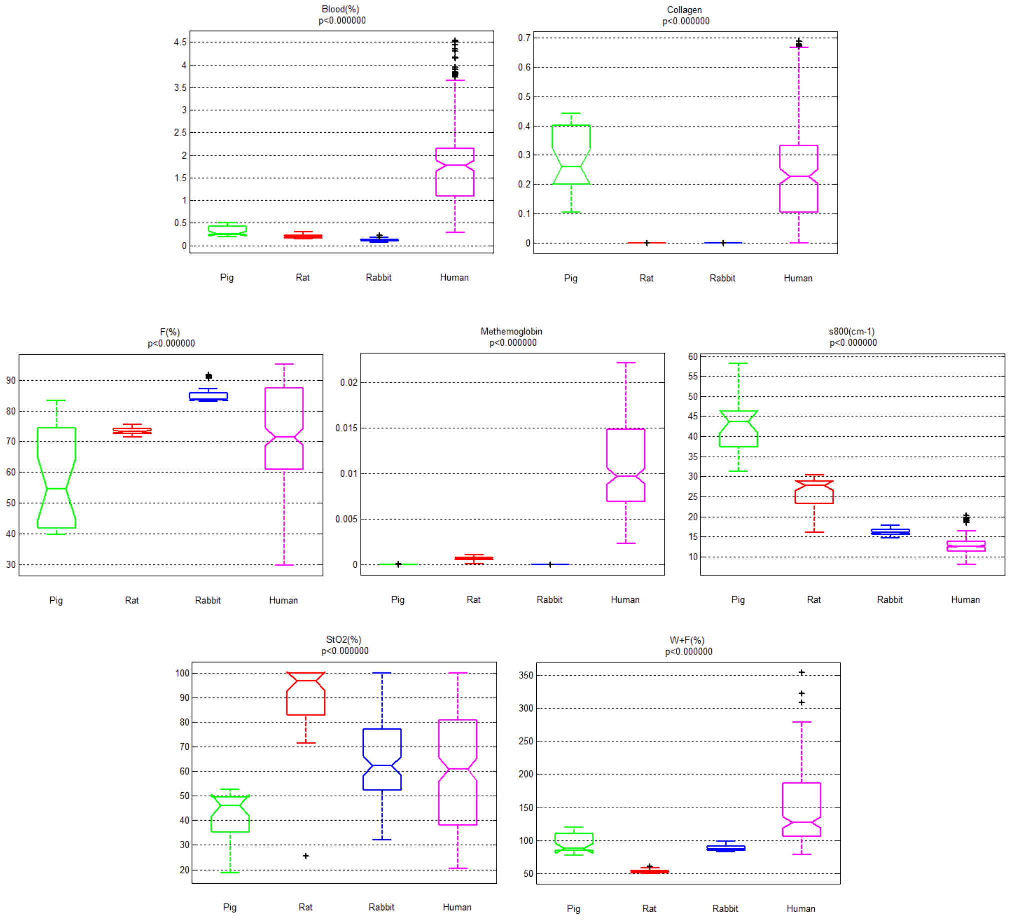

Figure 3.5: *Comparison between chromophores concentrations in different Animals and Human's Fat tissues*

mans data were collected from cadavers more than one day after death and this could explain either the blood percentage and the methemoglobin increases. As said in paragraph3.1.3, dead tissues which are stored in cold temperatures have a slower metabolism than live tissues, which implies a less oxygen request from cells, and accordingly, less blood consumption[37]. Furthermore, after death, part of the hemoglobin in the tissues is expected to convert in methemoglobin with passing of time[38].

Collagen has shown to be higher for human cadavers and pig fat than for rabbit and rat ones, while pig fat tissues resulted to have a higher scattering coefficient value at 800 nm in respect of other species.

No particular trends are shown for fat percentage and oxygen saturation.

Figure3.6 displays box plots comparing various parameters for muscle tissue measured from animal and human cadavers. As observed for subcutaneous fat data, blood percentage, water fraction and methemoglobin content are higher in human cadaver samples than animal samples. In this case, also the fat percentage in humans has been found to be higher than in animals. Collagen, Scattering coefficient value at 800 nm and oxygen saturation percentage show a comparable results for all the species.

Figure3.7 box plots comparing various parameters for muscle tissue measured from animal and human cadavers. A recurrent pattern is visible for methemoglobin and water plus fat percentage, which are in all cases higher for human samples than for animals. As seen in case of muscle samples, also for nerve tissue the fat percentage resulted higher in human than in animals. Total hemoglobin content (blood(%)) and the value of the scattering coefficient at 800 nm resulted to be comparable in all the species. No particular trend has been noticed for collagen content.

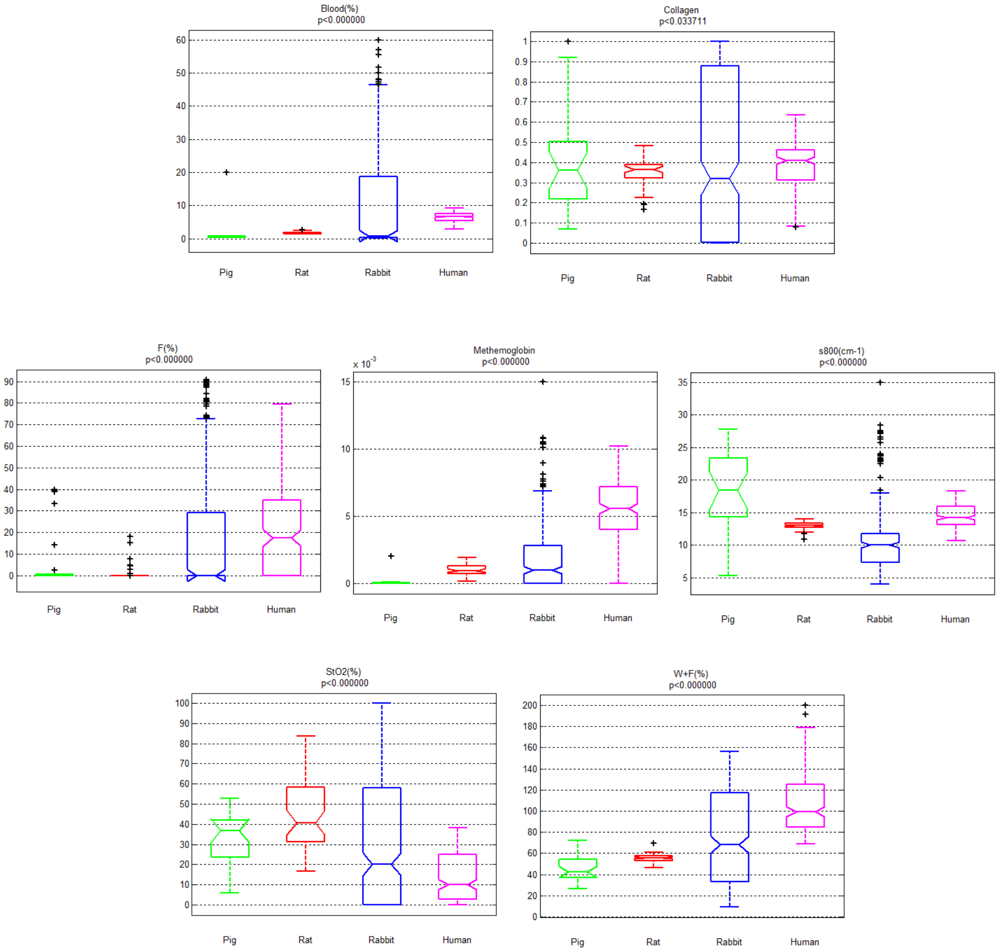

Figure 3.6: *Comparison between chromophores concentrations in different Animals and Human's Muscle tissues*

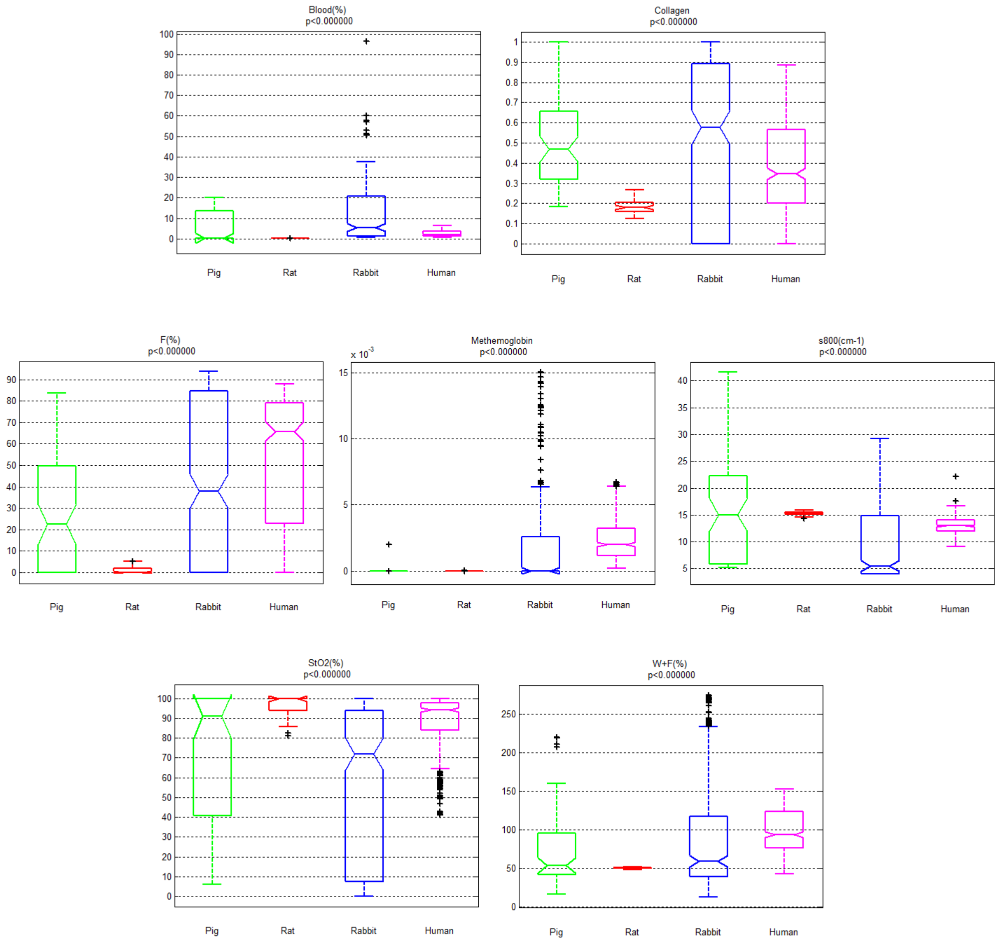

Figure 3.7: *Comparison between chromophores concentrations in different Animals and Human's Nerve tissues*

3.3 Conclusions

In this chapter, variability in chromophores concentrations and scattering properties of tissues were investigated. Two different studies have been made, a comparison between tissue before and after cold storage and a comparison between different animal species and human cadavers.

The first comparison, between tissue before and after cold storage, confirmed that methemoglobin, collagen and water fraction increase after cold storage, as confirmed by literature, while the blood content was found to be higher after cold storage, in disagreement with results from previous studies.

From the second comparison, methemoglobin resulted to be higher in humans than in all animals for all tissue types. This cannot be considered as an intrinsic feature of humans compared to animals, but it is probably due to the longer period of time after death before the measurements. The same conclusion can be made for the water fraction concentration, while fat percentage was found to be constantly higher in human cadavers than in animals, but no literature has been found which can confirm this result.

Chapter 4

Liver studies

4.1 Introduction

In the last decade, optical sensing by means of diffuse reflectance spectroscopy (DRS) has developed into a promising technique that could significantly contribute to clinical improvements. By allowing specific differentiation between tissues, DRS has the potential to be incorporated into optical tools for diagnosis and therapy of diseases like, for example, cancers[].

Studies on the use of diffuse reflectance spectroscopy on liver tissue are scarce[]. Recently it has been demonstrated that bile is an important chromophore for hepatic tissues, enabling DRS analysis to overall discrimination of normal from metastatic tissues[3]. To proceed with further clinical implementation, latest studies investigated the possibility to assess the presence of hepatic steatosis, a limiting factor for extensive liver resections after prolonged chemotherapy[39]. Steatosis is a medical condition where there is an abnormal retention of lipids by the liver cells. This is a reversible condition which is usually due to excessive consumption of alcohol and it is relevant when major liver surgery is considered. Hepatic steatosis in deceased-donor livers is considered to be the main risk factor for poor or non-function of the transplanted organ and it has also been associated with increased morbidity and mortality after resection[40]. Among living liver donors, the residual liver with a fat content of less than 5% shows better regeneration than the one with a fat content of 5-30%. In addition, the possibility of hepatic dysfunctions and renal failures in the recipient escalates if the amount of donor hepatic steatosis increases from mild to moderate (30%) to severe (60%)[40]. Severe steatosis is also considered responsible for early mortality and ischemia-reperfusion injuries in recipients of liver transplants^{citefattyliver}.

Histopatology analysis is the reference standard to detect and quantify fat in liver tissues, but the results are vulnerable to sampling errors and it can cause complications. For these reasons it cannot be repeated often enough to monitor treatment responses. Moreover, its results need time to be available and a liver cannot stay outside the body for more then 18 hours. Medical images are considered much less invasive, but each method comes with some disadvantages or limitations. Ultrasonography, for instance, is effective for detecting moderate or severe fatty infiltration but is limited by lack of inter-observer reliability and intra-observer reproducibility. Computed tomography (CT) allows quantitative and qualitative evaluation and it is in general accurate and reliable, but the results may be confounded by changes due to other hepatic diseases like cirrhosis. Magnetic resonance (MR) imaging, with appropriate sequence, and MR spectroscopy provide unique advantages but they are both too expensive and complex to be used to monitor steatosis[40]. Due to those problems more research groups are nowadays trying to characterize liver tissues with DRS, evaluating its potential as a cheap, efficient and minimally invasive diagnostic tool.

In this study, different healthy animal livers will be analyzed with diffuse reflectance spectroscopy in order to validate its capability of discriminate different types of tissues in livers.

4.2 Materials and Methods

The spectra were collected from different samples with the same set up used for the previous analysis, which has been explained at paragraph 2.2. Also the calibration was performed in the same way as in the previous study, while, for the fitting of the acquired spectra, bile, bilirubin and lycopene had been added to the model as parameters of choice, together with collagen, beta-carotene, methemoglobin and the standard ones seen in theory (see paragraph 2.2.2).

4.3 Tissue classification

Different types of tissue in livers were investigated. In this section, optical features of them will be discussed, based on the results of DRS measurements.

4.3.1 Tissue Samples

The spectra were taken ex vivo from different animals, in particular livers from two rats, one rabbit and two pigs were measured. In Figure4.1 a picture of one liver from swine and one from rabbit are shown.
As done for the hind limb tissues, the rat livers and the rabbit livers were collected from Life Science Facility of Philips, while HemoLab provided the organs from the

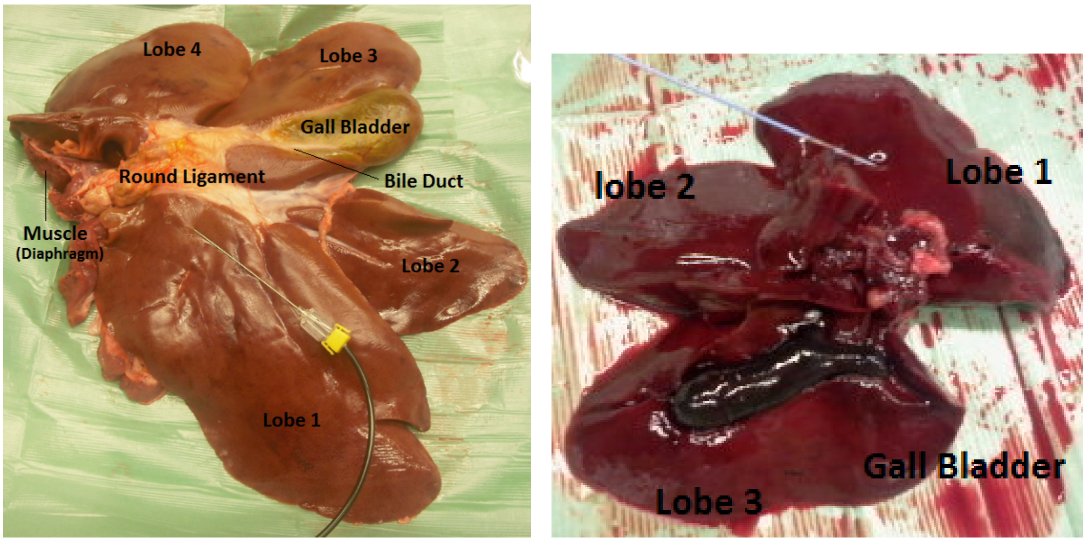

(a) Pig Liver (b) Rabbit Liver

Figure 4.1: *Measured Pig Liver (a) and Rabbit Liver (b)*

swines. All the samples were excised and measured within 12 hours after the animal's death. There was no local or systemic illness of the animals to cause any pathological tissue alterations prior to sample extraction.

From the pigs' livers, lobe, gall bladder, bile duct, round ligament and muscle samples (probably the diaphragm) were measured, collecting 5 spectra per 10 location in each different tissue type (see Figure4.1). Spectra from the lobes, the gall bladder and the round ligament were acquired from the rabbit liver, but no bile ducts were clearly distinguished and no muscle samples were present. Due to the small sizes of the rat livers, it was not possible to identify the gall bladder, but data from the lobes, blood vessel and the ligament were collected.

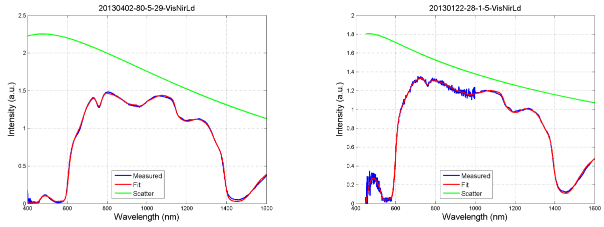

(a) Rabbit Liver lobe (b) Rat Liver lobe

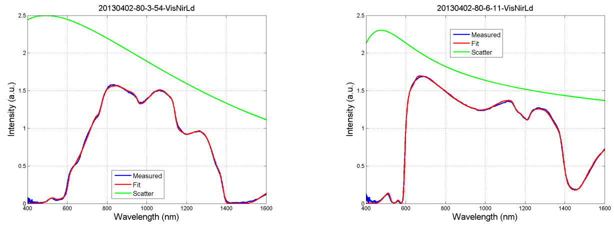

(c) Rabbit Gall Bladder (d) Pig Round Ligament

Figure 4.2: *Examples of spectra collected from different tissues in different livers*

4.3.2 Spectral Measurements and Fitting Results

In this section the measurements results and the corresponding fitting for the various tissues will be discussed.

In Figure4.2 a few examples of measurements on different types of liver tissue are shown.

In general a good fit for the DRS data can be observed.

In the wavelength range between 400 and 600 nm it is possible to notice the constant presence of a flat spectra area. This is due to the prominent presence of blood which shows absorption in this region. This is supported by the fact that liver is a homogeneous organ, which is well perfused with blood. As seen in paragraph 1.1.1, the presence of bile and beta-carotene strongly influences the wavelength range between 500 and 900 nm, while, in the range between 900 and 1600 nm, the main chromophores are fat, collagen and water.

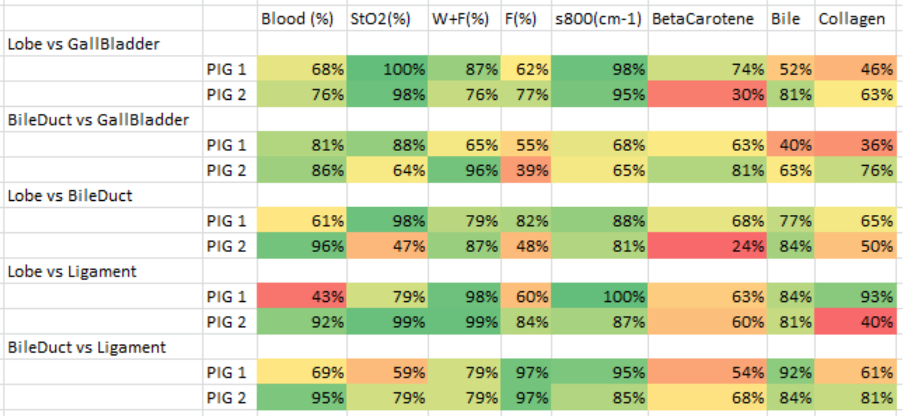

		Blood (%)	StO2(%)	W+F(%)	F(%)	s800(cm-1)	BetaCarotene	Bile	Collagen
Lobe vs GallBladder									
	PIG 1	68%	100%	87%	62%	98%	74%	52%	46%
	PIG 2	76%	98%	76%	77%	95%	30%	81%	63%
BileDuct vs GallBladder									
	PIG 1	81%	88%	65%	55%	68%	63%	40%	36%
	PIG 2	86%	64%	96%	39%	65%	81%	63%	76%
Lobe vs BileDuct									
	PIG 1	61%	98%	79%	82%	88%	68%	77%	65%
	PIG 2	96%	47%	87%	48%	81%	24%	84%	50%
Lobe vs Ligament									
	PIG 1	43%	79%	98%	60%	100%	63%	84%	93%
	PIG 2	92%	99%	99%	84%	87%	60%	81%	40%
BileDuct vs Ligament									
	PIG 1	69%	59%	79%	97%	95%	54%	92%	61%
	PIG 2	95%	79%	79%	97%	85%	68%	84%	81%

Figure 4.3: *trend analysis*

4.3.3 Statistical Analysis

Trend Analysis

During a first step the data from each single animal were compared with the data from the other animal of the same specie, in order to avoid interspecies variability. In figure the percentages of successful classifications in pigs' livers are shown. The evaluation was implemented comparing two tissues each time and calculating the percentage of successful classifications in each session of measurement, which corresponds to one measured location. The average values for all positions are displayed per each parameter which resulted to be more significant in this study. As shown, the best parameters for classification resulted to be the oxygen saturation percentage, the scattering coefficient value at 800 nm and the water fraction, but also blood (%), fat (%), beta-carotene, bile and collagen resulted to be good classifiers in more than 50(%) of cases.

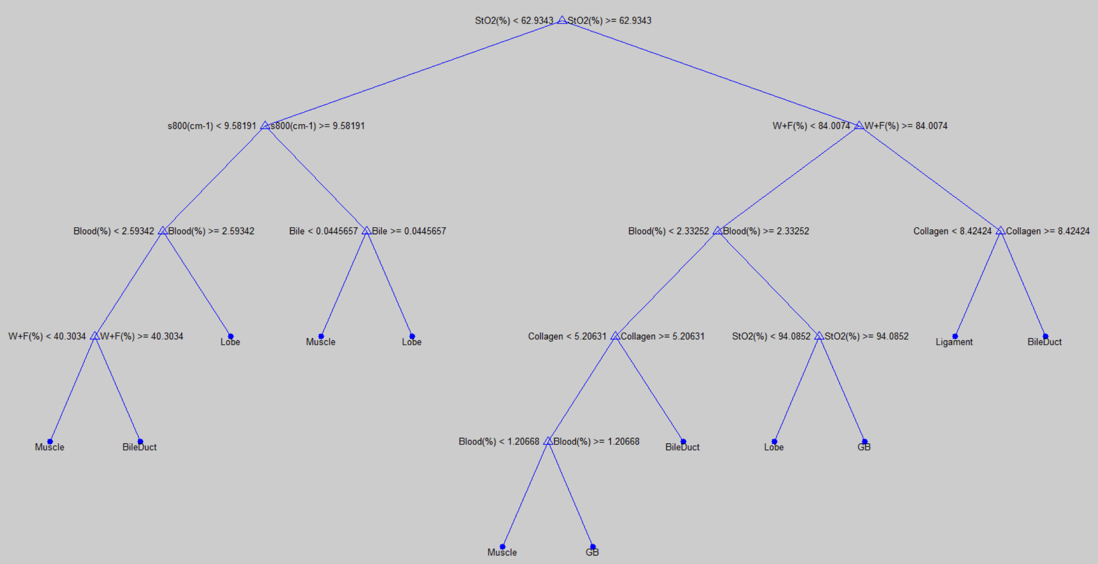

Figure 4.4: *Decision tree for the LOO method for liver different tissues*

Collective Analysis

A Classification And Regression Tree (CART) algorithm was used to implement the classification of the collected data into the defined tissue types, based on the main parameters used for the fitting. The parameters chosen for the CART analysis were the blood content (%), water plus fat percentage, fat content (%), bile, bilirubin, beta-carotene and collagen concentration, scattering coefficient value at 800 nm and oxygen saturation (%). The result of this analysis is shown if Figure4.4.

Table4.1 displays the classification accuracy of the decision tree in Figure2.12 for all optical DRS measurements considered in the study when compared with the experimental knowledge. As shown, a total of 200 spectra out of 211 for ligament, 548 out of 570 for lobe, 174 out of 200 for gall bladder, 178 out of 200 for bile duct and 79 out of 100 for muscle were correctly classified, which lead to the following sensitivity and specificity values:

$MeasuredTissue/DRS$	Li	GB	Lo	BD	M
$Ligament(211)$	200	1	2	8	0
$GallBladder(570)$	0	548	5	3	14
$Lobe(200)$	10	5	174	9	2
$BileDuct(200)$	6	11	5	178	0
$Muscle(100)$	0	18	0	3	79

Table 4.1: *Confusion Matrix associated to the classification*

$Se_{Ligament} = 95\%$, $Sp_{Ligament} = 98\%$,

$Se_{Lobe} = 96\%$, $Sp_{Lobe} = 95\%$,

$Se_{GallBladder} = 87\%$, $Sp_{GallBladder} = 99\%$.

$Se_{BileDuct} = 89\%$, $Sp_{BileDuct} = 98\%$,

$Se_{Muscle} = 79\%$, $Sp_{Muscle} = 99\%$.

4.4 Parameters Variability after cold storage

As done in chapter3, in this section changes in the main chromophores and scattering properties in tissues after cold storage will be discussed. Samples were frozen, defrosted and remeasured when they reached again the room temperature. The results were compared with the ones collected from fresh tissue samples.

4.4.1 Tissue Samples

As soon as all the measurements on fresh tissues were taken, the swine livers and rabbit livers were put in a freezer at -8℃ where they stayed over night. Once frozen, they have been taken out of the freezer and put in a fridge at 4℃ to unfreeze. Rabbit livers took one day to be completely defrosted, while pig livers took two days, due to the bigger dimensions. Once defrosted, the samples stayed outside the refrigerator,

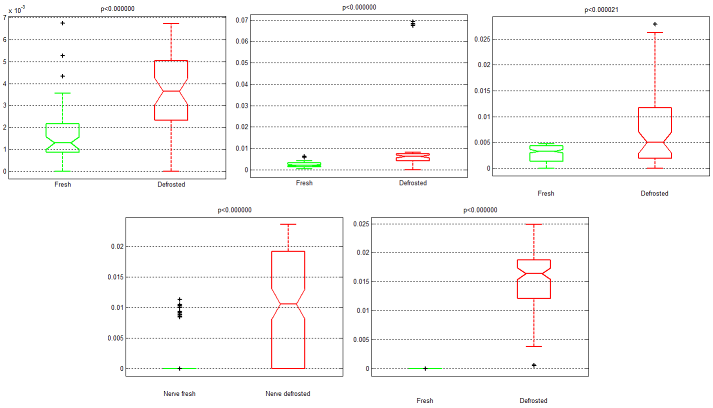

Figure 4.5: *Methemoglobin variation in Round Ligament, Gall Bladder, Lobe, Bile Duct and Muscle during cold storage*

in the photonic laboratory, to reach the room temperature (25℃) before the start of the experiments.

4.4.2 Collective analysis

In this section boxplots will be used to compare the concentrations of the main chromophores and scattering elements used in the fitting model between fresh tissue and defrosted tissue. The results that will be proposed show effects of freezing on the concentration of some of the main chromophores in the measured tissues in pig livers. In all the figures, data taken from lobe, gall bladder, bile duct, ligament and muscle will be displayed in this order.

Figure4.5 shows methemoglobin behavior for all different types of tissue measured. As mentioned before, methemoglobin is a product of changes in hemoglobin after tissue death whose concentration increases with time[37]. Shown results confirm that DRS has potentials to correctly detect this increase.

Another important chromophore in liver tissue is bile. The results displayed in Figure4.6 show a decrease of bile after cold storage. This loss in bile is confirmed by

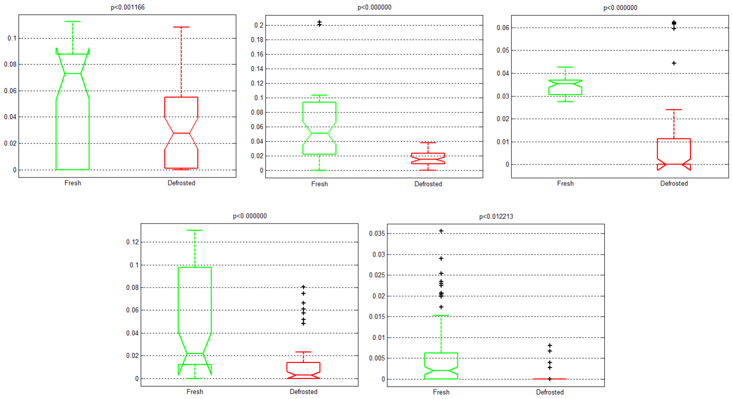

Figure 4.6: *Bile variation in Round Ligament, Gall Bladder, Lobe, Bile Duct and Muscle during cold storage*

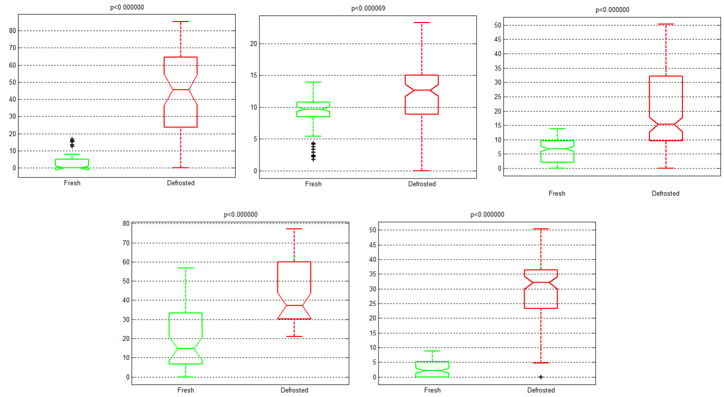

Figure 4.7: *Bilirubin variation in Round Ligament, Gall Bladder, Lobe, Bile Duct and Muscle during cold storage*

the boxplots in Figure4.7, which show that bilirubin, a product of bile, constantly increases in all different types of tissue.

Figure4.8 shows that the total blood concentration is higher after cold storage than in fresh tissue. This result is in agreement with the ones discussed in Chapter3 for different tissue types from animals' hind limbs and with a previous study conducted in Philips Research[39].

Due to death, collagen should increase and cause fibrosis of tissue and this is in

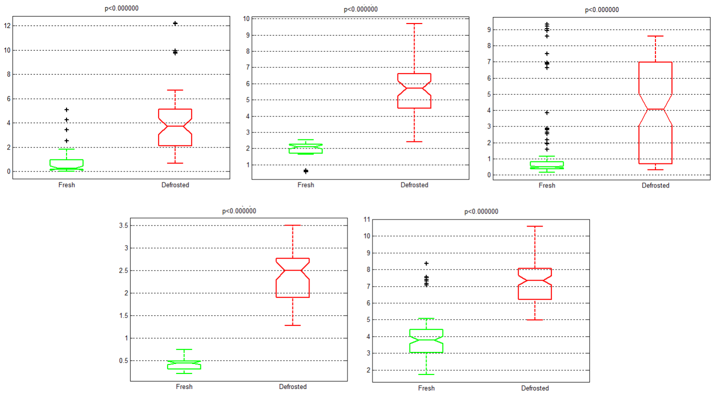

Figure 4.8: *Blood (%) variation in Round Ligament, Gall Bladder, Lobe, Bile Duct and Muscle during cold storage*

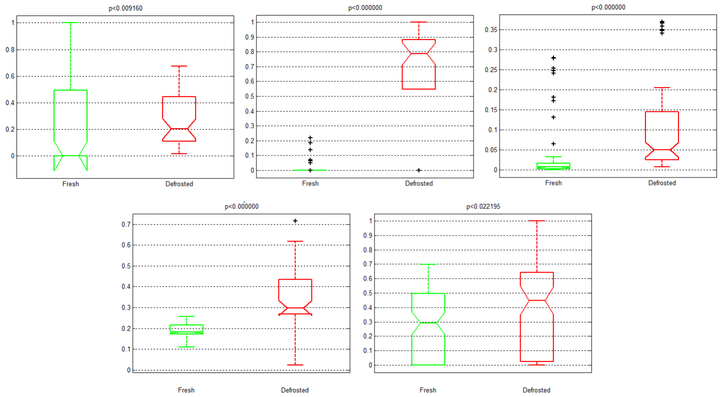

Figure 4.9: *Collagen variation in Round Ligament, Gall Bladder, Lobe, Bile Duct and Muscle during cold storage*

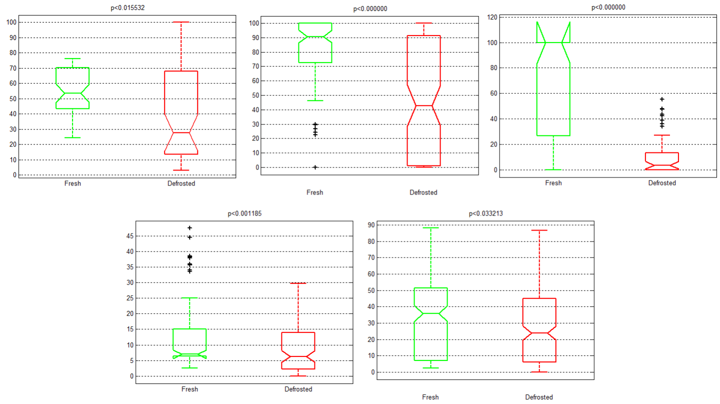

Figure 4.10: *Oxygen saturation (%) variation in Round Ligament, Gall Bladder, Lobe, Bile Duct and Muscle during cold storage*

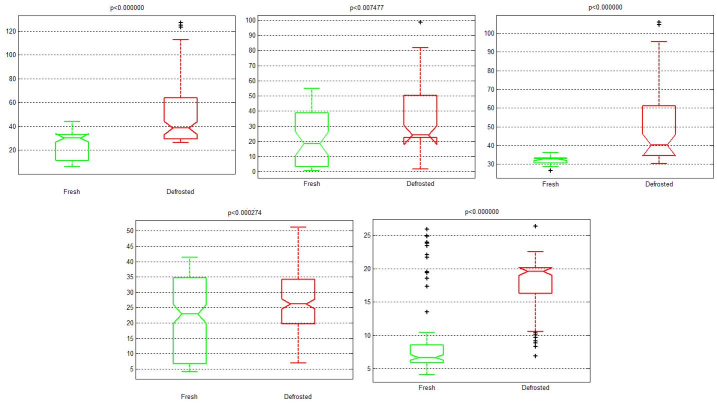

Figure 4.11: *Water plus Fat (%) variation in Round Ligament, Gall Bladder, Lobe, Bile Duct and Muscle during cold storage*

agreement with the DRS results shown in Figure4.9, in which measurements before and after cold storage are compared.

In the last two figures, Figure4.10 and Figure4.11, the percentage of oxygen saturation and of water are shown to be higher after cold storage. As seen in the previous study (Chapter3), the oxygen saturation results to decrease in all different tissue types due to the lack of perfusion, while, the water fraction increases, in agreement with previous results in literature[34] , due to the time passed after the sacrifice.

4.5 Conclusions

In this section, the feasibility of liver tissuse studies with diffuse reflectance spectroscopy has been investigated.

From this study DRS resulted to be a good technique for classification of different tissue types in liver. The spectra acquired showed characteristics which are known from literature to be associated to particular chromophores in each tissue type. After a statistical analysis based on CART algorithm, sensitivity values between 79% and 96% and specificity value between 95% and 99% have been calculated. The effect of cold storage on liver tissues has been analyzed. From the results of this study, similar behaviors as found for tissues in animal limbs after cold storage (see chapter3) were noticed. Bile resulted to decrease in time, while an increase in bilirubin, which is a product of bile, was detected.

Chapter 5

Liver Vitality monitoring during Preservation

5.1 Introduction

Maintaining liver vitality during preservation is important for optimal graft function and survival.

Static cold storage (CS) is currently the the most widely used technique in clinical use for liver preservation and it is simply based on suppression of metabolism and catabolic enzymes by hypotermia[38]. Although this traditional organ preservation method is sufficient for preserving most liver for transplantation, it fails to maintain viability in part of the grafts of suboptimal quality, or so-called extended criteria donor (ECD) grafts. ECD allow, for example, organs from elderly, steatotic livers or after cardiac death donors (DCD) to be considered for a graft, but those are all situations at high risk of moderate to severe preservation injury (PI) and PI-related biliary complications[41]. Severe PI may contribute to primary nonfunction (PNF) and a need for retransplantation in 3–7% of all liver transplants.

As the discrepancy between available donor organs and the number of patients waiting for transplantation increases, more ECD grafts are requested and the development of new and better preservation methods is becoming a needed priority[42][43].

A relatively simple option is hypotermic machine perfusion, which preserve the organ keeping it at a low temperature (0-4℃) and offering it oxygen supply and the removal of waste products. However, although it has achieved adequate results in near-clinical and clinical settings[43], its use seems to offer little protection in case of suboptimal grafts[44]. Moreover, hypotermia can cause side effects such as cell swelling or acidosis.

Normothermic perfusion (37℃) of donor livers offers potential to meet the requirements to preserve ECD grafts.

Important advantages of this methods are the full metabolic support and the possibility to assess grafts viability before transplantation. In addition liver grafts could potentially be optimized by pharmacological conditioning. On the other hand it requires challenging, near-physiological conditions. Promising results on discarded human ECD livers have been reported[7].

Liver viability monitoring is helpful to better understand how the donor liver behave over the preservation time. An accurate method for continuous assessment of liver vitality could be of great value for predicting the outcome of liver surgery and transplantation. Currently, pathology studies are used to check the vitality of donor livers before transplantation. The main problem with this analysis is that the results require time to be available. Due to the short life of a donor liver out of a patient, a real-time method for vitality check is needed.

Diffuse Reflectance Spectroscopy has been proven to be an effective method for estimating biological tissue compositions. During liver preservation, DRS should potentially be able to give real-time feedback about physiological and biological parameters such as oxygenation saturation and lipid content, which can be used as indicators of donor liver viability.

In this study DRS data from taken three descarded human ECD livers will be discussed. While two livers were measured during 6 hours without being perfused, one was measured during normothermic perfusion.

5.2 Materials and methods

5.2.1 DRS setup

For this study, the same console used for the measurements explained in previous chapters was used (see paragraph 2.2). The complete setup was shifted to the University Medical Center Groningen (UMCG), where experiments on human ECD livers under normothermic machine perfusion are currenty running. After a brief introduction regarding the set up, doctors responsible of these experiments acquired the DRS data which have been analyzed and whose results are shown in this section.

5.2.2 Donor liver

Three human livers derived from a donor that was declined for transplantation by all three transplant centers in the Netherlands were included in this study. The relatives of the donors gave the permission to use the livers for research purposes. The studies were approved by the medical ethical committee of UMCG and the Nederlandse Transplantatie Stichting, the competent authority for organ donation in the Netherlands.

All liver procurement procedures were performed by one of the regional multi-organ recovery teams, in The Netherlands. The livers were packed in standard sterile donor organ bags and stored in boxes with crushed ice and subsequently transported to UMCG. Immediately upon the arrival of one of the three livers in the operating room, an experienced transplant surgeon realized all the black-table procedures[7] and attached it to the preservation machine. From a pathology analysis, it is known that the liver which was attached to the perfusion machine was steatotic (fat level higher than 30%) and this was the main reason for which it was descarded. No steatosis was fond in the other two livers studied.

5.2.3 Normothermic machine perfusion

For normothermic perfusion of the donor liver, a CE marked (European Union certification of safety, health and environmental requirements) devise that enables dual perfusion via both the hepatic artery and the portal vein in a closed circuit (Liver Assist, Organ Assist, Groningen, The Netherlands; Figure5.2).

As shown schematically in Figure5.1, two rotary pumps provide a pulsatile flow to the hepatic artery and a continuous flow to the portal vein. Two hollow fiber membrane oxygenators provide oxyganation of the perfusion solution, as well as removal of CO_2. The system is both pressure and temperature controlled, which allows auto regulation of the blood flow through the liver, with constant pressure at variable flow rates[7]. Pressure was limited to a mean of 50 mmgH in the hepatic artery and 11 mmgH in the portal vein. The temperature was set to 37°C and a new sterile disposable set of tubing, reservoir and oxygenators was used.

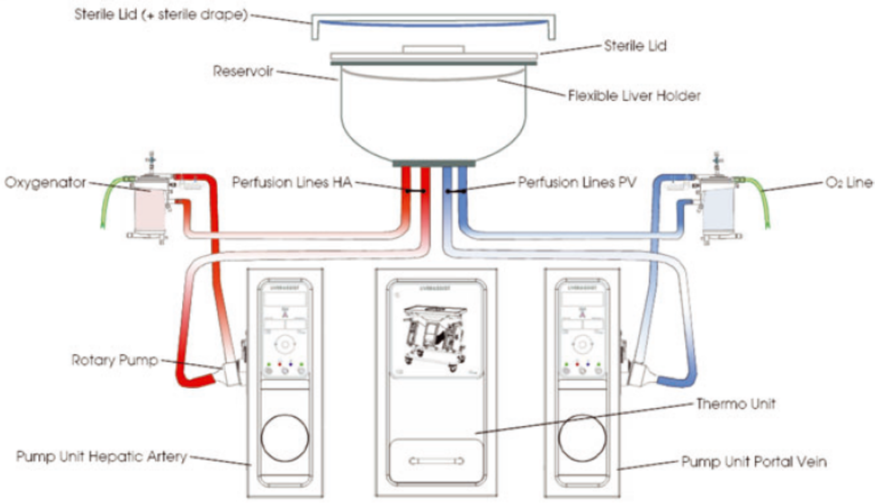

Figure 5.1: *Schematic drawing of the perfusion machine used for normothermic perfusion of human donor livers (Liver Assist, Organ Assist, Groningen, The Netherlands)*$^{c}iteumcg$

Figure 5.2: *Photo of the perfusion machine used for normothermic perfusion of human donor livers (Liver Assist, Organ Assist, Groningen, The Netherlands)*[7]

The perfusion fluid used is composed of human packed red blood cells and fresh frozen plasma. Blood group and Rhesus factor are identical to the donor liver. These blood products were obtained from the local blood bank and derived from third party blood donors. Because of the relatively low hematocrit of the perfusion solution, the pO_2 was targeted at supernormal values (60 kPa) in order to provide sufficient oxygen to the liver. Heparin was added for anticoagulation, and vitamins, glucose, amino acids and trace elements were added to provide sufficient nutrients for the liver. Antibiotics were added to prevent bacterial growth and graft infection under normothermic conditions[7].

5.2.4 Experimental protocol

Optical measurements from the left lobes of the livers were collected during a period of time of 6 hours. In Table5.1 and Table5.2, the area measured and the number of DRS spectra acquired at each time point for the three livers are shown. While the first liver was measured during perfusion, the second and the third liver were measured out of the perfusion machine. As shown, for the first liver it was not precisely clear which zone of the lobe was measured at each time point, while for the second and the third liver 10 spectra from the periphery of the lobe, 10 from the middle of the lobe and 10 from the central part of the liver were acquired at each time session.

Tissue Type	Time (min)	#Spectra
Liver1, peripheral	0	21
Liver1, lobe	20	10
Liver1, lobe	50	10
Liver1, lobe	60	31
Liver1, lobe	150	15
Liver1, lobe	180	20
Liver1, lobe	210	10
Liver1, lobe	240	20
Liver1, lobe	270	11
Liver1, lobe	300	20
Liver1, lobe	330	20
Liver1, lobe	360	20

Table 5.1: *Protocol of UMCG DRS measurements for the liver under perfusion*

Tissue Type	Time (min)
Liver2,3, peripheral, middle, central lobe	0
Liver2,3, peripheral, middle, central lobe	30
Liver2,3, peripheral, middle, central lobe	60
Liver2,3, peripheral, middle, central lobe	90
Liver2,3, peripheral, middle, central lobe	120
Liver2,3, peripheral, middle, central lobe	150
Liver2,3, peripheral, middle, central lobe	180
Liver2,3, peripheral, middle, central lobe	210
Liver2, peripheral, middle, central lobe	240
Liver2,3, peripheral, middle, central lobe	270
Liver2,3, peripheral, middle, central lobe	300
Liver2, peripheral, middle, central lobe	330
Liver2, peripheral, middle, central lobe	360

Table 5.2: *Protocol of UMCG DRS measurements for the two livers out of the perfusion machine. 10 spectra per each location at each moment were collected*

5.3 Results

In this section, results from the DRS measurements taken during the three experiments developed in UMCG are presented.

5.3.1 Spectral Measurements and fitting results

Figure5.3, Figure5.4 and Figure5.5 show some examples of spectra collected at the beginning and at the end of each experiment from the perfused liver ad the two not perfused livers respectively. Spectra collected at each time session of each experiment are shown in appendix C.

For the fitting of the acquired spectra, bile, bilirubin and lycopene had been added to the model as parameters of choice, together with collagen, beta-carotene, methemoglobin and the standard ones seen in theory (see paragraph 2.2.2). The fitted spectra match properly the measured signals, in almost all the cases.

The shape of the signal is comparable to the one of the spectra collected from animals livers. It is affected by the high presence of blood in liver, in the visual region, between 400 and 700 nm, by the presence of water in the NIR region, between 1300 and 1600 nm by lipids, which major peak is visible at 1210 nm and by collagen, which absords at around 1000 nm.

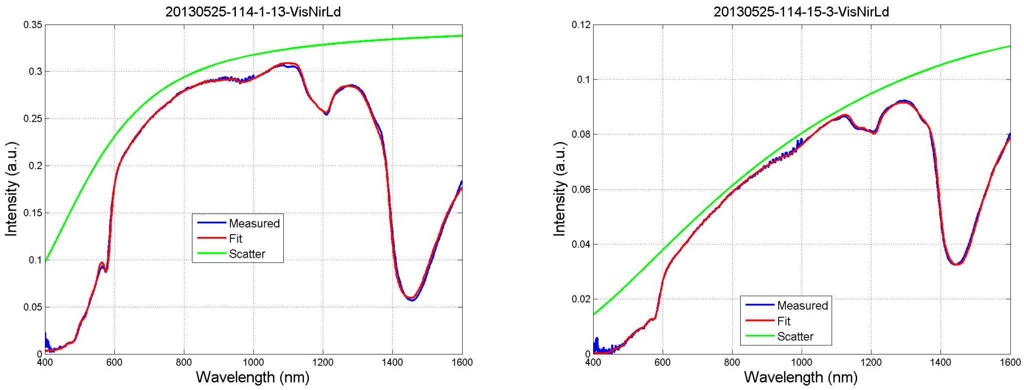

Figure 5.3: *Examples of spectra collected from the perfused liver at time 0 and after 6 hours*

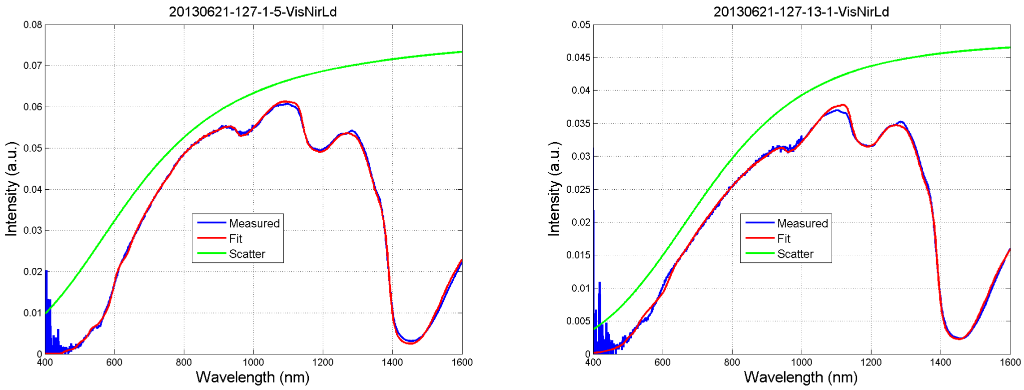

Figure 5.4: *Examples of spectra collected from the first not perfused liver at time 0 and after 6 hours*

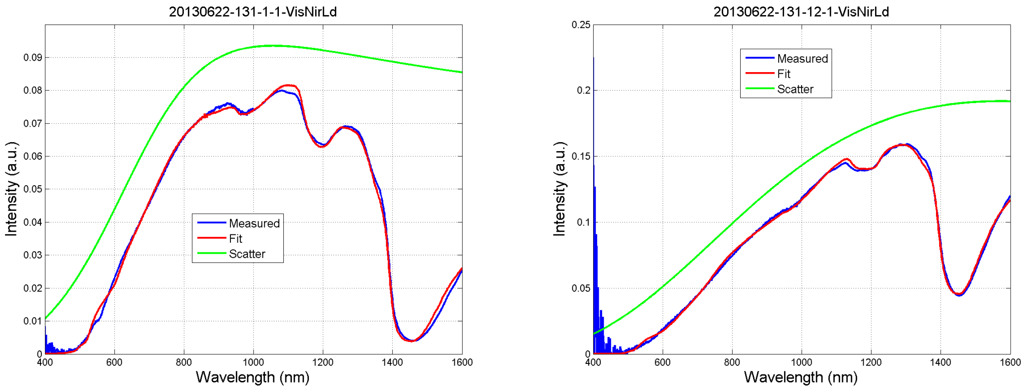

Figure 5.5: *Examples of spectra collected from the second not perfused liver at time 0 and after 6 hours*

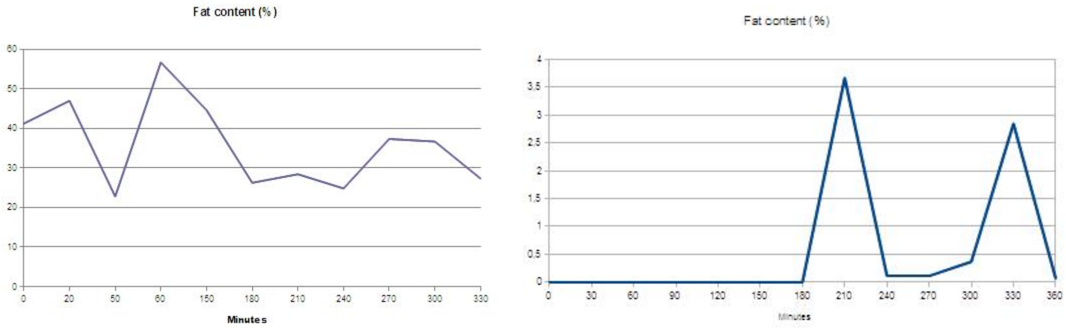

(a) (b)

Figure 5.6: *Variation of Fat(%) over 6 hours in the steatotic liver, under perfusion (a) and one of the non steatotic not perfused liver (b)*

5.3.2 Parameters variation in time

In this section the variation over the period of time studied (6 hours) of the main parameters used for fitting the measured spectra are presented.

In Figure5.6 the contents of fat at each time session in the steatotic liver and in one of the non steatotic ones are shown. As said, a liver is considered steatotic if its fat content is higher than 30%. The results in Figure5.6 confirm that DRS is able to detect the amount of lipids in a liver lobe in order to distinguish between an healty and a steatotic liver. More studies on perfused steatotic livers need to be done to confirm this diagnostic potential of DRS measurements on livers during preservation.

Figure5.7 shows the results for bile over the entire period of the experiment. UMCG doctors expected the level of bile to decrease in case of not perfused livers, while during perfusion it should maintain a constant level or decrease slowly. DRS results show a decrease in all cases and the decrease in case of perfused liver is slower than the not perfused livers, but the difference is not significant and more studies on perfused livers need to be done. Furthermore, these experiments were the first

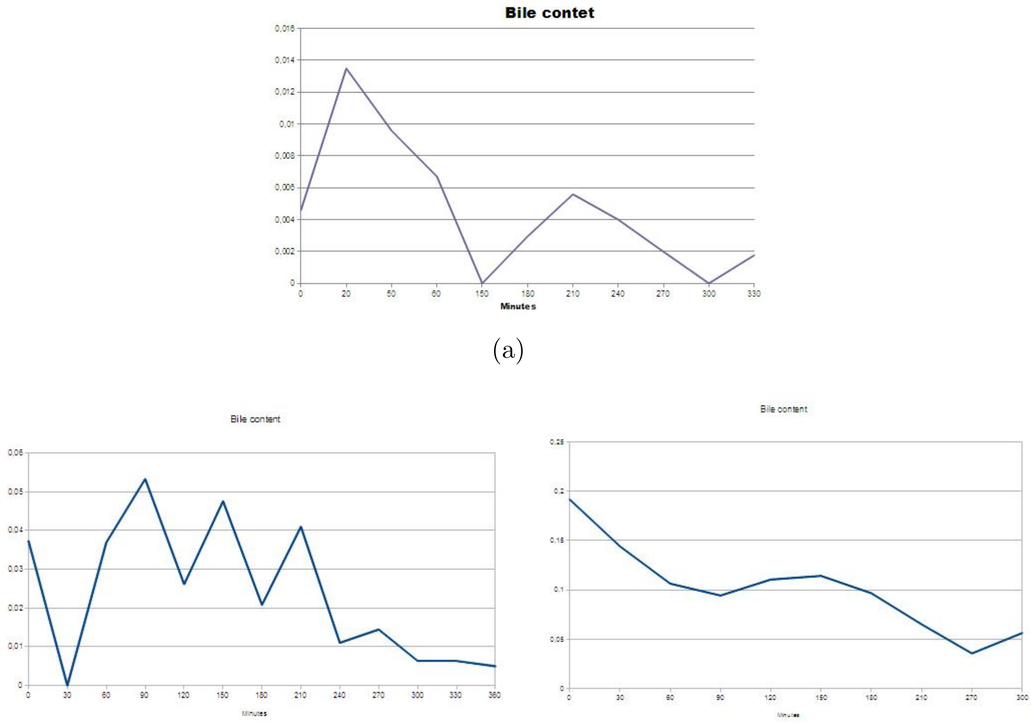

(a)

(b) (c)

Figure 5.7: *Bile variation over 6 hours in the perfused liver (a) ad the not perfused livers (b,c)*

experiences of UMCG doctors with DRS measurements and some improvements in the protocols are needed. As said, it was not possible to know which areas in the lobe of the perfused liver were measured in each time session. This could explain the presence of some discrepancies between two measurements close in time (see appendix D).

In general, decreases in water fraction, methemoglobin and collagen were found for all the three livers studied in all the measured areas of the lobes, while an increase in the scattering coefficient at 800 nm has been detected in all cases.

No significant differences between the perfused liver and the not perfused livers were found which could be due to the different preservation methods used. More studies on human discarded livers need to be performed.

5.4 Conclusions

This study showed that DRS offers potentials to give a real-time feedback on liver during preservation before transplantation. DRS could correctly estimate the level of fat in the liver lobe, which means that this technology has potentials to replace pathology for steatosis monitoring and diagnosis. Further studies on discarded donor livers need to be done.

Chapter 6

Conclusions and Recommendations

In this thesis two main studies have been developed.

Firstly, Diffuse Reflectance Spectroscopy was used to classify different tissue types. The principal aim was to understand if DRS has potentials to be integrated in surgery tools to allow percutaneous image guidance. It should be able to give a real-time feedback on the tissue type during a procedure, confirming the exact position of the tip of interventional probes in the region of interest.

The results showed good and promising sensitivities and specificities in the classification between fat tissues, muscular tissues, nerve tissues and blood vessels, while it was more difficult to correctly recognize ligaments.

Further in-vivo experiments need to be done to avoid differences due to dead tissues. Swines tissues resulted to be more similar to human cadaver tissues in comparison with rabbit or rat tissues, so experiments on pigs are recommended.

The same tissues studied in the first step were then frozen and defrosted in order to evaluate the effect of cold storage on biological tissues. The results showed trends in agreement with literature for methemoglobin, water fraction and collagen which were found to increase with the freezing process. On the contrary, the blood content was found to decrease with cold storage, in disagreement with literature. Further experiments are needed to better understand this result, giving attention to the position in which the tissues are stored. The effect of gravity on blood in the tissue may be a reason of the observed increase of it in the measured area.

The main goal of the second study was to assess the capability of Diffuse Reflectance Spectroscopy in monitoring the vitality of a liver during preservation. Currently pathology analysis are used, but the results need time to be available and they can not be given in real time to the doctors. Donor livers can not stay more than 18 hours out of a patient and this often doesn't give enough time for pathology analysis. Furthermore a pathology analysis can not be repeated and it doesn't allow continuous monitoring over time.

The DRS data analysis showed promising results in the use of this technology for diagnosis of steatosis in livers, but, as only one steatotic liver has been analyzed, further studies need to be done. Moreover it should be possible to monitor the response of steatotic livers during pharmacological treatments, in combination with normothermic machine perfusion. Furthermore DRS measurements of the bile duct should be taken to see if it is possible to use this technology to monitor the level of collagen in order to predict stenosis, which is a consequence of lack of oxygen in tissue. Stenosis of bile duct tissue results in thickening of the walls due to fibrosis, which might cause post operation complications, such as a lack of bile supply from the liver to the intestine due to duct obstruction.

Further analysis on the level of bile during perfusion need to be done to assess the potentials of normothermic machine perfusion in comparison with the current preservation technique based on simple cold storage.

Bibliography

[1] R. Nachabe, J. W. A. van der Hoorn, R. A. van de Molengraaf, R. Lamerichs, J. Pikkemaat, C. F. Sio, B. H. W. Hendriks, and H. J. C. M. Sterenborg, "Validation of interventional fiber optic spectroscopy with MR spectroscopy, MAS-NMR spectroscopy, high performance thin layer chromatography and histopathology for accurate hepatic fat quantification," *J. Biomed. Opt.*, 2005.

[2] W. G. Zijlstra, A. Buursma, and O. W. Assendelft, *Visible and Near Infrared Absorption Spectra of Human and Animal Haemoglobin.* VSP Publishing, 2000.

[3] R. Nachabe, D. J. Evers, B. H. W. Hendriks, G. W. Lucassen, M. van der Voort, J. Wesseling, and T. J. M. Ruers, "Effect of bile absorption coefficients on the estimation of liver tissue optical properties and related implications in discriminating healthy and tumorous samples," *BIomed Optics Express*, 2011.

[4] E. L. P. Larsen, L. L. Randeberg, E. Olstad, O. A. Haugen, A. Aksnes, and L. O. Svaasand, "Hyperspectral imaging of atherosclerotic plaques in vitro," *J. Biomed. Opt.*, 2011.

[5] R. Nachabe, D. J. Evers, B. H. W. Hendriks, G. W. Lucassen, M. van der Voort, E. J. Rutgers, M.-J. V. Peeters, J. A. Van der Hage, H. S. Oldenburg, and J. . Wesseling, "Diagnosis of breast cancer using diffuse optical spectroscopy from 500 to 1600 nm: comparison of classification methods," *Journal of Biomedical Optics.*

[6] E. Marieb, *Human Anatomy and Physiology*, 1995.

[7] S. op den Dries, N. Karimian, M. E. Sutton, A. C. Westerkamp, M. W. N. Nijsten, A. S. H. Gouw, J. Wiersema-Buist, T. Lisman, H. G. D. Leuvenink,

and R. J. Porte, “Ex vivo normothermic machine perfusion and viability testing of discarded human donor livers,” *American Journal of Transplantation*, vol. 13, 2013.

[8] R. Nachabe, *Diagnosis with near infrared spectroscopy during minimally invasive procedures.*

[9] A. J. W. W. F. Cheong, S. A. Prahl, “A review of the optical properties of biological tissues,” 1990.

[10] P. Bouguer, “Essai d optique sur la graduation de la lumiere,” 1729.

[11] J. H. Lambert, “Photometria siva de mensura et gradibus luminis, colorum et umbrae,” 1760.

[12] A. Beer, “Bestimmung der absorption des rothen lichts in farbigen flussigkeiten,” *Ann. Physik*, vol. 86, pp. 78–88, 1852.

[13] R. Nachabe, B. H. W. Hendriks, A. E. Desjardins, M. van der Voort, and M. B. van der Mark, “Estimation of lipid and water concentrations in scattering media with diffuse optical spectroscopy from 900 to 1600 nm,” *J. Biomed. Opt.*, 2010.

[14] D. R. White, E. M. Widdowson, H. Q. Woodard, and J. W. Dickerson, “The composition of body tissues (II). fetus to young adult.” *British Journal of Radiology*, 1991.

[15] S. C. Kanick, C. van der Leest, J. G. J. V. Aerts, H. C. Hoogsteden, S. Kascakova, H. J. C. M. Sterenborg, and A. Amelink, “Integration of single-fiber reflectance spectroscopy into ultrasound-guided endoscopic lung cancer staging of mediastinal lymph nodes,” *J. Biomed. Opt.*, 2010.

[16] P. Taroni, D. Comelli, A. Pifferi, A. Torricelli, and R. Cubeddu, “Absorption of collagen: effects on the estimate of breast composition and related diagnostic implications,” *J. Biomed. Opt.*, 2007.

[17] S. Wang, J. Zhao, H. Lui, Q. He, and H. Zeng, “Monte carlo simulation of near infrared autofluorescence measurements of in vivo skin,” *J Photochem Photobiol B.*, December 2011.

[18] C. F. Bohren and D. R. Huffman, *Absorption and Scattering of Light by Small Particles.* John Wiley and Sons, 2008.

[19] W. P., "Approximation formulae for the light scattering coefficient of dielectric spheres," *Brit. J. Appl. Phys. 15*, July 1964.

[20] M. G., "Contribution to the optical properties of turbid media, in particular of colloidal suspensions of metals," *Ann. Phys. (Leipzig)*, 1908.

[21] F. P. Bolin, L. E. Preuss, R. C. Taylor, and R. J. Ference, "Refractive index of some mammalian tissues using a fiber optic cladding method," *Appl. Opt. 28*, 1989.

[22] S. T. Flock, B. C. Wilson, and M. S. Patterson, "Total attenuation coefficients and scattering phase functions of tissues and phantom materials at 633 nm," *Med. Phys. 14*, 1987.

[23] H. C. van de Hulst, *Multiple light scattering.* Academic Press, 1980.

[24] M. S. Patterson, B. Chance, , and B. C. Wilson, "Time resolved reflectance and transmittance for the non-invasive measurement of tissue optical properties," *Applied Optics, Vol. 28*, 1989.

[25] D. Contini, F. Martelli, and G. Zaccanti, "Photon migration through a turbid slab described by a model based on diffusion approximation. I. theory," *Applied Optics*, 1997.

[26] B. C. Wilson and S. L. Jacques, "Optical reflectance and transmittance of tissues: Principles and applications," *IEEE Journal of Quantum Electronics, VOL. 26*, 1990.

[27] T. J. Farrell, M. S. Patterson, and B. Wilson, "A diffusion theory model of spatially resolved, steadystate diffuse reflectance for the noninvasive determination of tissue optical properties in vivo," *Med. Phys. 19*, 1992.

[28] A. Kienle and M. S. Patterson, "Improved solutions of the steady state and the time resolved diffusion equations for reflectance from a semi infinite turbin medium," *J. Opt. Soc. Am. A, Vol. 14*, 1997.

[29] I. S. Saidi, S. L. Jacques, , and F. K. Tittel, "Mie and rayleigh modeling of visible-light scattering in neonatal skin," *Applied Optics, Vol. 34*, 1995.

[30] G. Zonios and A. Dimou, "Light scattering spectroscopy of human skin in vivo," *Optics Express, Vol. 17*, 2009.

[31] R. Nachabe, B. H. W. Hendriks, M. van der Voort, A. E. Desjardins, and H. J. C. M. Sterenborg, "Estimation of biological chromophores using diffuse optical spectroscopy: benefit of extending the uv-vis wavelength range to include 1000 to 1600 nm," *Biomed Opt Express.*, 2010.

[32] K. Furutsu, "Diffusion equation derived from space-time transport equation," *JOSA, Vol. 70*, 1980.

[33] ——, "Modelling light distributions of homogenous versus discrete in light irradiated turbin media," *Phys. Med. Biol., Vol. 42*, 1997.

[34] F. Stelzle, K. T. Gerk, W. Adler, A. Zam, M. Schmidt, A. Douplik, and E. Nkenke, "Diffuse reflectance spectroscopy for optical soft tissue differentiation as remote feedback control for tissue-specific laser surgery," *Lasers in Surgery and Medicine 42.*

[35] W. H. Kruskal and W. A. Wallis, *Use of Ranks in One-Criterion Variance Analysis.* American Statistical Association, December 1952, vol. 47.

[36] L. Breiman, J. Friedman, R. Olshen, and C. Stone, *Classification and Regression Trees.* Belmont, USA: Wadsworth International Group, 1984.

[37] B. J., "Post mortem formation of methaemoglobin in red muscle," *Biochem J.*, vol. 23, 1929.

[38] F. O. Belzer and J. H. Southard, "Principles of solid-organ preservation by cold storage," *Transplantation*, vol. 45, April 1988.

[39] Z. Quian, "Diffuse reflectance spectroscooy for liver vitality check," september 2012.

[40] A. Wieckowska, A. J. McCullough, and A. E. Feldstein, "Noninvasive diagnosis and monitoring of nonalcoholic steatohepatitis: Present and future," *Hepatology*, vol. 46, no. 2, pp. 582–589, 2007.

[41] R. M. Merion, N. P. Goodrich, and S. Feng, "How can we define expanded criteria for liver donors?" *Journal of Hepatology*, vol. 45, 2006.

[42] J. V. Guarrera and N. A. Karim, "Liver preservation: Is there anything new yet?" *Current Opinion in Organ Transplantation*, vol. 13, April 2008.

[43] J. V. Guarreraa, S. D. Henrya, R. O. B. Samsteina, M. Kinkhabwalad, M. J. Goldsteina, L. E. Ratnera, J. F. Renzc, H. T. Leeb, R. S. Brown, Jr., and J. C. Emonda, "Hypothermic machine preservation in human liver transplantation: The first clinical series," *American Journal of Transplantation*, vol. 10, 2010.

[44] F. C., H. AJ, and M. M. et all., "Hypothermic oxygenated machine perfusion in porcine donation after circulatory determination of death liver transplant," *Transplantation*, vol. 94, 2012.

[45] R. V. Veen, W. Verkruysse, and H. Sterenborg, "Diffuse-reflectance spectroscopy from 500 to 1060 nm by correction for inhomogeneously distributed absorbers," *Optics letters, Vol. 27*, 1980.

Appendix A

Tissue Classification. Spectra Results

In this section,some examples of spectra measured from each animal are shown.

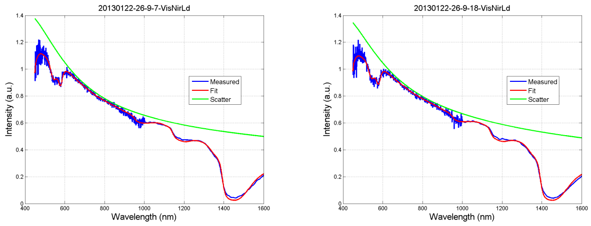

(a) Rabbit

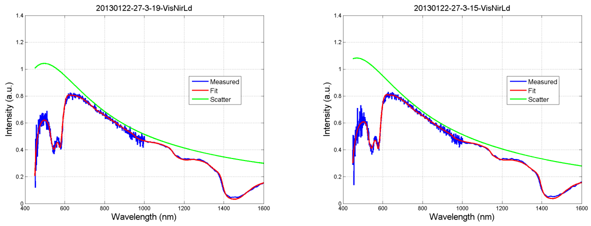

(b) Rat

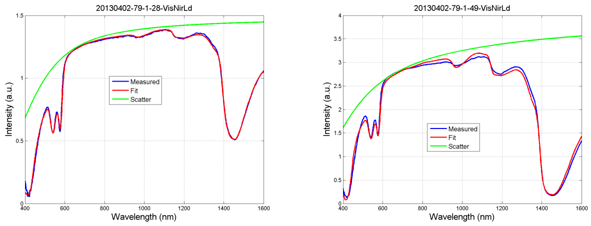

(c) Rabbit

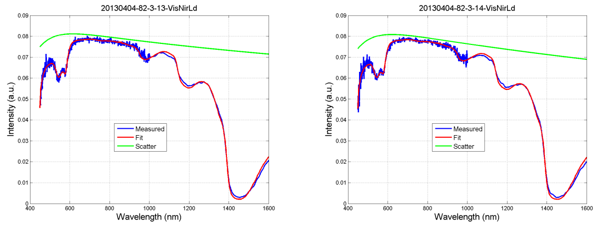

(d) Piglet

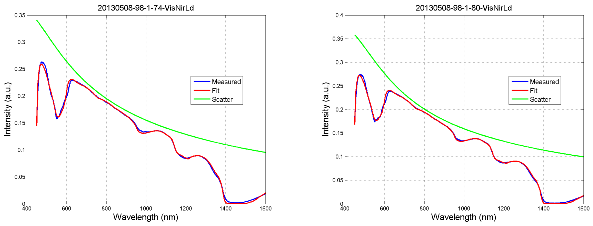

(e) Piglet

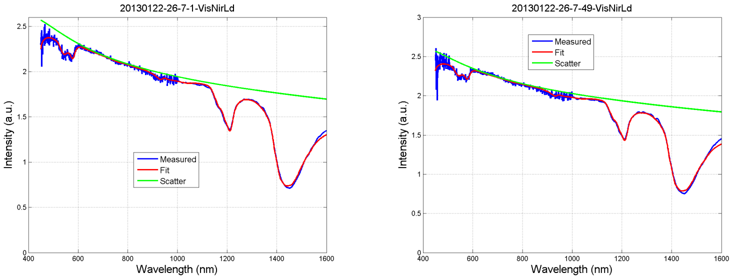

(f) Rabbit

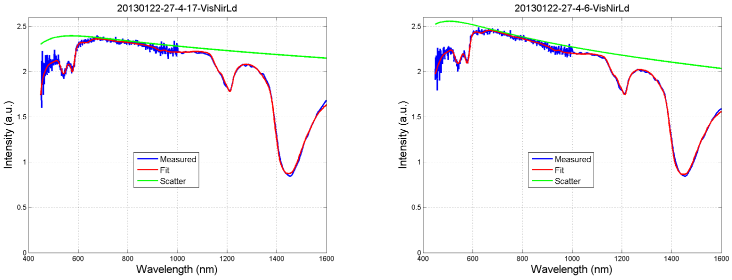

(g) Rat

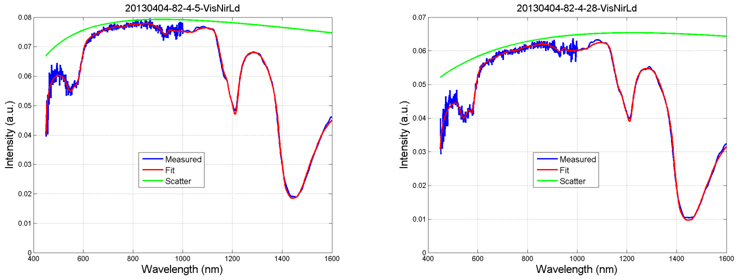

(h) Piglet

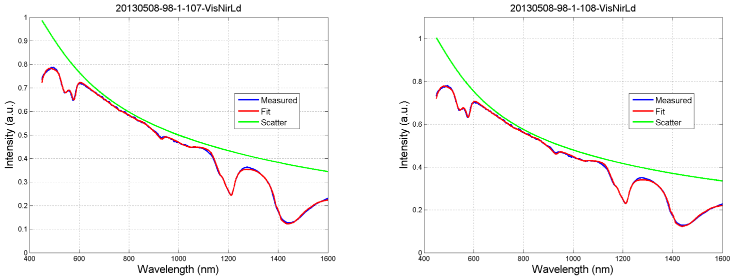

(i) Piglet

Figure A.1: *Example of spectra collected from subcutaneous fat tissues in swine*

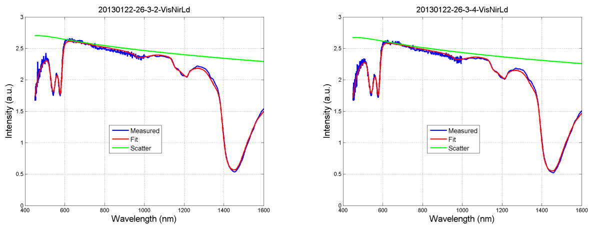

(a) Rabbit

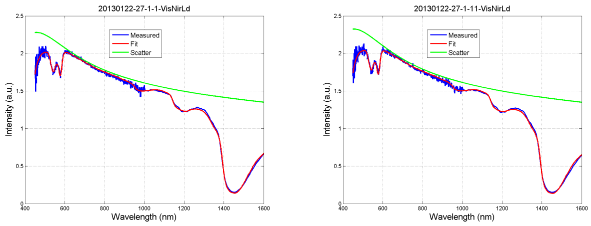

(b) Rat

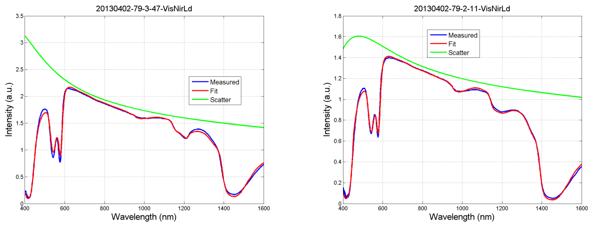

(c) Rabbit

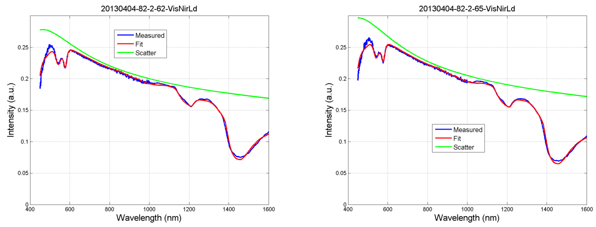

(d) Piglet

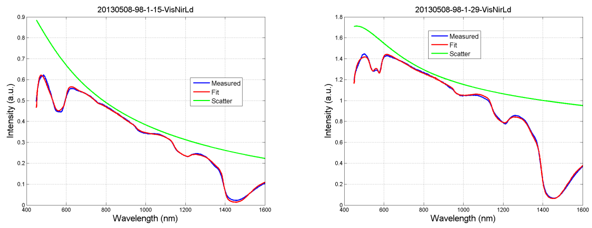

(e) Piglet

Figure A.2: *Examples of spectra collected from nerve tissues in animals (a, b, c, d and e)*

Appendix B

Cold Storage effects. Boxplots

In this section, the effects of cold storage on pig and rabbit muscle and nerve are shown. boxplots have been chosen to present the results.

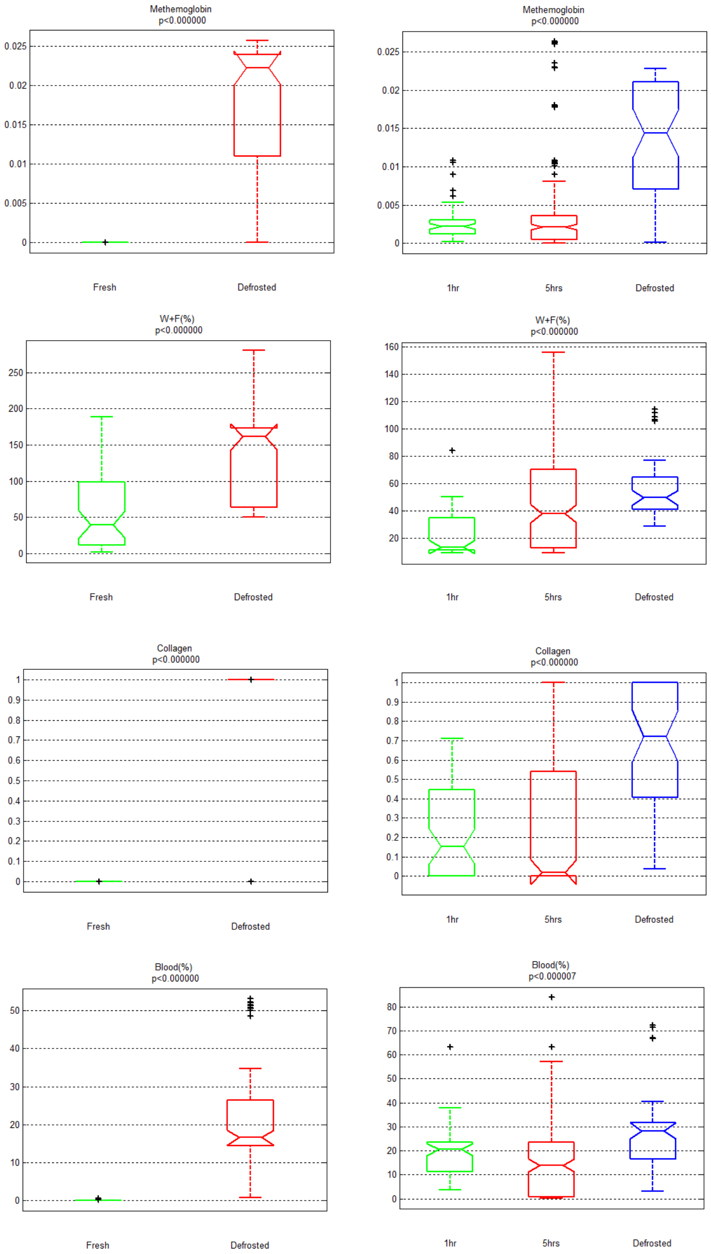

Figure B.1: *Time-Temperature variability of chromophores concentrations in Pig and Rabbit muscle tissue*

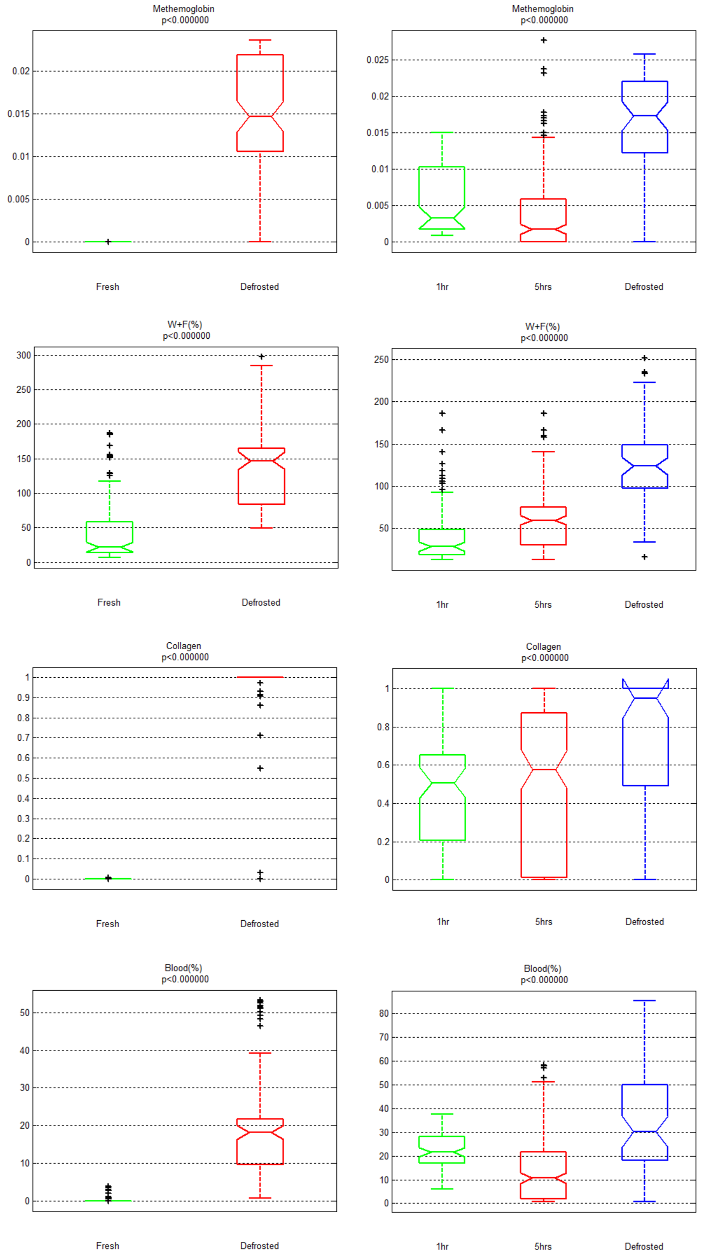

Figure B.2: *Time-Temperature variability of chromophores concentrations in Pig and Rabbit nerve tissue*

Appendix C

UMCG Spectra Results, examples

In this section, examples of spectra acquired at each time session on the three descarded human livers in UMCG are shown.

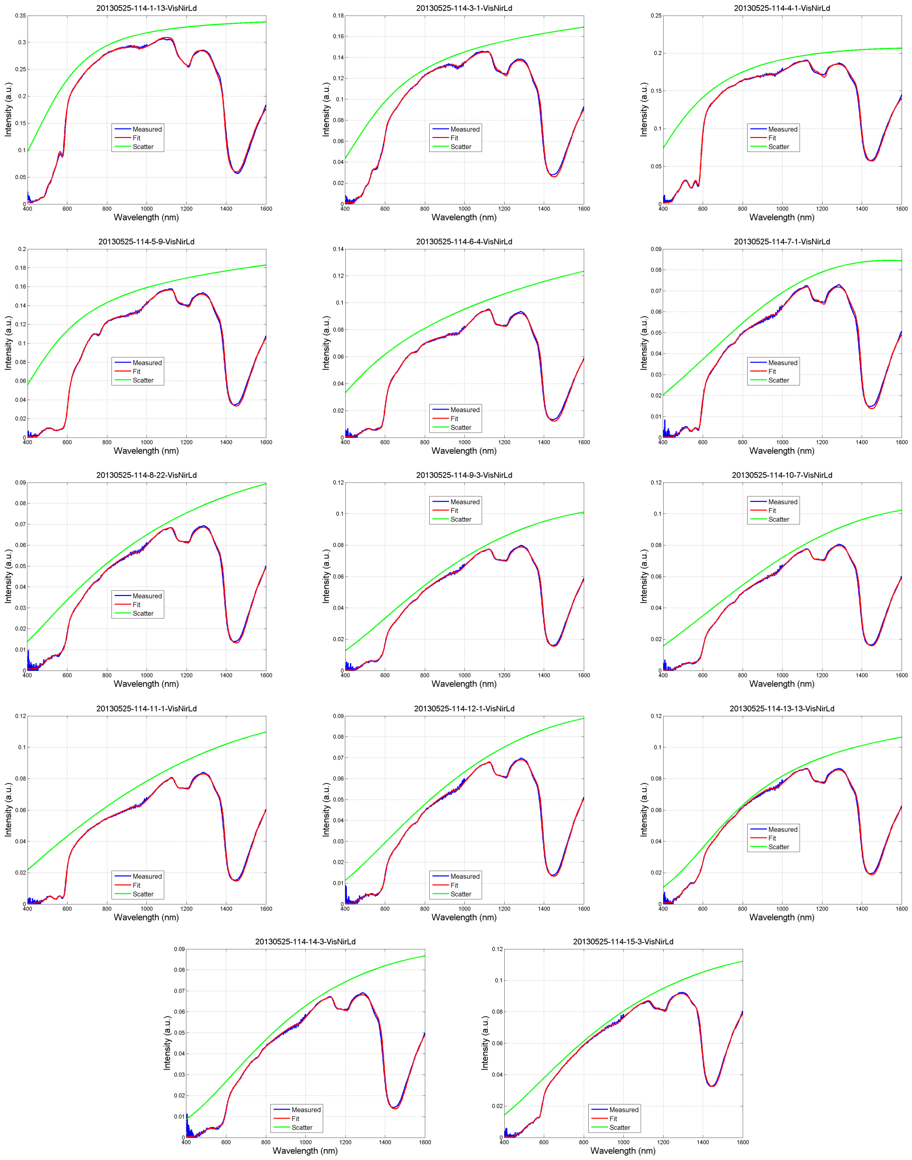

Figure C.1: *Examples of spectra collected every 20-30 minutes during 6 hours from the perfuse liver in UMCG*

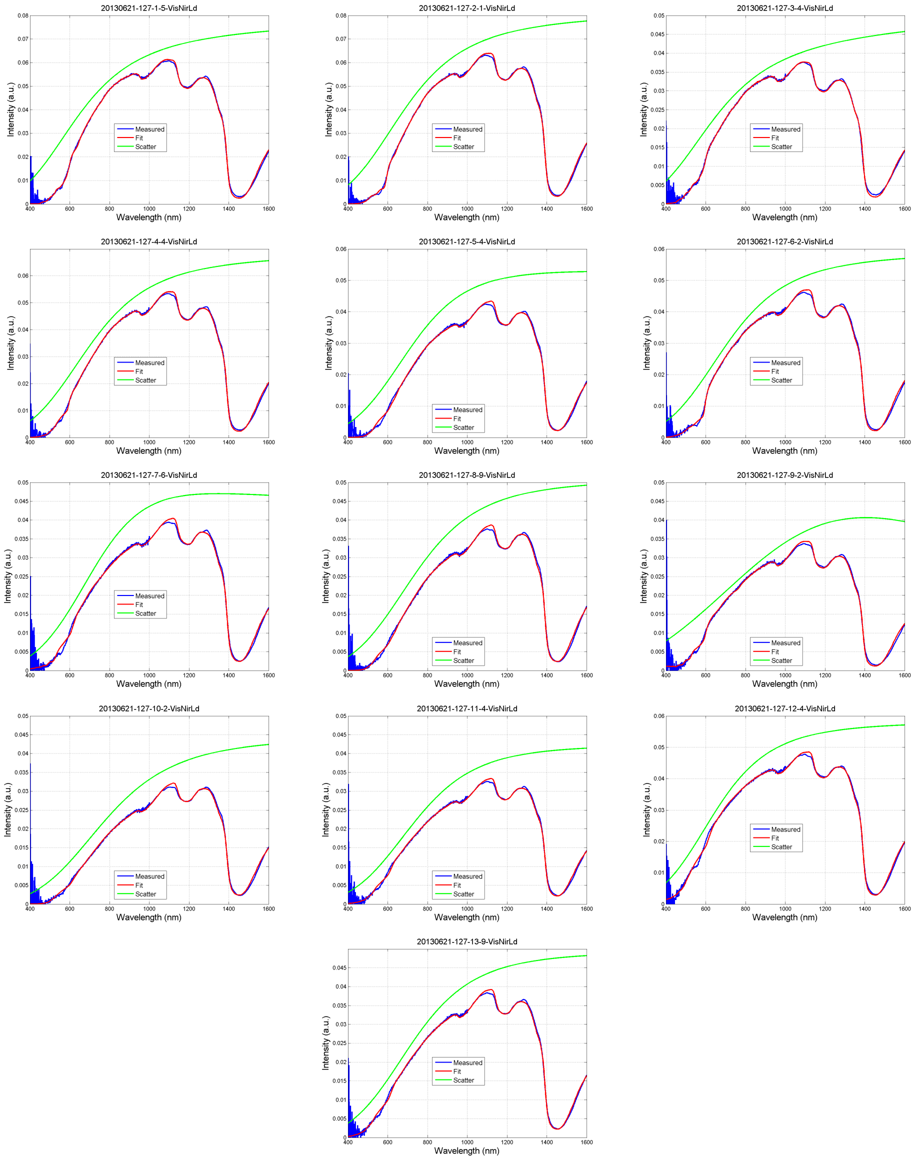

Figure C.2: *Examples of spectra collected every 30 minutes during 6 hours from the not perfused human liver in UMCG*

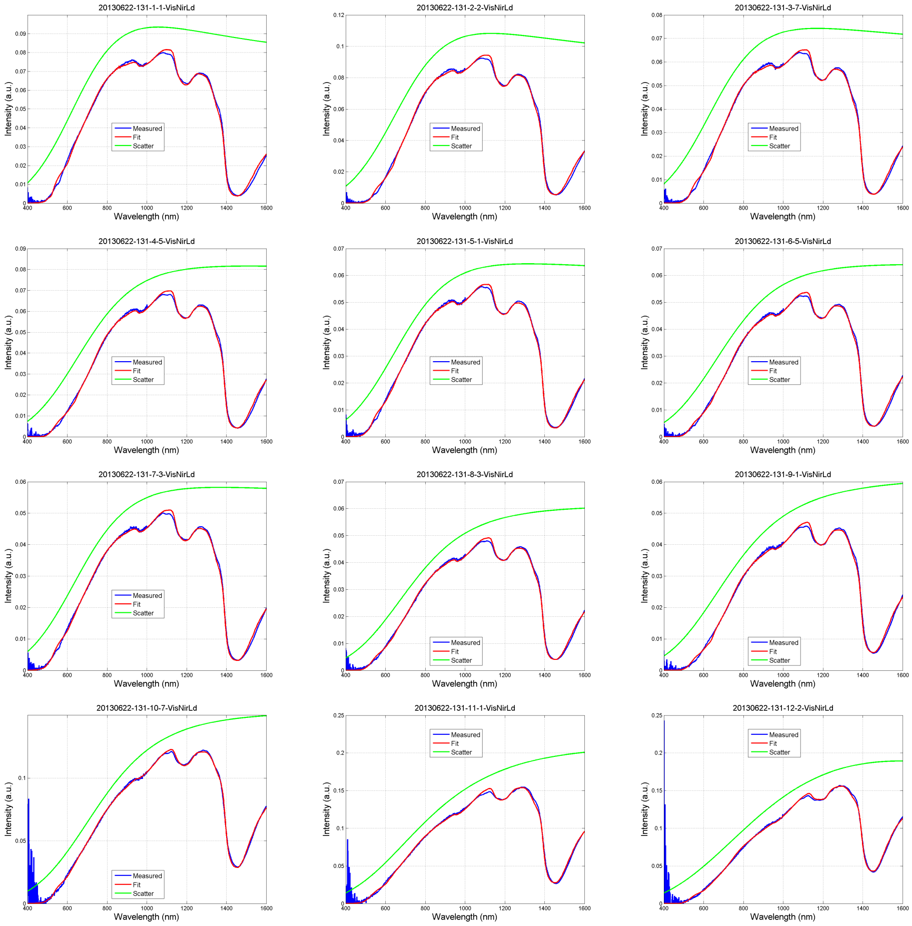

Figure C.3: *Examples of spectra collected every 30 minutes during 6 hours from the not perfused human liver in UMCG*

Appendix D

UMCG, Parameters variability over time

In this section, the trend of the principal fit parameters over the 6 hours of the experiments are presented for the three livers studied.

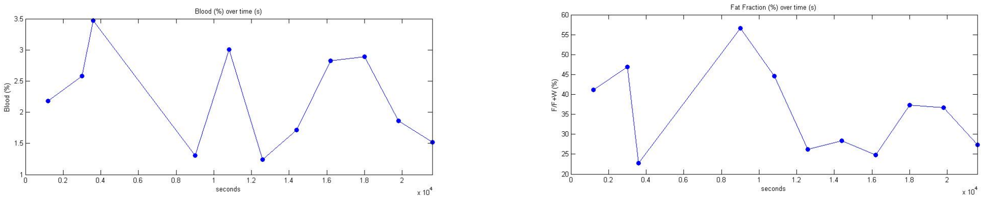

(a) Blood (b) Fat

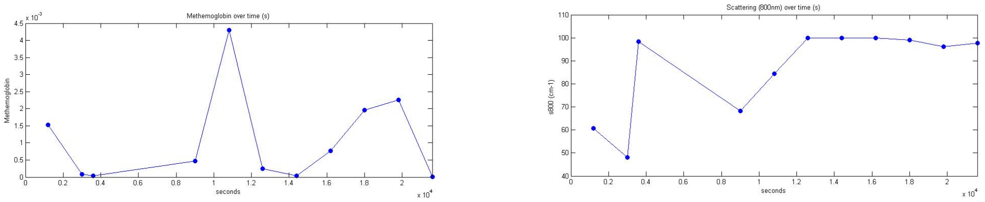

(c) methemoglobin (d) s800

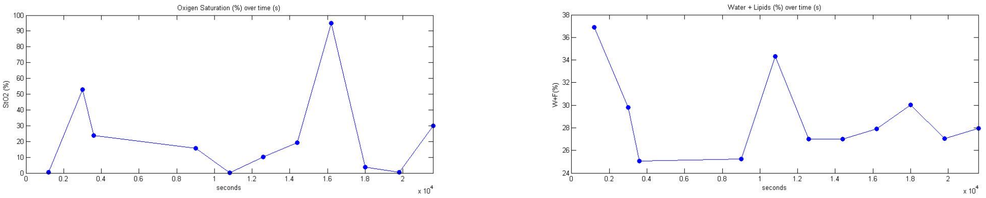

(e) StO2 (f) water + fat

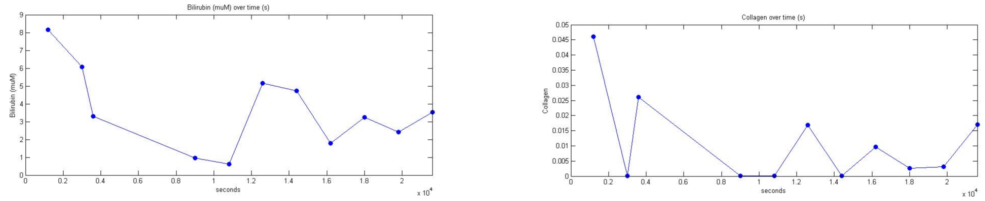

(g) Bilirubin (h) Collagen

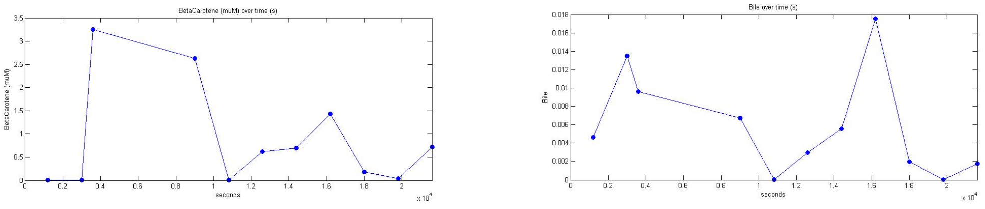

(i) Beta-Carotene (j) Bile

Figure D.1: *Parameters trends over 6 hours in the perfused liver*

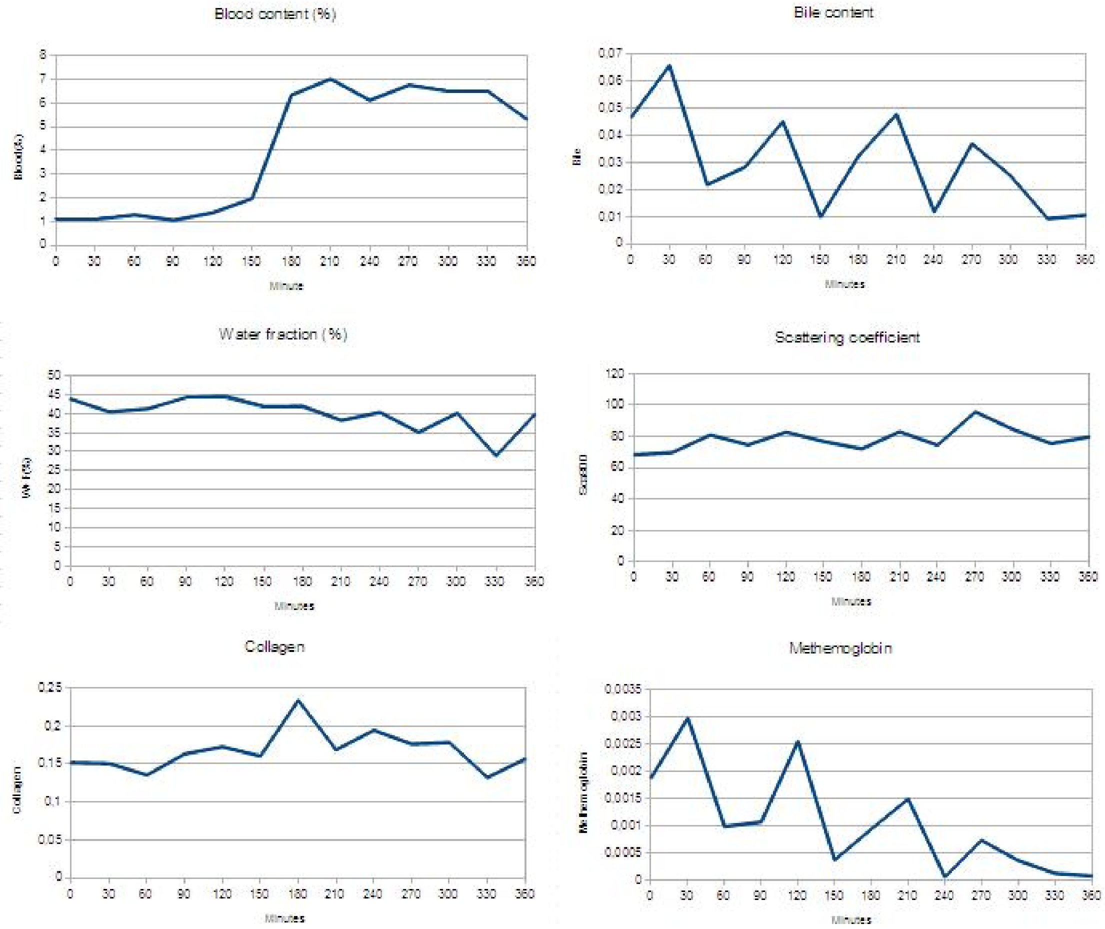

Figure D.2: *Parameters trends over 6 hours in the not perfused liver, peripheral lobe*

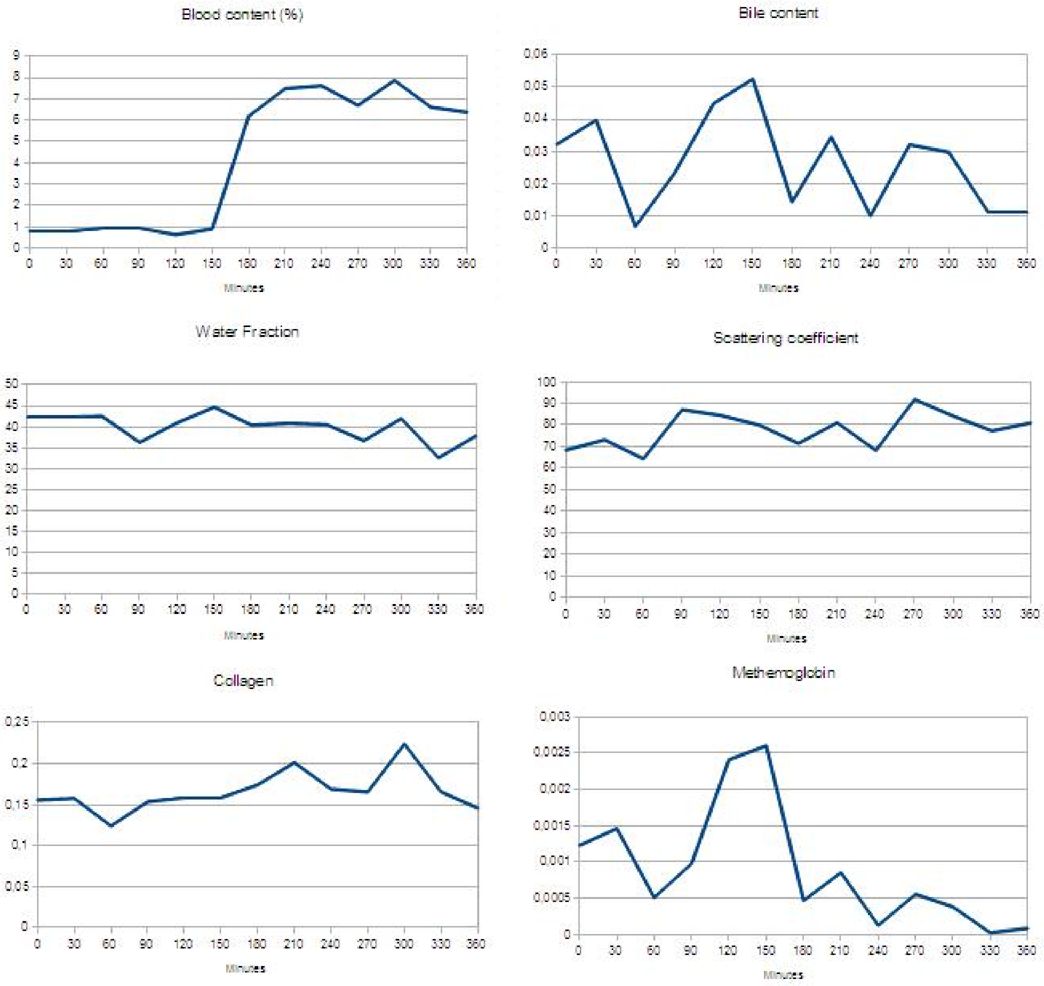

Figure D.3: *Parameters trends over 6 hours in the not perfused liver, middle lobe*

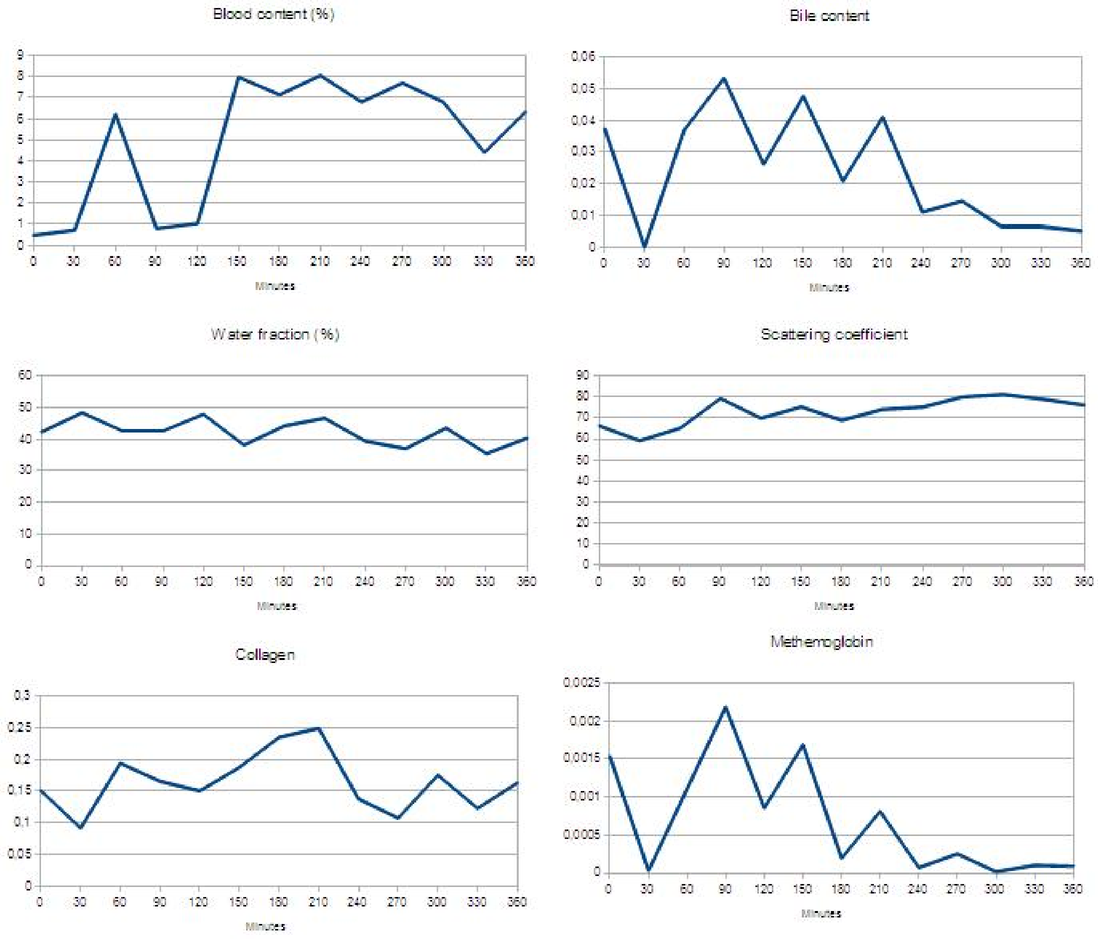

Figure D.4: *Parameters trends over 6 hours in the not perfused liver, central zone*

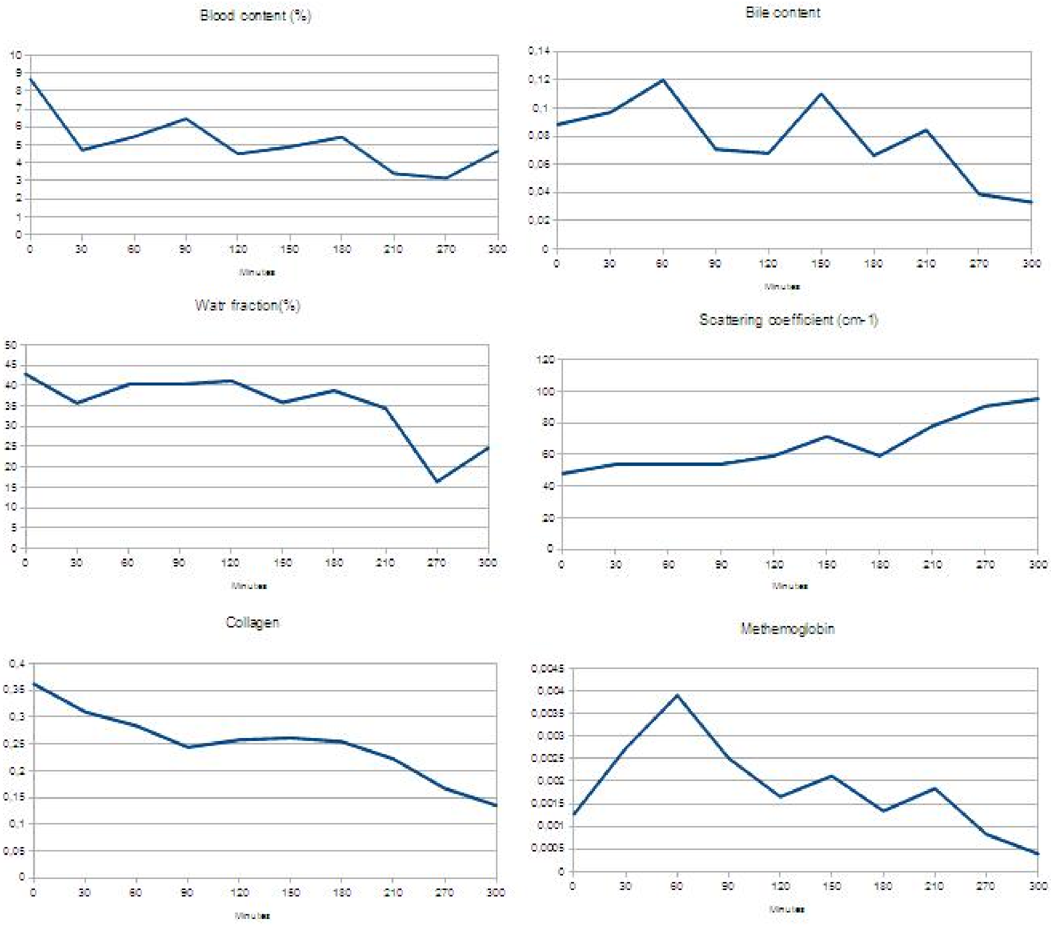

Figure D.5: *Parameters trends over 6 hours in the not perfused liver, peripheral lobe*

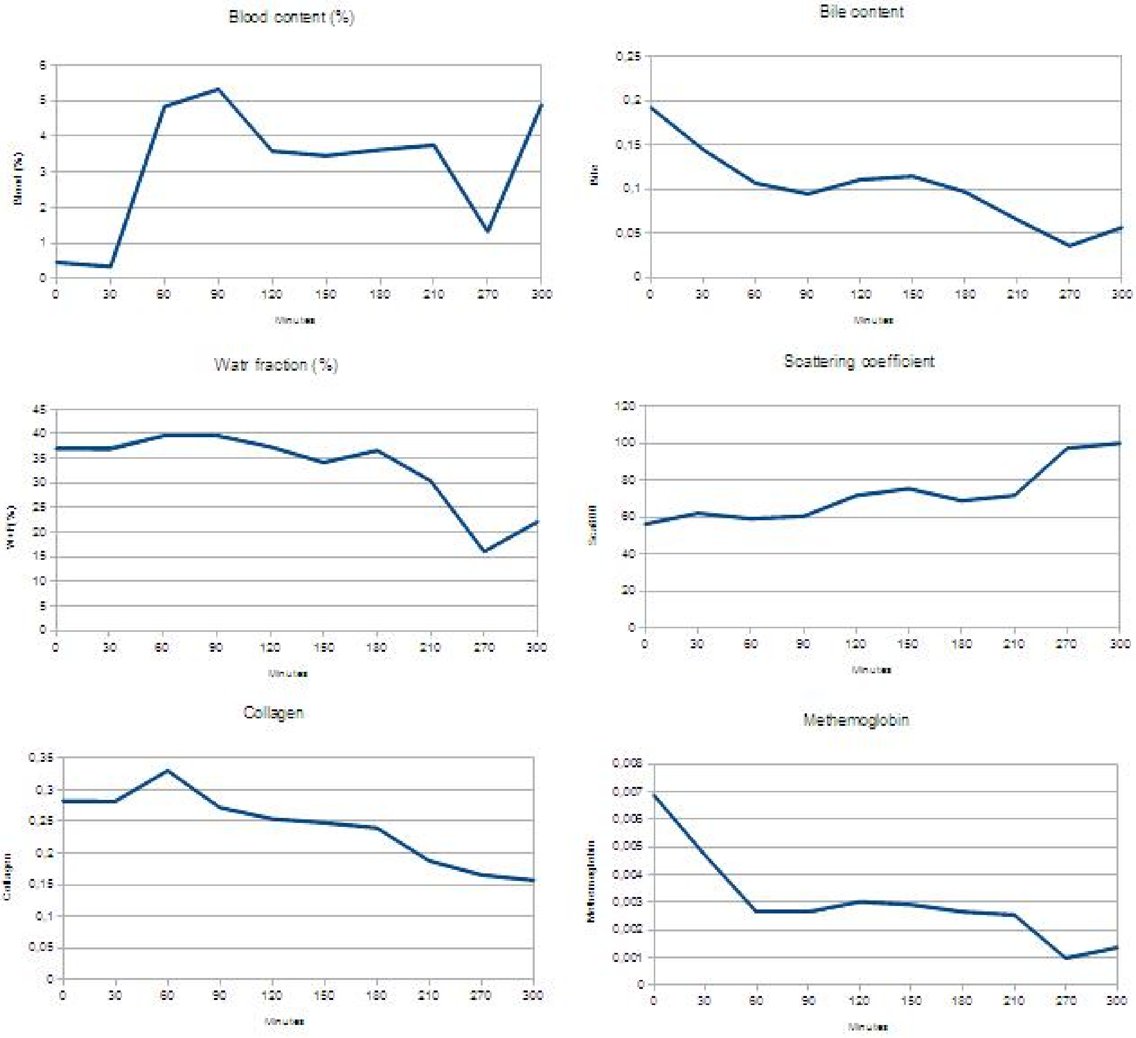

Figure D.6: *Parameters trends over 6 hours in the not perfused liver, middle lobe*

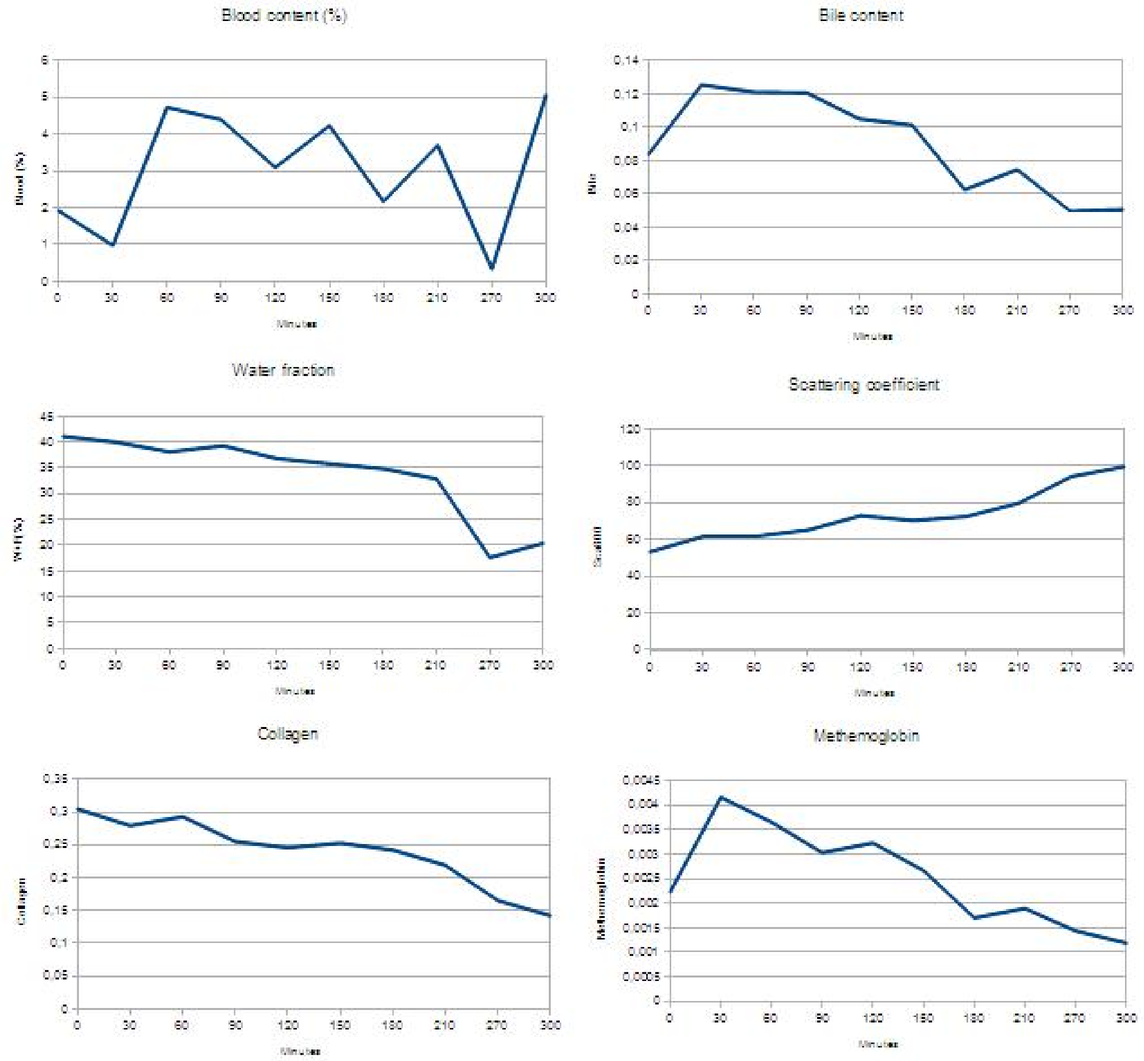

Figure D.7: *Parameters trends over 6 hours in the not perfused liver, central zone*

A journey is best measured in friends rather than in miles